EP/L014106/1
SUPERGEN Wind Hub

Deliverables:

D3.2 Report on wind farm control algorithms to meet power systems requirements

Delivered by:	University of Strathclyde
Author(s):	Dr Alex Giles, Professor Olimpo Anaya-Lara, Professor Bill Leithead,
	Dr David Campos Gaona
Delivery date:	September 2019
Distribution list:	Management Committee

Sponsored by:

Prologue

In this report, the investigation of wind farm control with the objective to meet power systems requirements is reported. It is shown that the full range of ancillary services including frequency support can be provided at the farm level. The architecture of the wind farm controller is hierarchical, decentralised and scalable. Although, only very weak feedback control is introduced at the turbine level, reasonably tight control is achieved at the wind farm level. It is demonstrated that offshore wind farms can be made to operate as virtual conventional plant through the Generator Response Following concept, whereby the power output of the farm is slaved to the power output from a small synchronous generator situated at the onshore end of the connection-to-shore. The sensitivity to communication delays and mitigating strategies are explored. The StrathFarm simulation tool has been used extensively in this work to evaluate the loads each turbine experiences when farm level control is used to provide ancillary services.

Following its remit to facilitate cooperation and collaboration, Supergen Wind Hub provided the cohesive element bringing together research from a number of programmes. The contributions from the following projects to the work reported here are gratefully acknowledged.

- EPSRC EP/L016680/1 DTC in Wind and Marine Energy Systems
- FP7-ENERGY-2013.10.1.6: 609795 IRPWind
- EPSRC EP/N006224/1 MAXFARM

The contributions of Lindsay Amos, Romans Kazacoks, Sung-Ho Hur, Luis Recalde Comacho and Adam Stock are, also, gratefully acknowledged.

CONTENTS:

DEPARTMENT OF ELECTRONIC & ELECTRICAL ENGINEERING

Supergen Wind

Title: Offshore Array Control

Alexander Duncan Giles, Olimpo Anaya-Lara and Bill Leithead

Wind Energy & Control Group
Department of Electronic and Electrical Engineering
University of Strathclyde

February 2018

Summary

With focus turning to the development of offshore wind farms to exploit the favourable wind resource, the control of such plants becomes of upmost importance, such that the projects remain as economically efficient as possible. The economic viability of an offshore wind farm is influenced by how effectively the wind farm can harvest energy, how the wind farm can operate in a manner amenable to a transmission system operator, and the level of mechanical loading to which the wind turbines are subjected.

In this work package, the University of Strathclyde developed a simulation tool, StrathFarm, for assessing the performance of wind farm controllers. Included in StrathFarm are state-of-the-art wind turbine control systems, turbine models and wind field models whose predictive capabilities have been demonstrated through comparisons with commercial software. With StrathFarm, it is possible to simulate the performance of a wind farm comprising one hundred turbines in real time on a standard desktop PC.

With StrathFarm, the University of Strathclyde have developed a control solution which demonstrates how a wind farm can provide ancillary services to a power system. Of particular importance is that this has been demonstrated when the wind is turbulent, a key detail which has often been ignored in previous work. While this was only demonstrated with a small wind farm comprising ten wind turbines in a regular layout, it should be noted that StrathFarm is sufficiently flexible for wind farm layouts such as the NORCOWE reference wind farm to be investigated. Similarly, while StrathFarm used Supergen wind turbine models, with appropriate lookup tables and knowledge of some physical properties, other wind turbines such as the DTU 10MW reference wind turbine could be simulated.

List of contents

1 INTRODUCTION

Historically, the control of wind turbines has focused on regarding said machines as individual, independent objects. However, with the proliferation of large wind farms, particularly offshore where farms may contain in excess of one hundred wind turbines, it is no longer appropriate to treat wind turbines within a farm as independent entities. This is for two reasons: first, the wind turbines within a farm are coupled through wake interactions; second, global objectives such as a target power output for the wind farm as a whole may not be achieved by turbine-level control alone when local wind speeds exhibit significant variance. To understand the latter reason, consider a wind farm where half of the turbines experience above rated wind speeds and the other half operating at some point below rated in the $C_{p_{max}}$ tracking region. By definition, the latter group of wind turbines can only increase their power output for a short period of time, drawing on the rotational kinetic energy of the rotor in the process; however, assuming the local wind speeds do not change, the former could, in principle, increase their power output indefinitely. In other words, a control mechanism should be introduced which takes into account the individual states/operating points of the wind turbines within the farm. Accordingly, control should extend to the farm level in addition to the turbine level.

To fully exploit the wind resource, offshore wind farms are also expected to be far-offshore. In order to minimise losses in the offshore transmission system, distant offshore wind farm will most likely be connected via HVDC systems. The implication of this is that the overall inertia of the AC system for which wind farms are providing power will be reduced following the displacement of conventional generation. It is expected that offshore wind farms, owing to their power ratings, will be required to compensate for the reduction in the system inertia along with providing other desirable functionality that conventional generation would have otherwise provided, all the while managing the mechanical loading experienced by the wind turbines so as to keep wind farms as economical as possible. Two ancillary services for which a wind farm may be expected to provide provision are frequency and voltage support. Voltage stability, particularly voltage stability issues surrounding the synchronization to the onshore power system, covers a set of stability problems which are predominantly solved through appropriate control of the onshore power converter in the HVDC system. Frequency stability, however, requires a system, in this case the wind farm, to change its power output and thus provide more/less energy, depending on the circumstances. Such a stability problem does involve farm-level control of the wind turbines.

During periods when ancillary services are not required, maximising the economic viability of a wind farm should become the primary objective. That is to say, a wind farm controller should be designed with one or both of the following objectives: maximise energy capture, or minimise mechanical loading. At a turbine-level, this may be achieved through approaches such as those proposed by Bossanyi or Leithead. In addition, at a farm level, this may be achieved through wake steering and/or de-rating of upwind turbines.

In order to evaluate the effectiveness of a wind farm controller, it is necessary to develop a model of the wind farm which is, ideally, both fast and accurate. Such a model must capture key dynamics associated with the wind turbine structures, and also those associated with the flow of air. This is then coupled to models of the control systems present in the wind farm.

The desire to develop such a tool has resulted in StrathFarm: a simulation package coded predominantly in C++ which uses MATLAB and Simulink to provide a user-friendly interface. The wind-field is coupled to engineering models of the wind turbine which currently employ the Frandsen wake propagation model. Lumped-mass structural models of wind turbines with state-of-the-art individual turbine controllers are also integrated into StrathFarm. In addition, each turbine is complimented by a Power Adjusting Controller (PAC) to facilitate the demands of the farm controller; finally, a central wind farm controller is included.

2 LITERATURE REVIEW

2.1 APPROACHES TO MODELLING THE PLANT

Wind farm dynamics are the combination of aerodynamics, structural dynamics, electrical systems and control systems. The first three combined form the plant which the control system attempts to manage. Hence, assessing the performance of the control system requires some representation of the plant. The aerodynamics and structural dynamics are far more coupled to each other than either is to the dynamics of the electrical system. This is primarily because the time scales associated with electrical systems are typically much shorter than those associated with aerodynamics and structures, thus occurring at frequencies well beyond the bandwidth of any control system for a mechanical component. Consequently, the main focus is on providing adequate representations of only the first two subcategories of engineering.

2.1.1 Aerodynamics

2.1.1.1 Engineering models

Historically, the most popular choice for representing the aerodynamics of wind turbines has been the Blade Element Momentum (BEM) theory approach. BEM models belong to a class of models known as engineering models; the defining characteristic of an engineering model is the focus on simplicity, where complex components of a system are quantitatively described using a small number of parameters and equations. For example, in BEM codes, the wake behind a wind turbine is entirely represented through two induction factors: the axial, a; and the tangential, a'. These represent the net velocities induced by the wake at the rotor. Lift and drag lookup tables are used during an iterative process which seeks to determine the induction factors for each and every blade element by balancing the axial force, as predicted by momentum theory, with the axial force, as predicted by blade element theory.

The shortcoming of engineering models is their reliance on modifications and/or empirical corrections. For example, the BEM equations in their original form assume that the wind speed is constant. In order to accommodate for this shortcoming, dynamic inflow models such as that of Pitt & Peters are applied [1]. Furthermore, the original BEM equations do not account for tip losses; accordingly, some variant of Prandtl's tip loss model is typically introduced [2]. However, given the wealth of experimental data available, such modifications have been developed and fine-tuned, yielding codes which have good levels of accuracy and have short computation times. Notable examples of reputable codes which employ the BEM equations are GL-Bladed and FAST [3][4].

In light of this success, engineering models have been applied to wind farm models, some being BEM-based [5][6], others being simpler models still [7][8]. In the case of the latter type, the wind turbine is represented through C_P and C_T lookup tables. In all aforementioned cases, the wake induction is represented through a simple parametric model, which is typically modified from the simple single-turbine wake model to accommodate for the multiple wakes present in the system. Examples of farm-level parametric wake models are the Frandsen model [9], the Jensen Park model [10], and the `New Analytical Wind Farm Model' [11]. Extensions of the Jensen Park model, capturing dynamic effects, are detailed in [12][13].

One might expect such simplistic representations to suffer from poor accuracy; however, somewhat surprisingly, models such as FLORIS, which is similar to the Jensen model, have been shown to predict wake losses accurately for a set of conditions, providing uncertainty is included in the calculation [14][15]. That being said, particular care must be taken over the combination of multiple wakes. Crespo illustrates that equivalent loads due to different wakes are not additive under multiple-wake conditions [16]. Typically, engineering models apply some additive form of wake combining, or the ``mosaic tile" approach, details of the latter may be found in [17]. In addition, the wake profile must be considered in engineering models. While it is generally accepted that the wake profile is Gaussian in shape, Frandsen showed that a model would suffer from no loss in generality by approximating the speed deficit by a top-hat profile instead of the Gaussian profile [9].

2.1.1.2 Physical models

Within the last couple of decades, advances in computing power and algorithms, specifically those which exploit graphical processing units, have made it possible for the aerodynamics of wind turbines to be predicted using solvers which are based either closely or explicitly on the Navier-Stokes equations. In their pure form, the Navier-Stokes equations are non-linear and require large amounts of computing power in order to produce meaningful solutions.

One class of Navier-Stokes solvers is known as Direct Numerical Simulation (DNS) flow models. For this class, the Navier-Stokes equations are solved on a very dense grid such that all the eddy scales are captured. Naturally, this leads to a high computational cost.

Another class of Navier-Stokes solvers is known as Large Eddy Simulation (LES) flow models. For this class, the Navier-Stokes equations are solved on relatively coarse meshes, thus capturing only the large scale eddies. Smaller scale eddies may be approximated with sub-grid models. Owing to the coarser mesh, the computation time associated with LES flow models is substantially lower than DNS flow models. For this reason, most high-fidelity wind farm flow solvers are LES flow models. Examples of LES flow models include the following codes:

- Simulator fOr Wind Farm Applications (SOWFA) [18]
- UTD Wind Farm (UTDWF) [19]
- SP-Wind (Leuven) [20]
- Parallelized LES Model (PALM) [21]
- Ellipsys3D [22]

SOWFA uses the same wind turbine model employed in FAST, with the wider flow field being represented through the LES flow model. Typical computation times are of the order of days or weeks [23]; consequently, SOWFA could not be considered sufficiently fast for either embedding into a controller or even evaluating the performance of a controller given the number of simulations that would need to be run. The other LES flow models listed above also suffer from the same computational costs; thus, LES flow models in general cannot be considered for wind farm modelling in the context of control engineering.

The Navier-Stokes equations are not tailored to any specific fluid system. Consequently, solvers based on the Navier-Stokes equations do not exploit any possible simplifications that can arise from appropriately relaxing the assumptions upon which the Navier-Stokes equations are based. For example, the bulk of the flow field associated with a wind turbine is inviscid, irrotational and incompressible.

Neglecting viscosity and assuming the flow field is irrotational and incompressible results in the Navier-Stokes equations being replaced by Laplace's equation [24]. This forms the basis of vortex codes, in which the wake is represented by a vortex lattice structure, comprising a plethora of vortex filaments. Each blade is typically segmented, as is done in BEM codes, with each segment featuring a vortex ring as shown in Figure 1. The bound vortex system is represented by the dashed lines. Each blade element is represented by one vortex ring comprising four vortex segments, one of which is aligned with the trailing edge, another aligned with the quarter-chord line, and the other two aligned with the blade element ends. The wake vortex system is represented by solid lines. Note - a vortex ring is defined to be a set of vortex segments which combined form a closed ring.

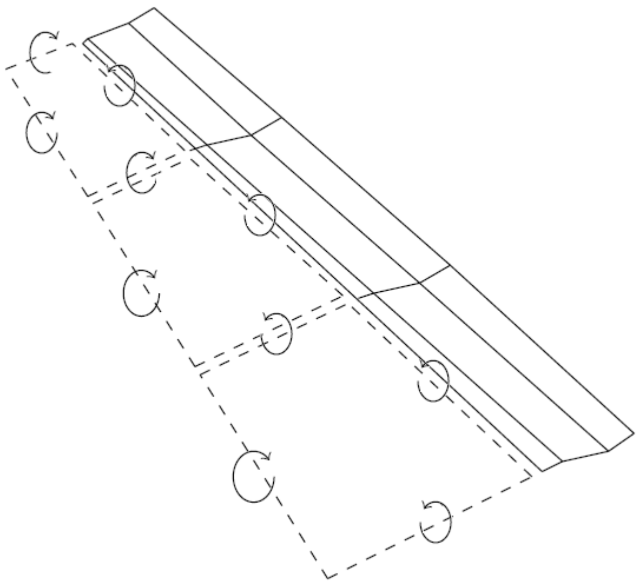

Figure 1: Lifting line representation of a blade (blade divided into three segments). Only the body vortex circulation has been illustrated.

The velocity of the air at any point in space is the vector sum of the free-stream velocity, the rotor velocity, the velocity due to the bound vorticity, and the velocity due to all vortices in the wake, including those most recently shed (whose strength is not known at the start of the iterative process for a given time step). Vortices are shed into the wake as a result of spanwise variation in the bound circulation, leading to `trailing vortices', and a result of temporal variation in the bound circulation, leading to `shed vortices'.

For each time step, the strengths of the bound vortices are set through an iterative process which uses lookup tables in conjunction with the Kutta-Joukowski theorem, finishing when the strengths of the bound vortices are such that the Kutta condition is satisfied all along the trailing edges of all the blades. The Kutta condition maybe formulated in a number of different ways; in its most accessible form, it is a statement that the local velocity at a trailing edge is zero. The iterative process employed also sets the strengths of the latest vortices to be released into the wake, in keeping with Kelvin's circulation theorem.

Through their formulation of the wake, vortex codes can naturally accommodate for time-varying winds. In addition, the phenomenon of tip losses is naturally accounted for.

Given that the velocity induced by the wake on some section of a blade is found by adding up all the individual contributions of the vortex filaments, each of these calculations can be carried out independently; hence, vortex codes lend themselves to parallel programming. Indeed, this feature of vortex codes, combined with the development of algorithms exploiting graphical processing units, has meant that it is now possible to simulate a wind turbine in a couple of minutes using vortex codes. This can be demonstrated using freely available software such as QBlade [25]. This advance in computation time has even made it possible to incorporate structural dynamics [26].

Branlard expanded on the application of vortex codes, modelling the free-stream turbulence using vortex lattice structures [27]. In this way, evolution of turbulence could be captured. Other extensions extend the system such that it comprises multiple rotors, as can be found in [28].

The bulk of the computational cost was evaluating the influence of wake vortex filaments on each other: for a system comprising N_v vortex filaments for a given time step, there are N_v^2 sets of calculations to be carried out. Hence, for systems involving multiple wakes, the computational cost can become high. One approach to reducing the computational cost is the vortex cylinder approach, which was explored by Branlard. In this approach, only the tip vortices are modelled. It was demonstrated that the velocity field could be calculated in approximately one second [29]. This computational efficiency did permit the modelling of wind farms using the vortex cylinder approach [30]. However, relatively little information is provided about details in the modelling such as how to accommodate for wake expansion and atmospheric stability.

2.1.2 Structural dynamics

Wind farm modelling must also ultimately include structural models if either a meaningful estimation of the cost a wind farm or the performance of a control system is to be made. In single-turbine simulation packages such as Bladed, the computational cost of the aerodynamics is sufficiently low that relatively advanced structural codes may be included. In recent versions of Bladed, a multi-body approach is adopted, specifically distributed models [3]. These models can capture the vast majority of dynamics witnessed in real life.

An alternative approach is the lumped parameter model. A blade, for example, may be represented by a pair of appropriately placed point masses; a higher order model of a blade would involve more point masses. It should be noted that the number of natural modes that a model can predict is fundamentally limited by the number of elements the model comprises; that is to say, a model of a blade comprising two point masses cannot capture the high frequency natural modes, while a multi-body representation can. However, by their very nature, the higher natural modes occur at frequencies beyond the bandwidth of any control system present, and also occur at frequencies where the power content (power in the spectral sense) of the wind confronting the turbine is low. Thus, of greatest importance are the first and second edgewise and flapwise blade modes, for which low-order lumped mass models are appropriate. The same logic can be extended to the drive-train and tower.

Interestingly, of the surveyed publications relating to wind farm modelling, very little information is provided about the elastic models used for the blades. The focus is on the drive-train and tower. In [7], a simple 3rd order drive-train model is employed, along with a 1st order generator model, 2nd order pitch actuator model, and a 2nd order tower model. No details of modelling the structural dynamics are included in [6]; this is presumably due to the focus of said work being on electrical systems.

2.2 WIND FARM CONTROL

Wind farm control is a relatively new area of research, within which there is a great level of diversity in multiple senses. For example, some wind farm controllers are designed to mitigate mechanical loads, while others are designed to maximise energy capture or track an externally driven power reference, such as one derived from frequency measurements of a power system. That is to say, wind farm control could be categorised according to objectives.

Within the literature available, a wide variety of inputs are used; the input will typically reflect the objectives that the wind farm controller is trying to achieve. For example, if the wind farm controller's primary objective is to reduce mechanical loads, some information such as blade root bending moment could be used as an input to the farm controller. Biegel et al assume that a measurement of the tower thrust is available, which is then used by a wind farm controller [31]. However, it is worth noting that standard turbines do not actually provide measurements of tower thrust. The tower thrust may be deduced, perhaps from an effective wind speed calculation [32]; however, effective wind speed calculations are themselves atypical. It has been proposed to use the ambient wind speed as the input for a wind farm controller. According to Knudsen, most of the relevant literature assumes the ambient wind speed is measurable [32]. However, this presents challenges since wind farms typically only have one met mast with which the wind speed can be measured in addition to nacelle-mounted anemometers. Nacelle-mounted anemometers are in the wake of a turbine, and so would not be appropriate for measuring ambient wind speed. Since there is usually only one met mast in a wind farm, there cannot be a full range of wind directions for which the met mast will not be immersed in a wake. Alternatively, a wind farm controller may take a measurement of the wind farm's total power output as its input. This lends itself to closed-loop control systems, where a wind farm controller sets a power reference for the wind turbines.

Alternatively, wind farm controllers may be categorised according to their structure; that is, a wind farm controller may be centralised, de-centralised, or hierarchical. De-centralised control structures are sometimes referred to as distributed control systems; hierarchical control structures are sometimes referred to as cascade control for reasons which will become self-evident.

Regarding centralised wind farm controllers, decisions are made for the entire wind farm by one controller. This requires the wind farm controller to process information from all sensors across the wind farm and dispatch commands to the actuators accordingly. This approach does lend itself to optimal operation; however, the computational demand of doing so would be prohibitively expensive. Indeed, while Horvat demonstrated that a centralised controller could increase energy capture, the results were confined to a wind farm comprising only eight turbines [33], far less than that which may be found in future offshore wind farms. Of course, computational costs can be mitigated by reducing the complexity of the model of the wind farm being used by the controller. However, even assuming that this is achieved, there is still the issue of what to do in the event of the central controller failing.

A closely-related control approach is the decentralised controller. In this case, the wind farm is broken down into blocks with each block comprising turbines that are in close vicinity to one another. Each block would then have its own `centralised' controller. Thus, failure of a single controller affects only a single block of the wind farm. However, each block would essentially be controlled under the assumption that it is independent, in all senses, of the other blocks in a wind farm. Consequently, in general, decentralised control may produce sub-optimal results. That being said, turbines are most influenced by the nearest upwind neighbour and influence the nearest downwind neighbour in turn the most. This suggests that blocking can be applied with some success. However, the blocking would have to adapt to changes in wind direction. Additionally, de-centralised controllers would not know how best to divide a global target, such as wind farm power output, among the blocks.

In the third approach, hierarchical control, there are multiple levels of control. In the case of a wind farm, the lowest level may be a wind turbine full envelope controller, which is designed such that a turbine follows a pre-defined control strategy, typically defined through a torque-rotor speed diagram. The highest level is the wind farm controller, where the wind farm power reference is calculated. Intermediate to the two may be control algorithms which accommodate for the individual turbine states and dispatch commands accordingly.

The means by which any of the three structures may achieve a set of control objectives can be split into two categories: those which attempt to achieve control objectives through influencing the strengths of the wakes downwind, usually achieved through the de-rating of upwind turbines; and those which attempt to achieve control objectives through wake steering, achieved through one or a combination of yaw, tilt and pitch action. The former approach is known as `axial induction control', while the latter is known as `wake redirection control'.

An important question that must be asked when implementing axial induction control is what is upwind and what is downwind? According to Knudsen, the available literature does not include evaluating the effect of changes in the wind direction [32]. This is a key oversight; if the wind direction changes relatively quickly, the ratings of the wind turbines must be updated quickly or else energy capture will be reduced. In fact, it has been suggested that the reduction in energy capture will exceed any gains that were produced from the original de-rating [32].

Furthermore, many control systems are tested using static wind speeds; when Johnson and Fritsch introduced time-varying wind speeds, the performance of the wind farm exhibited strong sensitivity to turbulence intensity [34]. Results demonstrated that the wind farm controller employed, an extremum-seeking control approach in the case of Johnson and Fritsch, the change in energy capture was +4%, +3%, +1% and -14% for constant wind and low, medium and high turbulence, respectively. That is to say, the proposed wind farm controller could easily result in net losses.

Vollmer et al investigated wake deflection on single turbines under different atmospheric conditions, presumably as a precursor to wind farm control using the wake steering approach; the types of atmospheric stability considered in this work were neutral, stable, unstable and thermal. It was demonstrated that changing the atmospheric stability did influence the wake shapes and the magnitude of deflection following a deliberate yaw misalignment [35].

Gebraad et al present a wind farm control strategy that optimises yaw settings of wind turbines for improved energy production of the wind plant [12]. They use a game theoretic approach using a control-oriented model that is able to predict the steady-state effects of yaw control on the wakes as well as the resulting effects on turbine power production. An increase in power production using the strategy was demonstrated in simulation, and an overall decrease in loads, although an increase in loads was found for those turbines then experiencing partial wakes. Perhaps the most significant short-coming of this approach is that the method requires manual tuning of parameters for different ambient turbulence intensities.

Raach et al focus on LIDAR based closed-loop wake redirection to address the issues regarding the uncertainty in direction of the wake produced by feed-forward control (i.e. the quality of the model used to compute optimal yaw angles highly influences the performance, and there is no observation of whether the wake is being redirected correctly) [36]. From an upfront financial-cost perspective, LIDAR installations are typically very expensive. Even when the cost is ignored, LIDAR devices have a certain number of shortcomings; of greatest significance in the context of wind farm control is the need for aerosols to be in the air.

The work of Raach is the main contribution that uses linear dynamic closed-loop control. In [37] a PID controller is designed for wake tracking, while in [36] and [38] a H_∞ controller is designed to steer the wake while employing a dynamic wind farm model.

Dar et al employ Dynamic Programming to the problem of wind farm power optimisation using yaw control [39]. While encouraging results concerning energy capture were presented, no accompanying assessment of the resulting impact on loads could be found. Moreover, it is possible that the use of a simple engineering wake model may well impact the application.

Fleming et al used CFD solvers to assess the effects of yawing a turbine [40]. It was demonstrated that if the yaw misalignment is 35 degrees, the wake of a turbine will have moved by only half a rotor diameter cross wind at a distance seven rotor diameters downstream of the turbine. In the same work, it was reported that tilt action was a significantly less effective means of wake steering: at a distance of seven rotor diameters downstream of a wind turbine, the wake had been moved by only 0.18 rotor diameters when a tilt of 18 degrees had been applied. While small gains in energy capture were reported, operating with a yaw misalignment as high as 35 degrees would increase mechanical loading considerably, most likely around 1P and 3P. It is important to note that the aforementioned results were produced using constant wind speed and direction.

Focusing only on papers derived from industrial applications of wind farm control, Knudsen notes that there is a limited supply of information. As of 2014, only three papers were produced by industry. While these papers claim to distribute a wind farm power set-point to individual wind turbine set-points, no detail is given on how this is done, or the results. The most information is given in [41], where it is revealed that each turbine attempts to obtain the maximum available power based on some estimation of free wind speed of each wind turbine. Knudsen concluded that, excluding periods when the transmission system operator demanded otherwise, wind farms are controlled as though the constituent turbines were independent entities. This being said, Knudsen notes that some industry contacts claimed that some wind farms run with the front row de-rated, with a very small gain to power production of less than 1% [32]. The lack of any sizeable increase may be due to the fact that what is defined to be the front row will not always refer to the same group of turbines, which introduces avenues for inefficiencies.

Bossanyi and Jorge of DNV-GL presented a paper at the European Control Conference in 2016 demonstrating a simplified engineering model. The purpose of the model was to allow for rapid optimisation of wind farms, with the aim being to optimise the cost of energy. This was achieved through trade-offs between energy production and turbine loading. Embedded in the model are multidimensional look-up tables for damage equivalent loads created from time series simulations in GL-Bladed. For a row of six turbines on flat terrain, simulations indicated that a total load reduction across all wind turbines of 12.6% could be achieved [42]. While the DNV-GL website advertises that their "*wind farm control system lets you optimize individual turbine speeds and torques to manage wake effects and maximize the overall energy capture of your farm while ensuring a long service lifetime*", experimental verification of the control system is not provided. This is, however, consistent with the sentiment of the paper's conclusion: "*wind farm control is in its infancy ... much further work is required to enable widespread commercial adoption*".
Moreover, it is acknowledged that much work is required on development and validation of wake models, the fatigue load databases, and also the difficulty in formulating the benefit function for the joint problem of maximising energy and minimising loads.

A survey of online resources for 2016's top 10 wind turbine OEMs found the following results:

- General Electric (GE) advertise their ”Wind Plant Wake Management” system [43], which aims to reduce wake losses through appropriate farm level cotnrol. By adopting the control system, energy capture over a typical year is said to be boosted by between 0.5% and 2%. While no detail is available regarding the algorithms used, it is most likely that a data-driven approach is adopted. They state that "*wind plant wake management integrates data from turbine-level and plant-level controls with real-time wind characteristics and micro-siting information, then adjusts individual turbine operational parameters such as pitch angle, tip speed ratio, and rotor speed in order to reduce wake losses and increase plant level energy output*.".
- Siemens Gamesa Renewable Energy appear to be developing data-driven solutions to optimising wind power plants called ”WinSight 360” [44]. Since the product is still in development, there are no results to comment on; however, it is claimed that the elements of WinSight 360 are "*creating a powerful basis for yield optimization*".
- Envision Wind Energy [45] offer products "Monitor and Control OS" and "Envision Ensight" which provide centralised control and wake loss analysis respectively; however, there is no apparent combined or coordinated solution.
- Enercon and Vestas detail ancillary services provided by wind farm control; however, the remainder of the ten OEM's (Goldwind, Nordex Wind, United Power and Mingjang Wind Power) have no mention of wind farm control solutions in the public domain.

The following solutions on offer from industry could also be found online:

- KK Wind Solutions "Wind Park Controller" [46] claims that it "*intelligently coordinates tasks between wind turbines in a wind park for optimized power output - including yaw untwist, wake control*" but doesn't give any detail or examples.
- Konsberg's "EmPower" [47] is an independent decision support system for wind farm management. This product claims to be capable of enabling a wind farm to provide ancillary services, or, if so desired, maximise energy capture and reduce mechanical loading. They state that "*The Dynamic Wind Farm Optimizer functionality represents uniqueness in EmPower with regards to control for increased energy yield and load reduction. The Wind Farm Control module will recommend, and if desired, automatically adjust, the set points for each individual turbine. This optimizes the total wind farm production and revenue according to current wind conditions, turbine state/condition,*

anticipated load and wear". However, no further details revealing either methodology or predicted results are available.

- DEIF Wind Power Technology offer a Wind Park Power Management (WPPM) system [48]. The primary focus of this control solution is on the provision of ancillary services; however, it also claims to include "*algorithms that enable to distribute set points individually to the different turbines based on several environmental inputs such as wind direction and temperature. With cluster control, an even distribution of the loads over time on all turbines in the wind park is achieved.*". According to the website, the company runs 30 wind parks in China.

3 WIND FARM CONTROL FOR ANCILLARY SERVICES

3.1 WIND FARM CONTROLLER

From a high-level perspective, a power system can be viewed as a combination of generators and loads interconnected by transmission and distribution systems. Conventional power systems were mainly powered by synchronous generators, typically fuelled by fossil fuels such as natural gas and coal. The combustion of coal releases thermal energy which in turn heats up a water supply, with the resulting steam being used to drive a turbine. The rate at which coal, natural gas, or any other fossil fuel is combusted is controllable and set according to the rotational speed of the rotor in the generator. That is to say, a control system known as a governor acts to ensure that the frequency of electricity produced by the generator is kept within tight limits. This control mechanism is referred to as droop control.

A control system such as the governor cannot react instantaneously; that is to say, in the immediate aftermath of an event which causes a frequency deviation, the governor is largely irrelevant. Any rotating object will continue to rotate at a given speed unless acted on upon by a net non-zero torque. For a generator in a coal plant, two sources of torque are present: the mechanical torque, due to steam; and electrical torque, due to the consumers' demand for electrical power. The former acts to accelerate the generator rotor, while the latter acts to decelerate it. Any imbalance between the two results in the rotor speed changing. The rate at which it does so is dictated by the magnitude of the net torque and the inertia of the generator rotor; high inertia rotors resist torque imbalances more than low inertia rotors.

During an event in which power demand exceeds supply, the net torque acts to retard the rotor; the power imbalance is compensated by the release of rotational kinetic energy from the generator. This basic physical response occurs instantly. It is referred to as inertial response.

With the reduced system inertia that accompanies the displacement of conventional generation by wind turbines, the wind turbines will need to provide both synthetic inertia and droop control. In addition, a wind farm may be required to curtail its power output, or make other adjustments in the power generated. Furthermore, it is necessary to demonstrate that a wind farm can deliver such services even when there are communication delays in the system, which can be expected to occur when HVDC links are used to connect generation to a power system. All aforementioned points are particularly true when considering projected sizes of far offshore sited wind farms, some being on the scale of 1GW with HVDC connection to shore.

It is important to recall that wind turbines in a wind farm cannot be regarded as independent. This is for two reasons: first, the performances of the wind turbines are coupled through wake interactions; second, a global objective may only be achievable by applying a non-uniform distribution of power change demands among the wind turbines, for example, when some wind turbines are operating in below-rated conditions. Accordingly, controlling turbines as individual entities without any consideration of the turbines as a collective body will, almost certainly, result in sub-optimal performance. Hence, it is appropriate to extend control to the farm level.

To deliver the full range of ancillary services, both the wind turbines and the wind farm will need to be operated flexible with the power output no longer dictated by the wind speed. The capability of the wind farm to deliver that flexibility of operation and so the full range of ancillary services is explored here. A suitable generic wind farm controller has been developed with the architecture is shown in Figure 2.

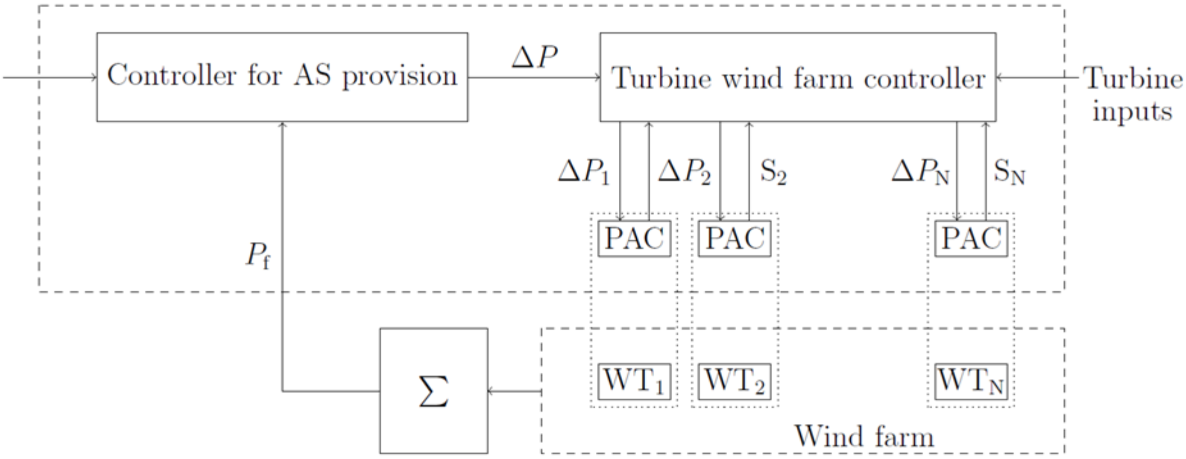

Figure 2: Structure of the wind farm controller

.The controller is hierarchical, decentralised and so readily scalable.

- The top layer, the *Controller for AS provision*, responds to onshore power system requirements to determine a target adjustment, ΔP, in the power output from the wind farm.
- It may operate open-loop, e.g. to reduce the power output by a fixed amount, or closed-loop, e.g. to curtail the output from the farm to a fixed power level. The latter feedback is based on feedback of the total farm output, P_F.
- The second layer, the *turbine wind farm controller,* determines the change in power required from each turbine, namely ΔP_1, for turbine 1, ΔP_2, for turbine 2, etc.
- The bottom layer is a generic interface to each turbine, the *Power Adjusting Controller (PAC)*.
- The only feedback permitted from each turbine to the first and second layers are flags containing information about the state of the turbines and an estimate of the local wind speed.

The turbine wind farm controller does not introduce additional feedback round an individual turbine, due to the fact that flags are the only direct communication between the turbines and the turbine wind farm controller [49]. As can be observed from Figure 2, there is an outer power feedback involving the network wind farm controller; however, this feedback loop is very weak. This may be inferred from a simple analysis, where the system is represented as shown in Figure 3.

The controller block denotes the wind farm controller, which is defined to have a transfer function, C. The wind farm controller receives as an input the difference between the power being demanded, say from a transmission system operator, and the power actually being produced by the wind farm. The difference is split among the turbines by the wind farm controller; the fraction of the total amount of the change in power that a given turbine, i, is to deliver is given by α_i. The dynamics of a given wind turbine are represented by G_i. Finally, each turbine is subjected to a unique wind speed disturbance, which is represented by d_i.

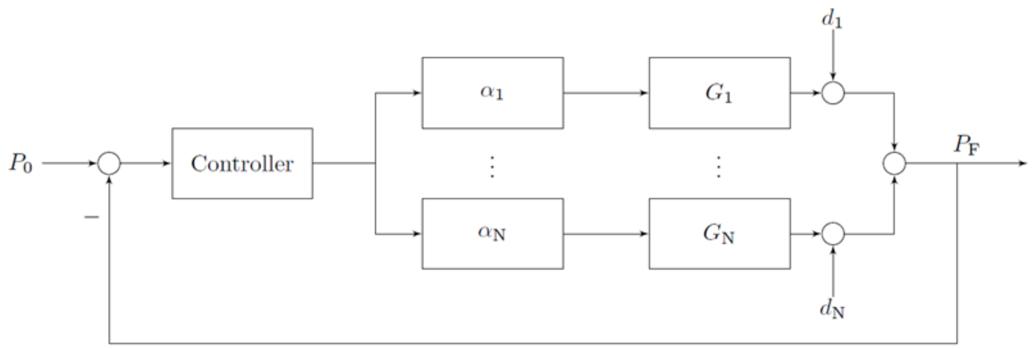

Figure 3: Simplified representation of the network wind farm controller [49]

Figure 3 may be simplified to a single system as shown in Figure 4:

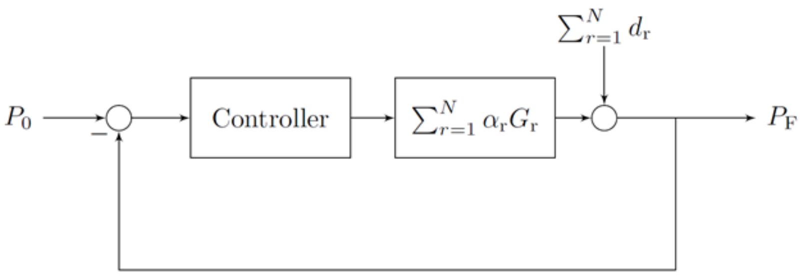

Figure 4: Feedback loop with turbines combined into single system [49]

The corresponding feedback for a single wind turbine, say turbine 1, is shown in Figure 5:

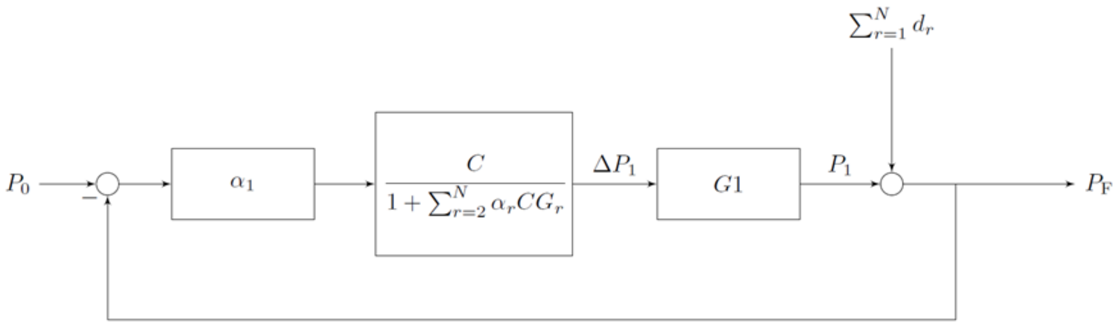

Figure 5: Feedback loop for single turbine in the wind farm [49]

While in the general case each turbine may have its own plant dynamics, for simplicity let the turbines all be the same. In other words, $G_i = G$. Accordingly, if an equal allocation of power adjustment is made, the open loop transfer function for Figure 4 simply becomes CG, whilst the open-loop transfer function for Figure 5 becomes, where N is the number of turbines in the farm.

$$TF = \frac{CG}{N\left(1 + \frac{N-1}{N}CG\right)} \quad (1)$$

Hence, as far as individual wind turbines are concerned, the wind farm controller does not introduce any additional significant feedback loops [49]. This is a desirable characteristic in a wind farm controller since it implies that no modification to the wind turbines' full envelope controllers is required.

3.2 Power Adjusting Controller

Conventional wind turbine controllers do not generally provide full flexibility of operation and in themselves cannot accommodate the requirements of the onshore power system. To accommodate this shortcoming, the PAC was developed [50]. The PAC works in conjunction with the full envelope controller; that is to say, it does not replace the full envelope controller, but simply enhances it to provide maximum flexibility of operation of the wind turbine as desired. The PAC has the following attributes:

- The PAC does not compromise the turbine controller since it is essentially feed forward in nature.
- It can be interpreted as changing the set point or operational strategy of the wind turbine albeit in a continuous and dynamic manner.
- The turbine is kept within a safe operating region through the use of the flags
- The change in output power from the turbine matches very accurately the change in power requested.
- Response of the turbine to the requested change can be very fast.
- Very little information about the turbine is required. No information is required on turbine dynamics or the turbine controller.
- It is easily retrofitted.

The PAC acts as a jacket wrapped around the turbine full envelope controller as shown in Figure 6.

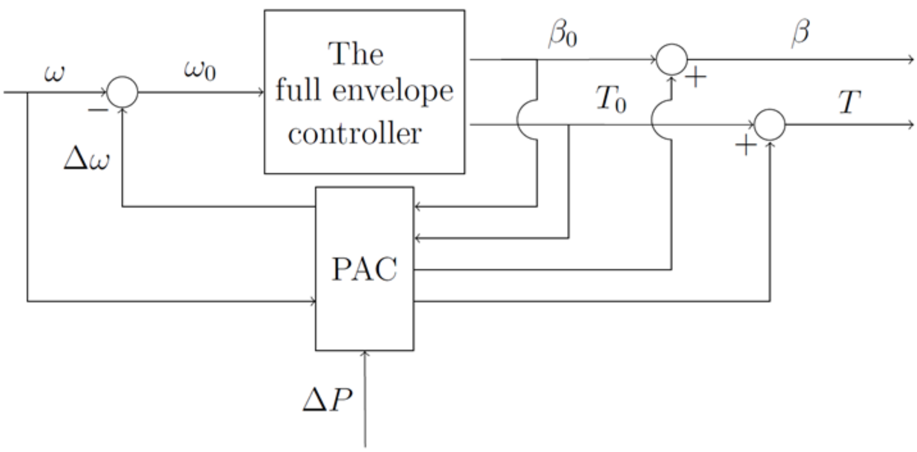

Figure 6: High level illustration of the PAC and its operation in conjunction with the full envelope controller

The controller input, generator speed, ω, and outputs, pitch demand, β, and generator torque demand, T_0, are additively modified. Since these adjustments are done in such a manner that no feedback around the full envelope controller is introduced, the operation of the full envelope is not compromised. The adjustments of pitch demand and torque demand are coordinated with the former slow acting and the latter fast acting to ensure that the achieved change in generated power matches the demanded change, ΔP.

The modification to generator speed, $\Delta\omega$, is made to ensure that the full envelope controller does not act in such a way as to counter the actions of the PAC, especially during below rated operating conditions. To understand why, consider an increment ΔT is added to the torque demand by the PAC. Assuming that the wind turbine was previously operating in steady-state, it follows that the rotor will accelerate/decelerate, depending on the sign of ΔT. The full envelope controller, without $\Delta\Omega$, would detect this rotor speed change and adjust the torque demand in such a way as to arrest the change in rotor speed and, thus, bring the machine back into equilibrium. This process can be thought of as being equivalent to a disturbance wind speed, which the full envelope controller is designed to reject. Thus, the PAC anticipates the change in rotor speed caused by the change in torque demand and adjusts the measured rotor/generator speed to 'fool' the full envelope controller into not rejecting the disturbance.

The structure of the PAC is presented in Figure 7. Contrary to appearance, even though it contains a feedback loop, the particular properties of turbine rotor aerodynamics and the design of the internal controller are exploited so that the PAC acts on the turbine as solely a feed forward controller. It includes an accurate estimate of wind speed that accounts for the effects of dynamic inflow [50]. For a particular wind turbine, the PAC only depends on a few parameters such as rotor radius and inertia. Hence, it is easily retrofitted.

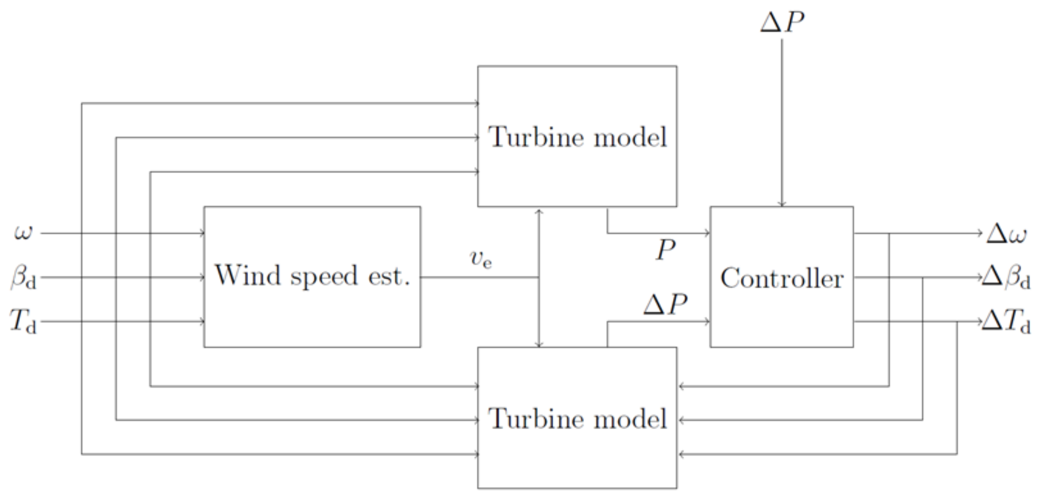

Figure 7: PAC structure

When the PAC is operating, the turbine deviates from its normal operating strategy. In essence, through causing the generated power of the wind turbine to deviate from that dictated by the wind speed, the operating strategy of the wind turbine is continuously modified by the PAC. However, in so doing, it must not cause the turbine to go out of the safe operating, e.g. from entering stall. Accordingly, the PAC includes a supervisory controller that continuously monitors the operating state of the turbine and prevents any action by the PAC that would put the turbine at risk. The current state of the turbine is recorded using a set of logic flags. These can only be set by the PAC. The wind farm controller can request a change to the status of a flag but that change will only be acted on if the PAC supervisory controller agrees. The status of all the flags is communicated to the wind farm controller so the changes in turbine's power requested power is appropriate. The supervisory rules related to these consist of two sets: black rules, defined by an absolute boundary on the torque/speed plane, which impose hard limits on the actions of the PAC; and traffic light rules, which impose restrictions on the actions that the wind farm controller might request, e.g. loss of generation (for which synthetic inertia would be required) or a lower-priority event (in the short term sense) such as curtailment.

An illustration of the traffic light rules is shown in Figure 8 which depicts the torque/speed plane diagram for a turbine. The black curve depicts the operating strategy for the turbine. The safe operating region is divided into green, amber and red zones. In the green zone, the allowed changes to generated power are relatively unrestricted other than by minimum/maximum limits. When the turbine enters the red zone, no change to generated power is permitted. If no request from the wind farm controller, that would cause the turbine to move back into the amber zone, is received then the PAC would itself go into recovery mode after a short interval and return the turbine to the normal operating point for the current wind speed. In the amber zone, the permitted changes in generated power are much more restricted than in the green zone to provide some cushioning. The black boundary lies just outside the red boundary. The PAC prevents this boundary from ever being breached.

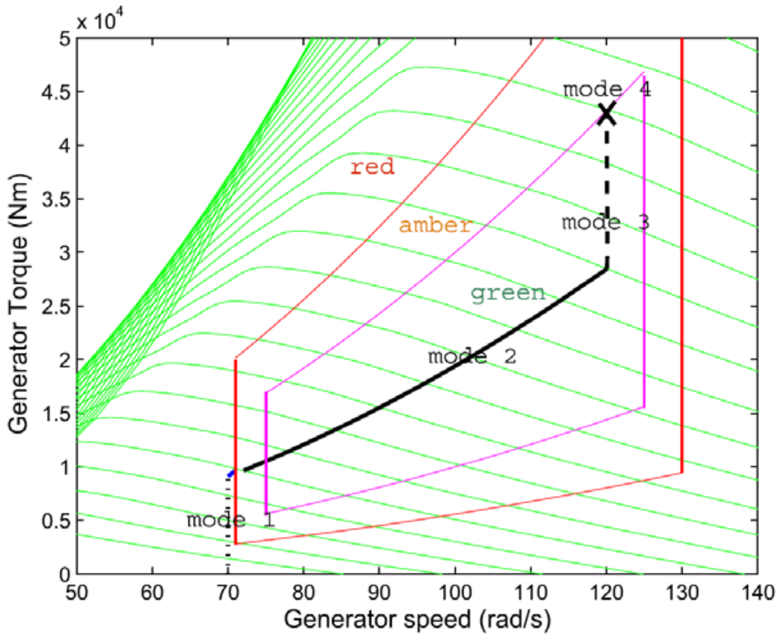

Figure 8: Illustration of the safety zones defined by the PAC

The general supervisory rules are as follows:

a. The requested change in power, rate of change in power and pitch rates are subject to limits and the permissible turbulence intensity and wind speed are subject to upper and lower limits, respectively. These limits and events designated high priority, e.g. Requests for synthetic inertia, are defined with agreement and cannot be changed without agreement of the OEM.
b. The PAC is activated following a PAC ON flag being sent by an external controller.
c. The PAC is deactivated when the PAC ON flag is reset either due to self-regulation such as when a limit has been reached, or by the PAC at a request from the wind farm controller. After being deactivated, the PAC goes into recovery mode; accordingly, the RECOVERY flag is set. The rate at which the recovery occurs is determined by the sub-flag (Fast/Slow). While the default setting is REOCVERY (Fast), the sub-flag

(Fast/Slow) can be reset at the request of the external controller.The PAC rejects any requested change in power during the recovery period; accordingly, The REJECTION (Recovery) flag is set by the PAC. On completion of the recovery mode, the RECOVERY (Complete) flag and sub-flag are set and the PAC ON flag is reset.

d. Only black supervisory rules apply to high priority events. The PRIORITY flag is set by the PAC at a request from the external controller.
e. If the limit for requested change in power is exceeded, the REJECTION (Power) flag is set by the PAC.
f. A power rate limit is incorporated into the PAC. Only if the PRIORITY flag is set will the PAC accept power rates in excess of these limits. If no PRIORITY flag is set, the rate limit applies and the REJECTION (Power rate) flag is set by the PAC.
g. If the turbulence intensity limit is exceeded, the PAC ON flag is reset and the PAC ON (Turbulence) sub-flag is set and latched by the PAC.
h. If the actuator pitch rate limits are violated by the turbine full envelope controller, the PAC ON flag is reset indefinitely and the PAC ON (Actuator) sub-flag is set indefinitely by the PAC.
i. If the low wind speed limit is exceeded, the PAC ON flag is reset and latched and the PAC ON (Wind Speed) sub-flag is set and latched by the PAC.
j. If the turbulent state is divergent such that normal operation is unreachable, the DIVERGENT flag is set by the PAC.

The black supervisory rules are as follows:

a. The boundary and maximum possible generator reaction torque are set with agreement and cannot be changed without agreement of the OEM.
b. The boundary should not be crossed under any circumstances. If the turbine state is outside the boundary, the PAC ON flag is reset by the PAC.
c. On the turbine state reaching the boundary, the REJECTION (Limit) flag and sub-flag are set by the PAC.
d. If the turbine state remains on the boundary beyond a pre-set limit, the PAC ON flag is reset by the PAC.
e. On a section of the boundary corresponding to the maximum possible generator reaction torque, the permitted time limit before resetting the PAC ON flag is zero.

The traffic light supervisory rules are as follows:

a. The boundaries can be set at a request from the wind farm controller.
b. The maximum magnitude of change of power in all regions can be set by the wind farm controller subject to the fixed upper limit, the maximum magnitude for the amber region being less than the maximum for the green region and the maximum/minimum change of power for that part of the red region to the left/right of the operating strategy being zero.
c. When the turbine state is in the green/amber/red region, the corresponding GREEN/AMBER/RED flag is set by the PAC.
d. When the demanded change in power exceeds the maximum or minimum, the corresponding REJECTION (Green limit)/(Amber limit)/(Red limit) flag and sub-flag are set by the PAC.

An analysis of the PAC dynamics, details of which may be found in [50], demonstrates that the PAC does not compromise the full envelope controller and that no modification to it is required. The effectiveness of the PAC is illustrated through Figure 9 and Figure 10. In Figure 9, a series of 100kW changes in generated power are requested for a 5MW wind turbine. In Figure 10, a synthetic inertial response is requested of the same wind turbine at 7, 10 and 20m/s. The response in each case is very similar other than the absence of a period of reduced power during which the energy depletion from the turbine rotor is replenished in the 20m/s response. The simulations are conducted in Bladed.

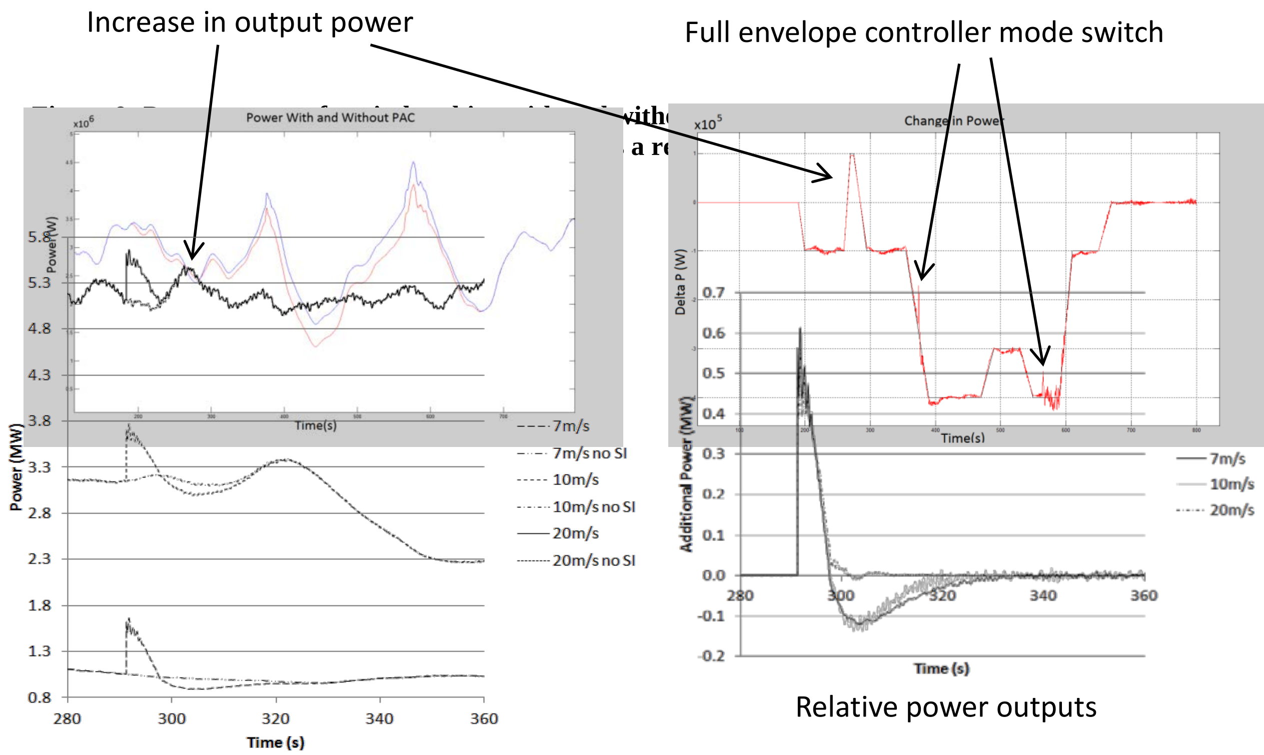

Absolute power outputs

Relative power outputs

Figure 10: Power from a turbine both when synthetic inertia is provided and when it is not for a range of wind speeds

Note that the PAC performance is subject to the accuracy of the C_P and C_T(thrust) lookup tables; a turbine's performance, as quantified by the aforementioned lookup tables, in reality may exhibit discrepancies from that found in a simulation model. Moreover, the performance may change with time. However, this issue can be circumvented by introducing machine learning algorithms to provide up-to-date lookup tables for the PAC to utilise, which process data acquired from already-installed instrumentation on a wind turbine.

Furthermore, it is important to recognise that the structures of the PAC and wind farm controller are such that they can easily be integrated with an extensive range of turbine-level controllers. This is for two reasons: first, the PAC modifies inputs and outputs to a turbine controller, namely the rotor speed measurement along with the pitch and torque demands, such that its effect is hidden from the turbine controller; second, the wind farm controller does not introduce any significant feedback into the system, thus dissociating turbine-level control systems from those introduced in [51].

4 StrathFarm Wind Farm Simulation

An analysis and design wind farm model and simulation tool, StrathFarm, which is depicted in Figure 11, has been developed with the following attributes:

- Wakes and wake interaction are modelled
- Turbines are modelled in sufficient detail that tower, blade and drive-train loads are sufficiently accurate to estimate the impact of turbine and farm controllers on loads.
- Commercial standard turbine full envelope controllers included.

- Wind farm controller and interface to turbine controllers included.
- Very fast simulation of large wind farms (run in real time with 100 turbines on a standard PC).
- Flexibility of choice of farm layout, turbines & controllers and wind conditions direction, mean wind speed and turbulence intensity.

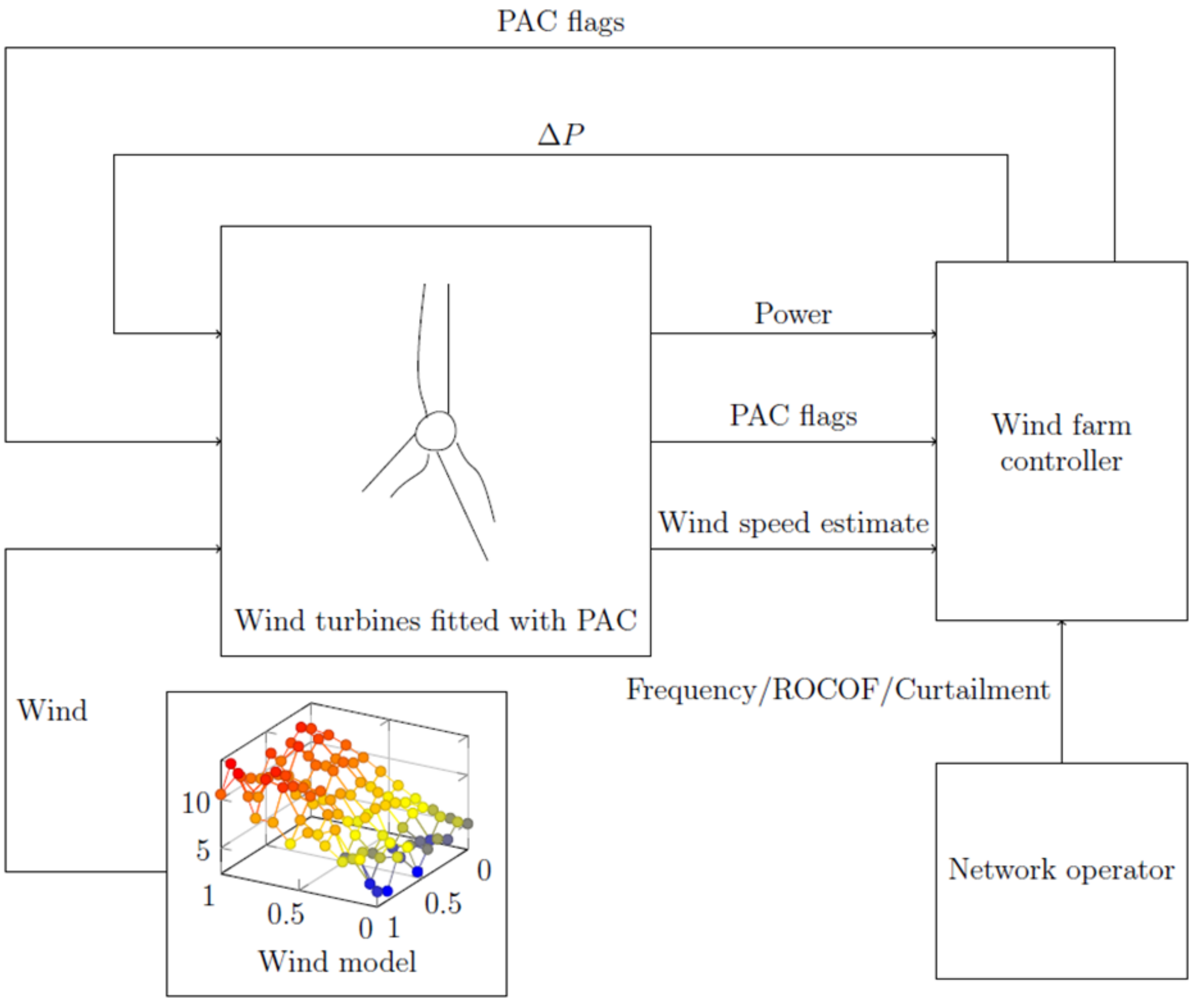

Figure 11: Illustration of StrathFarm

4.1 Wind Field Modelling

The wind field that confronts a wind turbine is complex, exhibiting both spatial and temporal variations. Specifically, the wind field is a combination of a mean wind speed, deterministic components such as wind shear, and stochastic components, i.e. turbulence. An example of a wind field that a rotor may experience is represented by Figure 12. Note that the wind field is illustrated for one instant in time only.

4.1.1 Wake deficit modelling

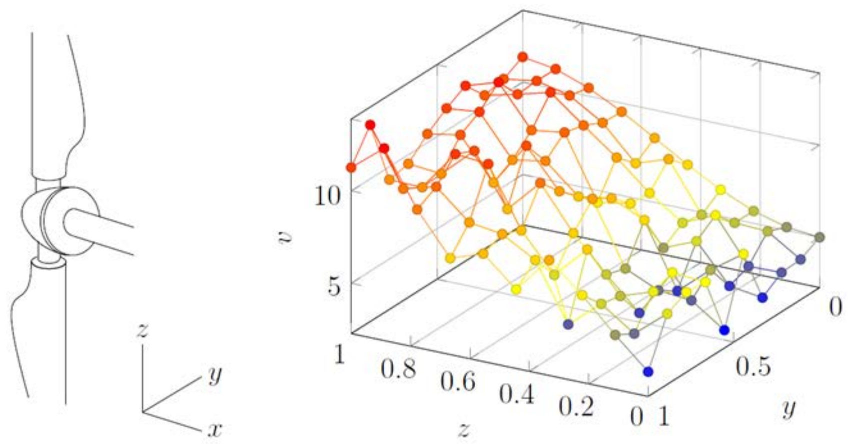

Figure 12: Point wind speeds at different points on a plane at an instant in time

At present, StrathFarm implements a wake model based on the kinematic explicit wake modelling approach of Frandsen [9]. In this approach, the wake effects including wake centre, wake diameter, and wake deficits are modelled as a function of distance from a wind turbine and the thrust coefficient of that same wind turbine. The wake centre is computed assuming an axisymmetric wake, meandering through the wind farm.

In the general case, the wind speed experienced by a given turbine may be a function of multiple wakes belonging to upwind turbines. To account for this, the upstream wake component of the wind speed is calculated by combining the effects of all relevant upwind wakes.

Lateral turbulent wind speeds are generated over the wind-field. These are included in the wind-field model to induce meandering of the wakes, see below.

4.1.2 Turbulence modelling

The stochastic element of the wind-field is represented as the addition of two components, a low frequency component and a high frequency component. Over frequencies less than the choice of bandwidth of the former, the wind speed is highly correlated over the rotor disc. Hence, it is sufficient to model the low frequency component as a time varying scalar wind speed. Over length-scales similar to those separating turbines in the wind farm, part of the low frequency component, at very low frequency, correlates highly. Any correlation of the high frequency component of the wind-filed occurs over length-scales less than or similar to rotor diameter. Indeed the amplitude of its spectrum tends to zero at very low frequencies. The different degrees of correlation of the above wind-field components, is exploited to construct a computationally economic model of the longitudinal element of the wind-field as described below.

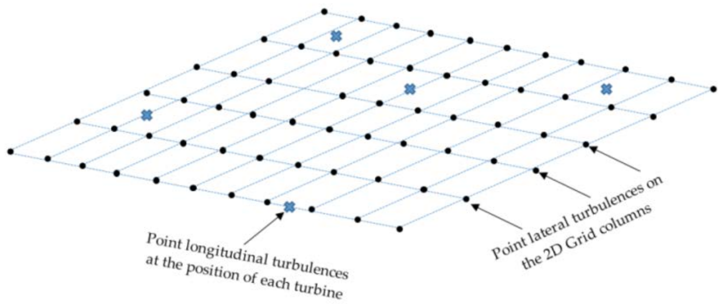

Figure 13: Illustration of the grid used for generating N correlated time series with each times corresponding to a point wind speed at a turbine hub [8]

With a relatively low sampling time of the order of 1sec, a set of correlated time series over an irregular grid of N points representing the position of the turbines in the wind farm, see Figure 13, is constructed using the Veers method [52]. Each series in the set represents the very low frequency part of the wind-field low frequency component. However, higher frequency representation of the wind-field is required as input to the wind turbine models; that is, a sampling time of the order of 0.02 sec is necessary. Because there is negligible correlation between turbines, this high frequency component of the wind field can be generated independently for each turbine. In addition, intermediate values over the long sampling time intervals for the wind-field low frequency component are constructed independently for each turbine with the correct correlation to the intervals' initial and final values. These two contributions to the non-correlated part of the wind – field are combined.

With regard to the wake meandering, the lateral turbulence need only be represented by a very low frequency scalar wind speed similar to the correlated part of the longitudinal turbulence. A set of correlated wind speed time series over a regular grid, with the spacing equivalent to the displacement at mean wind speed over 1sec, is constructed, again using the Veers method [52].

The above representation of the stochastic elements of the wind-field enables the use of a split-level integration algorithm. The longitudinal very low frequency part, combined with the mean wind speed and wakes model, and the lateral turbulence are numerically integrated with step length of 1sec. The longitudinal non-correlated part, combined with the deterministic parts, namely, wind shear and tower shadow, are integrated with a step length of 0.02secs.

In StarthFarm, the blades of a turbine rotationally sample, locally to that turbine, the wind-field constructed as above. The wind-field model is sufficiently detailed to represent such rotor/wind-field interactions up to 6P.

4.1.3 Creating the wind field in StrathFarm

The wind farm layout is defined through two user interfaces. The first, Figure 14, is used to specify the number of turbines in the farm. StrathFarm has the flexibility to model regular structures, such as a 5-by-2 wind farm, or irregular structures, such as the NORCOWE wind farm. This is done through an additional user interface. It is presented after the user selects whether he/she wishes to define the farm layout by grid rows and columns. If yes, the resulting user interface contains fields for the following inputs: the number of rows to be included in the wind farm; the number of columns to be included in the wind farm; the spacing between rows; and the spacing between columns.

StrathFarm is defined such that a column is parallel to the x-axis and a row parallel to the y-axis. If no, the user has to specify vectors containing the coordinates of the turbines.

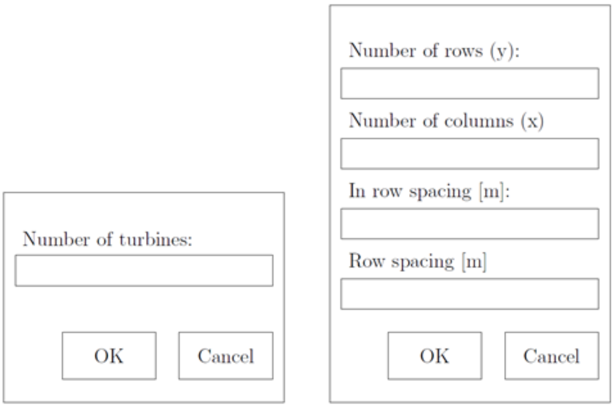

Figure 14: The user interface with which the user defines the basic layout of the wind farm

When using StrathFarm, the wind field is defined using the definition of the wind farm and additional inputs from a separate user interface, Figure 14. The requested inputs for the third user interface are as follows: mean wind speed, expressed in m/s; wind direction, expressed in degrees; turbulence intensity, expressed as a fraction i.e. 0.1=10% turbulence intensity; wind field length, expressed in metres; wind field width, expressed in metres; surface roughness length, expressed in metres; sample time, expressed in seconds; and simulation time, expressed in seconds.

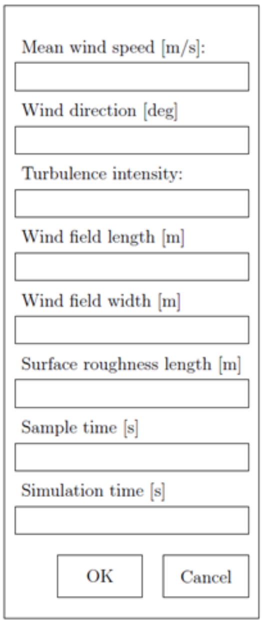

Figure 15: The user interface with which the user defines the basic properties of the wind field

4.2 WIND TURBINE AND CONTROLLER

4.2.1 Wind Turbine Model

A model, illustrated in Figure 16, which captures the structural dynamics and aerodynamics of a wind turbine is included in StrathFarm. The bulk of the model can be split into two high level components: one which represents the rotor, and one which represents the drivetrain.

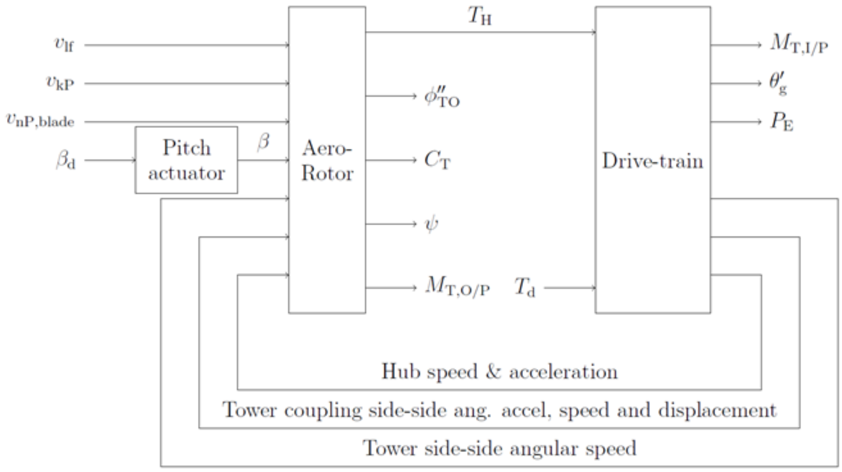

Figure 16: Overview of the wind turbine model used in StrathFarm

The rotor block receives as inputs the various components of the wind field model previously described. In addition, the pitch angle, hub speed & acceleration, tower side-side angular acceleration, speed & displacement and the tower side-side angular speed are also inputs. The outputs of the rotor block are the hub torque, the tower fore-aft acceleration (ϕ''_{TO}), the thrust coefficient (C_T), the azimuthal angle (ψ), and the tower fore-aft root-bending moment ($M_{T,O/P}$).

The rotor block itself, illustrated in Figure 17, may be split into three components: an aerodynamics block, which uses an aerodynamic model which includes dynamic inflow effects; a rotor dynamics block in which the rotor dynamics derived using Lagrangian methods [53], embedded in which is a representation of the tower fore-and-aft dynamics; and a lumped-mass model of the blade, through which edge and flap motions/forces may be calculated.

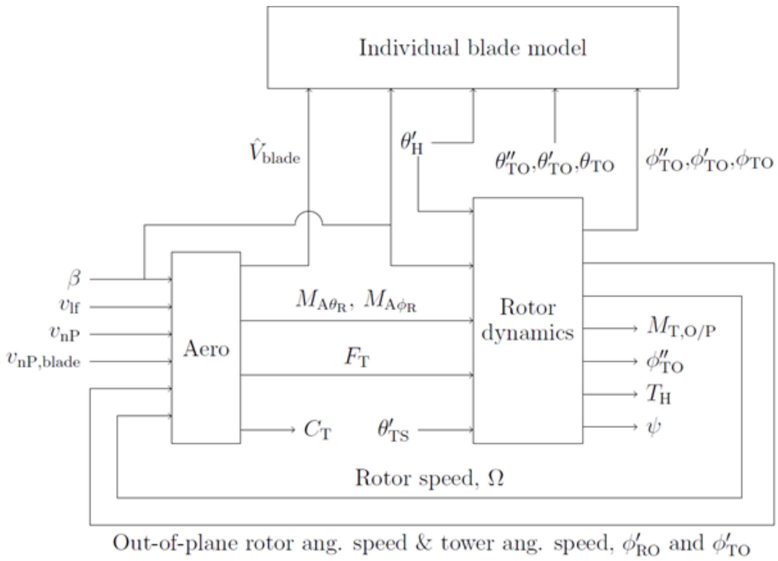

Figure 17: Overview of the wind turbine rotor model used in StrathFarm

The drive-train block accepts as input the hub torque and the torque demanded set by the controller. Tower side-to-side response is also calculated in the drive-train block. Specifically, the following variables are calculated, tower side-to-side angular speed, θ'_{TS}, tower coupling side-side angular acceleration, speed & displacement, θ''_{TO}, θ'_{TO} and θ_{TO} respectively, hub speed and acceleration, θ'_H and θ''_H respectively, tower side-side root bending moment, $M_{T,I/P}$, generator speed, θ'_g and electrical power, P_E. Low-order models representing all essential aspects of the drive-train dynamics are employed.

4.2.2 Comparison of wind turbine models to Bladed.

Simulation runs for similar wind conditions were performed for both the wind turbine model incorporated into StrathFarm and a corresponding Bladed model. The spectra for wind turbine loads are compared in Figure 18. Because of the difference in representation of the wind-field models, the speeds for each model are inevitably different. Nevertheless, the agreement is sufficiently good to determine whether one wind farm controller is better than another.

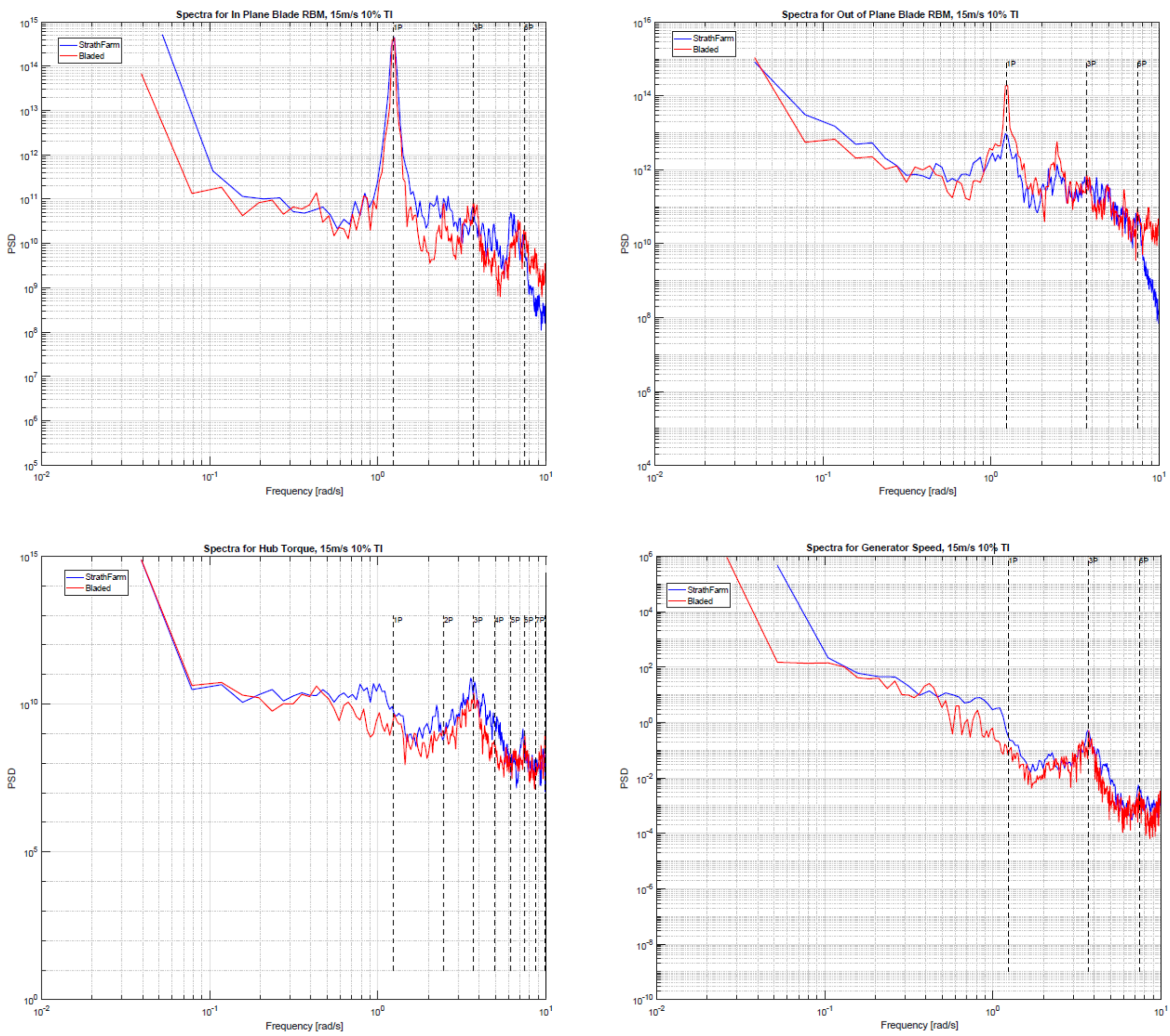

Figure 18: Clockwise from top left: in-plane root bending moment, out-of-plane root bending moment, hub torque and generator speed. All simulations were conducted using a mean wind speed of 15m/s with turbulence intensity set to 10%

4.2.3 Full Envelope Wind Turbine Controller

At the lowest control level is the full envelope controller, which causes the wind turbine to follow some choice of operating strategy, e.g. that shown in Figure 19. This strategy, broadly speaking, can be split into two parts: a below-rated part and an above-rated part.

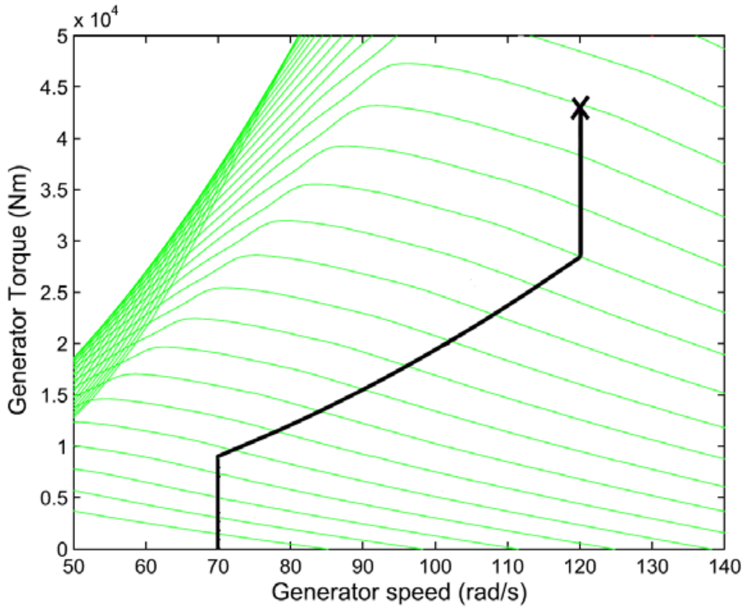

Figure 19: Control strategy for a Supergen wind turbine. The pitch controller is introduced at the cross

The basic objectives of the above-rated controller are to maintain the rotor torque and speed at their rated values. Assuming the wind turbine has a fully-rated converter, the first objective may be achieved by having the power converter set a fixed generator reaction torque. Power electronics are very fast acting devices. Thus, the first objective can be achieved through open loop control alone [49]. To achieve constant rotor speed, the pitch angles of the wind turbine blades are adjusted in unison in response to a measurement of rotor/generator speed. That is, with the basic controller, all blades have the same pitch angle. Accordingly, the basic wind turbine control structure is as shown in Figure 20:

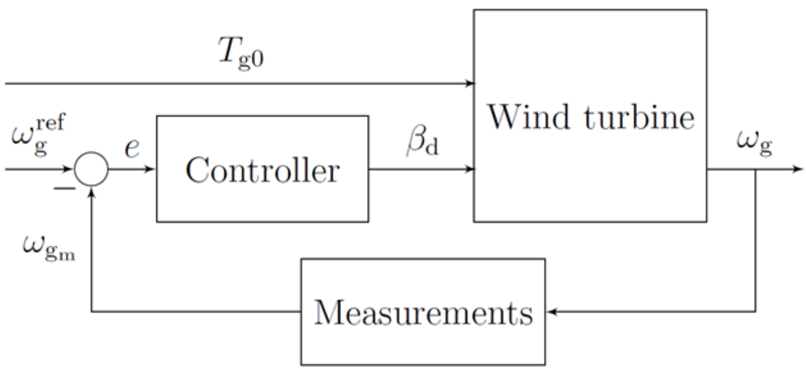

Figure 20: Basic structure of a wind turbine full envelope controller

The below-rated controller may itself be split into three components: two constant-speed modes separated by a variable speed mode, during which the controller attempts to hold the wind turbine at optimal aerodynamic efficiency over a range of wind speeds. To regulate the rotor speed in this region, torque control is applied.

Additional to the above strategy, a drive-train filter can be included so as to dampen the first drivetrain mode.

A fully functional industry standard controller is incorporated into each turbine model.

4.2.4 Choosing wind turbines in farm layout.

While declaring the wind farm layout, a GUI is provided, see Figure 21, whereby the user chooses from a library the model for each turbine. In addition, whether to log the outputs from each turbine or not, can be chosen.

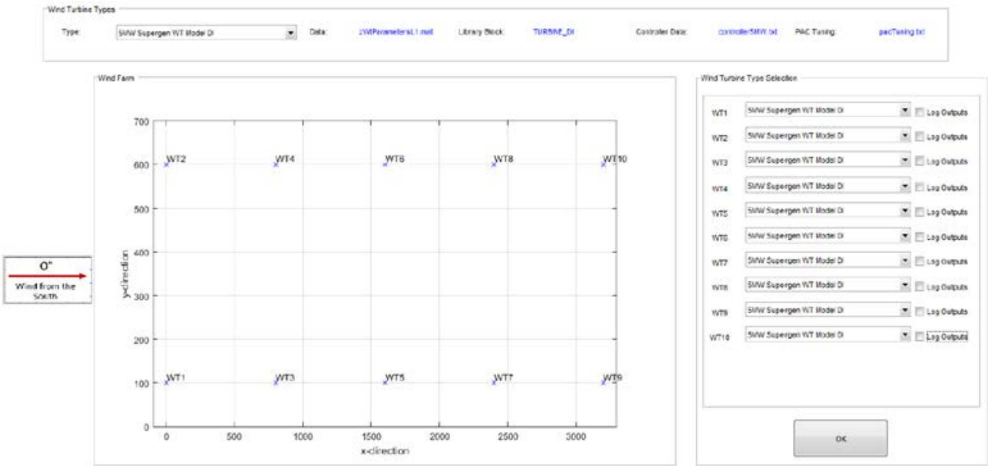

Figure 21: Choosing StrathFarm wind turbine models

Note that StrathFarm permits easy integration of an extensive range of turbine-level controllers, such as those found in [51]; these would simply need to be coupled to a turbine model, which then forms an integrated model which gets embedded into the farm model (see figure 21).

5 PROVISION OF GRID SUPPORT FROM WIND FARMS

5.1 CURTAILMENT

A wind farm comprising 10 Supergen 5MW wind turbines is used to demonstrate the ability of a wind farm to curtail its power output when appropriate control algorithms are employed.

Figure 22 shows the correlated spatially filtered wind speeds to which the turbines are subjected:

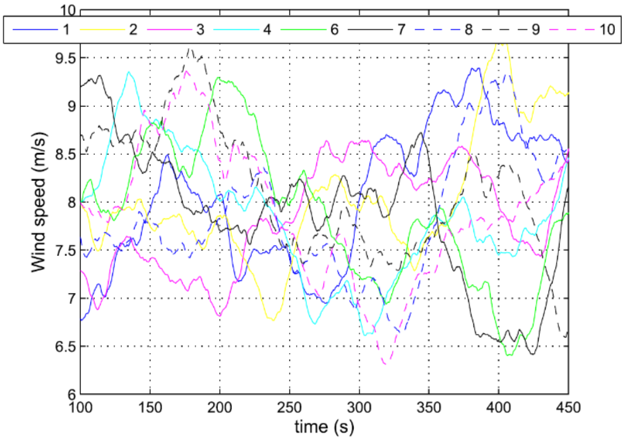

Figure 22: Wind speeds that each rotor experiences

In the first simulation, the wind farm controller is given a signal to curtail the power output of the wind farm to 12MW. The mean wind speed across the wind farm is set to 8m/s. Had no such signal been sent, the combined power output of the ten turbines when confronted by the winds shown in would be that given by the red line in. When the wind farm controller is applied, the PAC is applied. Figure 24 shows the power output of each turbine throughout the simulation when wind farm control is applied.

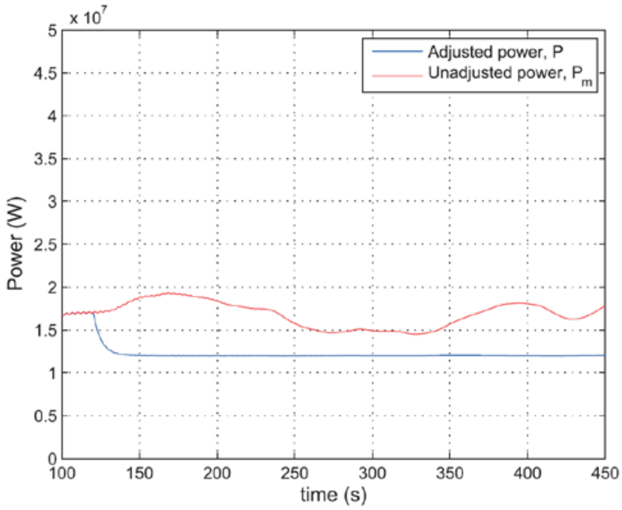

Figure 23: Curtailment of a wind farm's power output (blue) compared with the wind farm's power output had no curtailment been applied (red).

The curtailed power output may be illustrated in terms of the power outputs of the individual wind turbines. Note how the power output of each turbine is not equal to the demanded wind farm power output divided by the number of turbines. Since each turbine sees a unique wind speed time series, it is logical that the wind farm controller should adjust the power outputs of the individual turbines in a non-uniform manner; this is particularly true since some of the turbines cannot produce 1.2MW of power without eventually moving towards stall. That is, the use of shared information/instrumentation can be exploited to achieve tighter control.

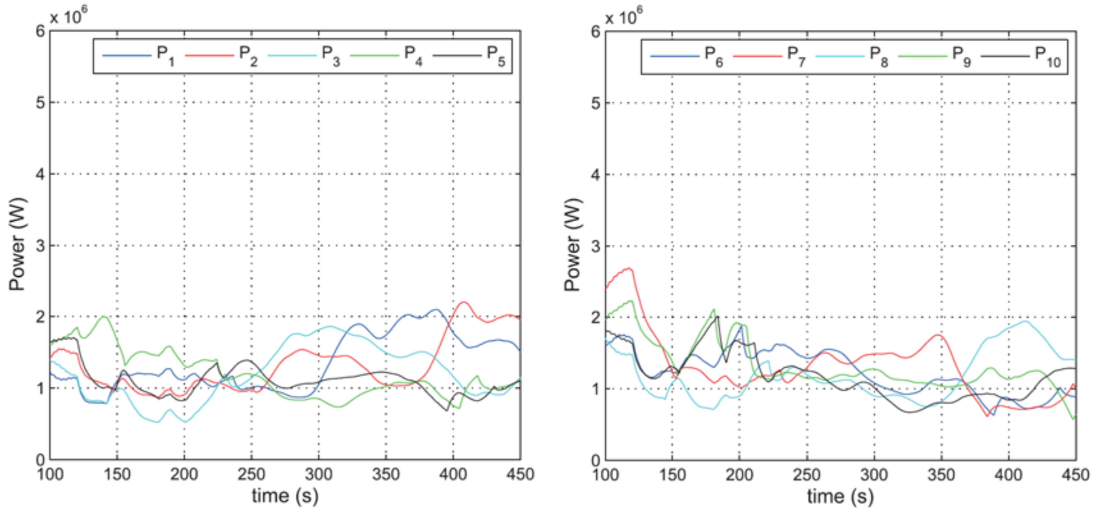

Figure 24: Power outputs of the individual turbines when curtailment is applied using a farm level controller

Indeed, if all turbines were asked to produce 1.2MW of power, some of the turbines would be incapable of delivering it at certain times, at which point the PAC rules would prohibit continued power extraction of the aforementioned level. After such a condition has been met, the turbines in consideration would enter recovery modes, which can be seen in Figure 25. The net wind farm power output when each turbine is asked to produce 1.2MW of power is shown in Figure 26. The advantage of windfarm control in enabling cross-compensation between turbines is clear

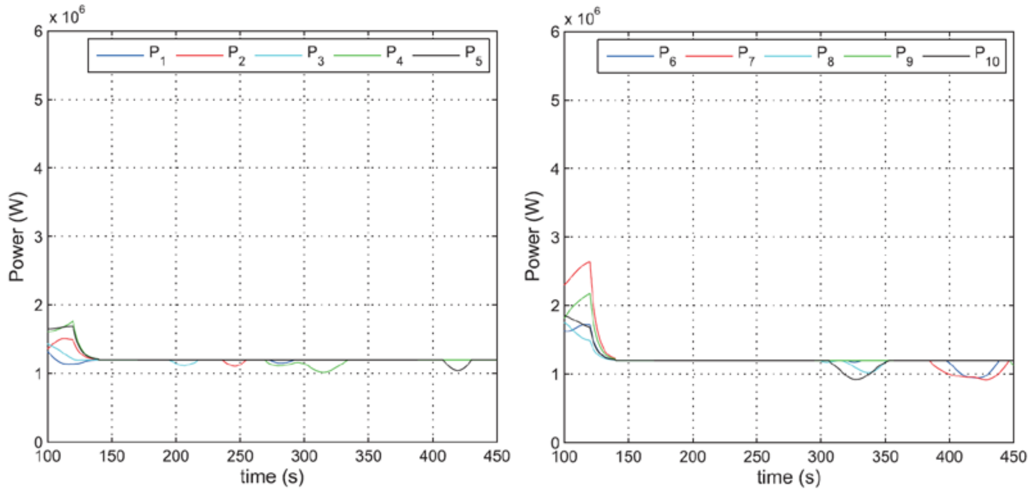

Figure 25: Power outputs of the wind turbines when each turbine is given a command to produce 1.2MW of power, giving a combined target power output of 12MW

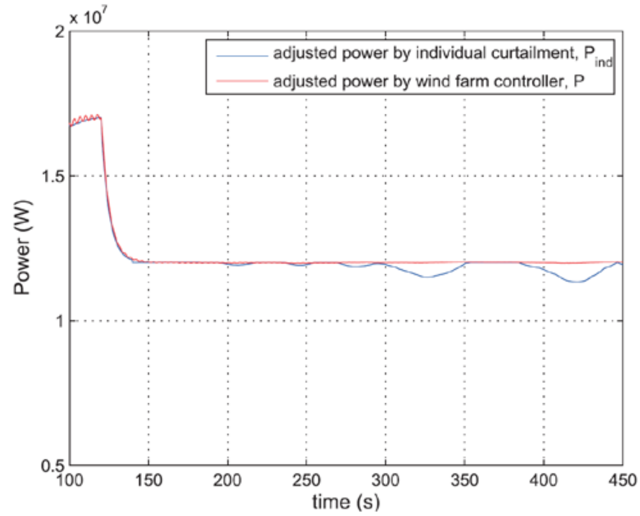

Figure 26: Combined power output of the wind farm when curtailment is applied only at the turbine level

Figure 28 illustrates the operating conditions of each turbine on torque/speed planes without wind farm control. The left hand diagram is when wind farm control is applied; the right hand diagram is when wind farm control is not applied. It can be observed that the turbines do not experience significant excursions out of the green zone. When a turbine does move from the green zone to the amber zone, that turbine is allocated a smaller power output change, allowing the turbine to return to the green zone. The change in power output that results from this action is then redistributed among the remaining turbines.

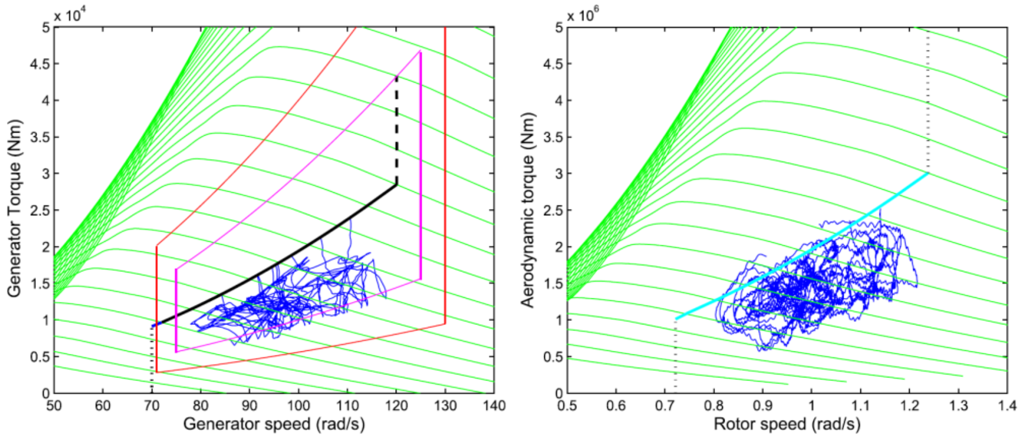

Figure 27: Behaviour of each turbine on the torque/speed plane.

5.1.1 Producing more power than is available from the wind alone

In the next simulation, the target power output of the wind farm was set to 17MW; the same wind speeds were used as in the curtailment simulation. In other words, the power target exceeds that which could be obtained from the wind alone. Naturally, this will result in energy being taken out of the rotors, causing them to slow down.

In a (comparatively) simple controller, once one of the wind turbines reaches a hard boundary, the number of wind farms available to provide additional power is reduced. As a result, the remaining available wind turbines have to produce even more power than they were before; this pushes turbines to the hard boundary at an increasing rate (as more wind turbines enter the recovery mode). That is, a cascading effect is observed, which leads to a sharp drop in the wind farm power output as can be seen in Figure 28. The rapid movement of each turbine towards the hard boundary can be visualised through the torque/speed diagram in Figure 29.

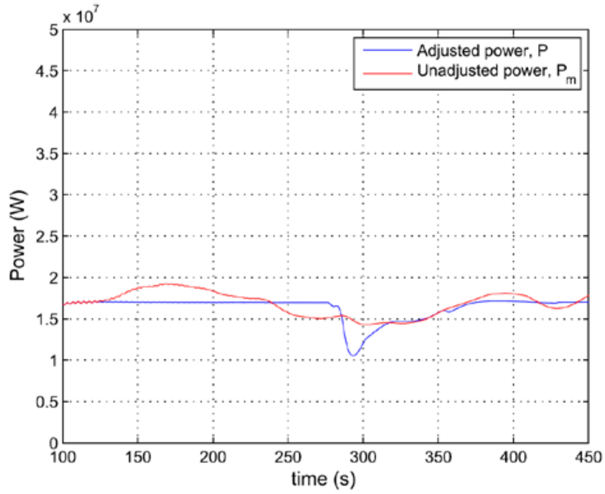

Figure 28: Power output of the wind farm when a wind farm controller is applied and the desired power output is 17MW (blue line) and the power output when no wind farm control is applied (blue line)

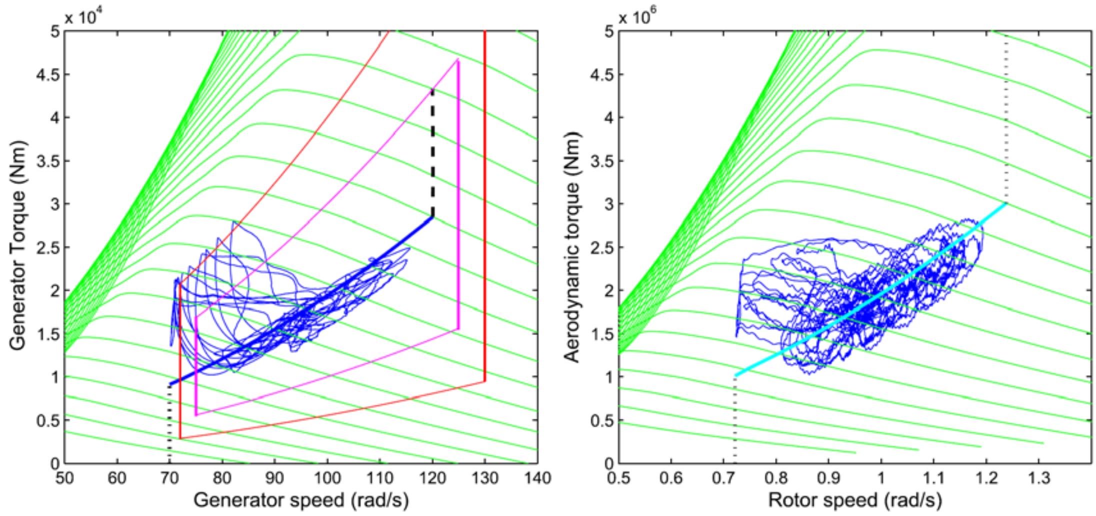

Figure 29: Behaviour of each turbine on the torque/speed plane

An alternative approach would be for the wind farm controller to adjust the wind farm power target in response to the flags being received; that is, as a turbine ceases to be available for providing additional power, the net wind farm power target is scaled down. This results in a slower fall in power, with the minimum output also being less severe than in Figure 28.

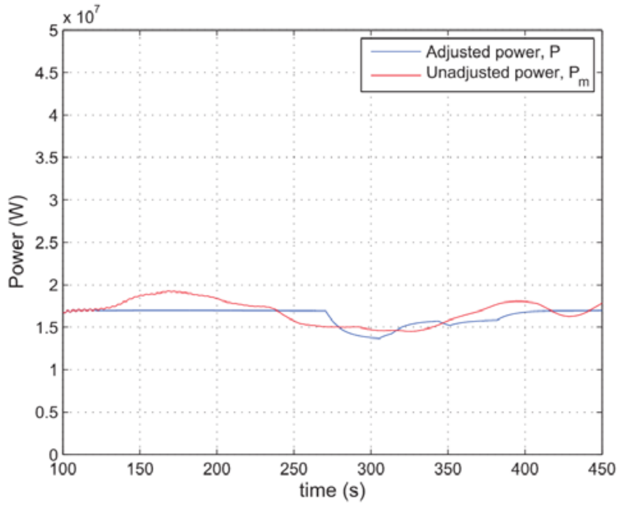

Figure 30: Wind farm power output using the alternative strategy

5.1.2 Decoupling of the wind farm controller and the wind turbines

Figure 31 demonstrates the degree to which the wind farm controller is coupled to a wind turbine. As can be seen, the spectra of tower and blade bending moments are unaffected by the presence of the wind farm controller; that is, the coupling between the wind farm controller and the full envelope controller is relatively weak as desired. This is an advantage since it means that the wind farm controller can be applied to a farm without any need to redesign the turbine controllers.

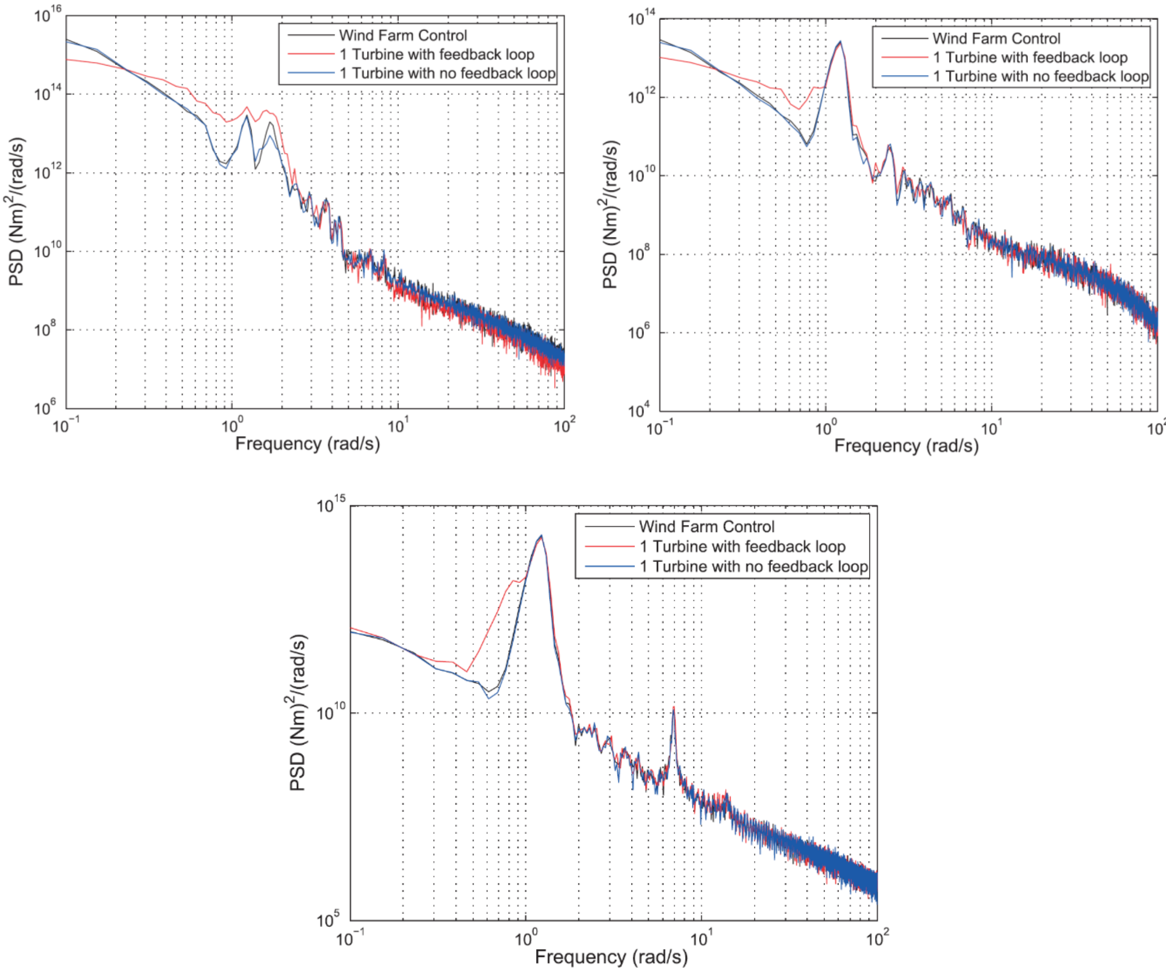

Figure 31: Clockwise from top left: tower fore-aft bending moment, out-of-plane bending moment and in-plane bending moment

5.1.3 Assessing the impact of delays:

In practice, there may be delays between the wind farm controller and the wind farm, both in terms of the controller dispatching commands, and in terms of the farm power output changes being detected by the wind farm controller. The most extreme delay considered in this work is a 12 second delay (6 seconds for each way). Even in the most extreme case, the power output is still within 10% of the target power output; this can be observed in Figure 32. The performance of the individual wind turbines for each delay considered is presented in Figure 33.

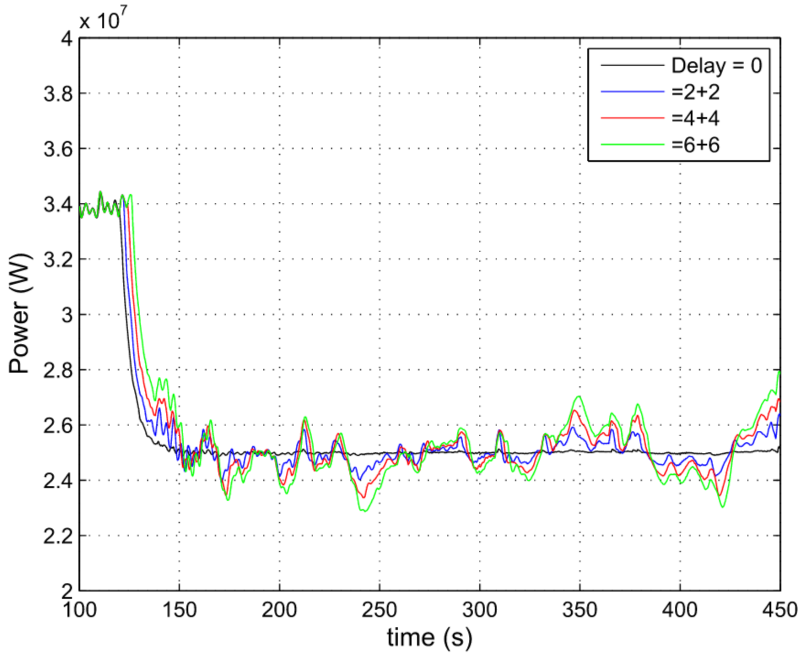

Figure 32: Adjusted power for different communication delays

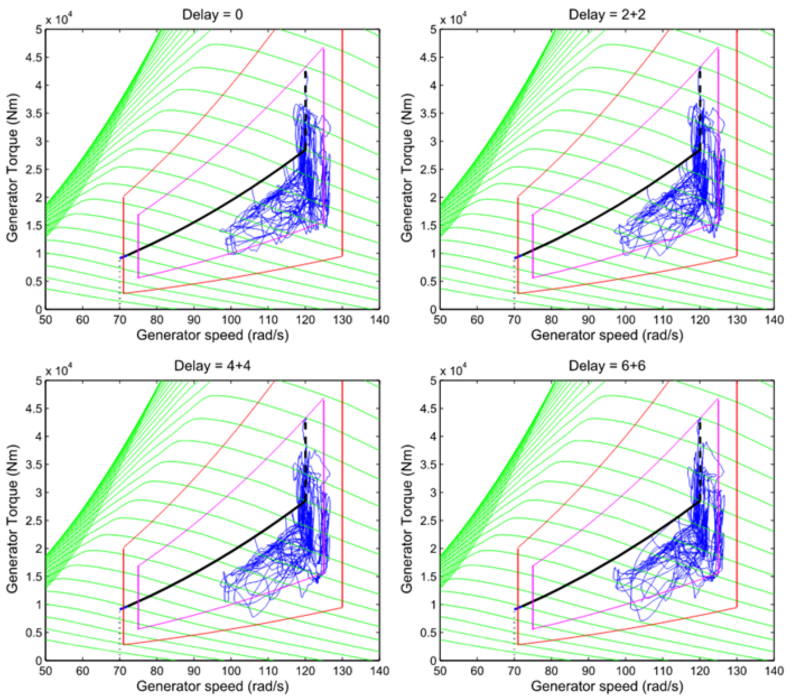

Figure 33: Behaviour of the turbines for different communication delays

5.2 SYNTHETIC INERTIA

To demonstrate the effectiveness of the wind farm controller, the turbines are subjected to wind speeds shown in Figure 34.

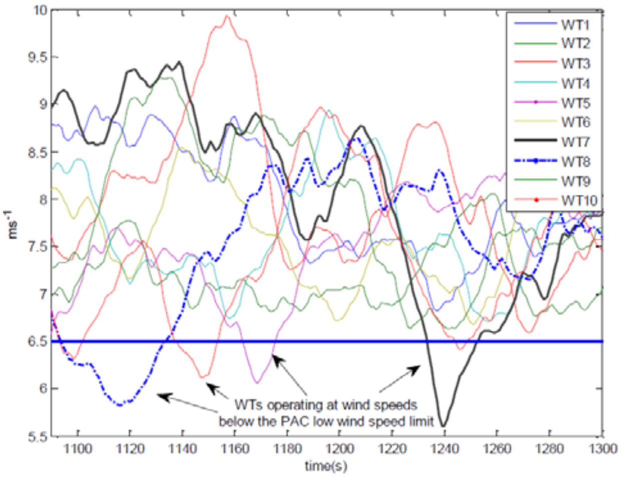

Figure 34: Wind speeds that each turbine experiences during the synthetic inertia and droop control experiments

An event is illustrated in Figure 35, coupled to which is a close up of the wind speeds during the time of the event.

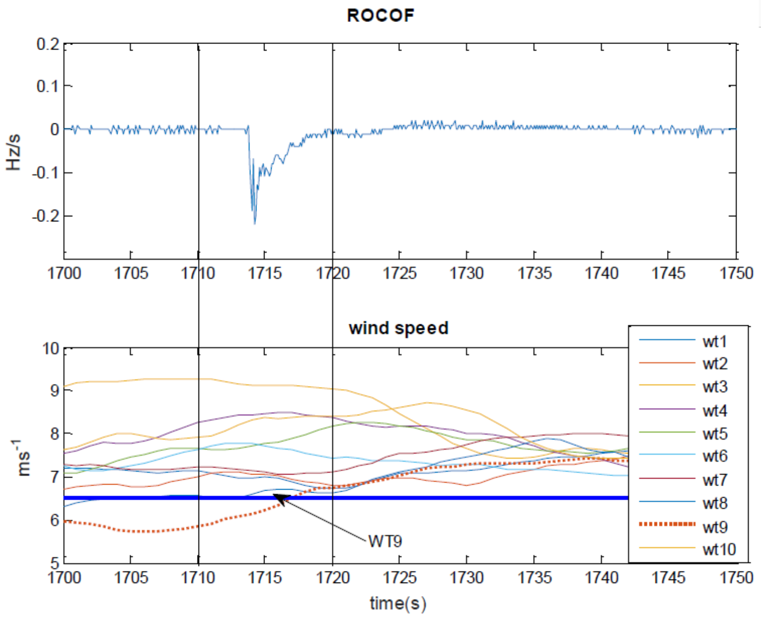

Figure 35: Frequency history during a significant event (top) and the wind speeds that each turbine experiences during that same period of time

Following the event, the wind farm controller is sent a signal to provide a rapid change in power output, which is then dispatched to the wind turbines. Figure 36 shows the response of the wind farm to this event:

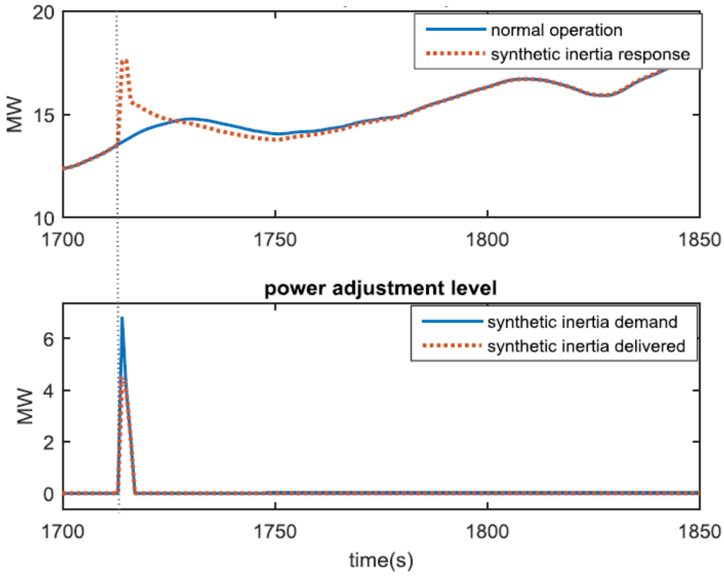

Figure 36: Wind farm response to the major event shown in Figure 35

The behaviour of the turbines can be expressed using torque/speed planes. It can be seen that the turbines are allowed to approach the black zone. This is because of the fact that the event is a rapid change in power system frequency, for which synthetic inertia is required.

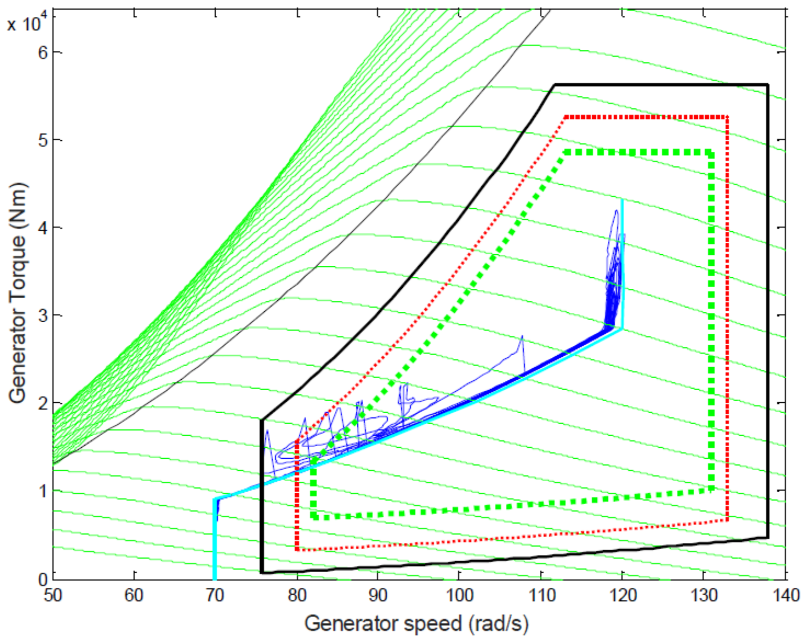

Figure 37: Wind farm response to the major event as illustrated through a torque/speed plane diagram

5.3 Droop Control

Synthetic inertia is the provision of additional power in the immediate aftermath of an event. This manages the rate of change of frequency. In the longer term, droop control is required to manage frequency itself. Accordingly, the power output of a wind farm may need to be altered for a prolonged period of time. However, the power change required for droop control is significantly less than that required for synthetic inertia. This can be seen in Figure 38.

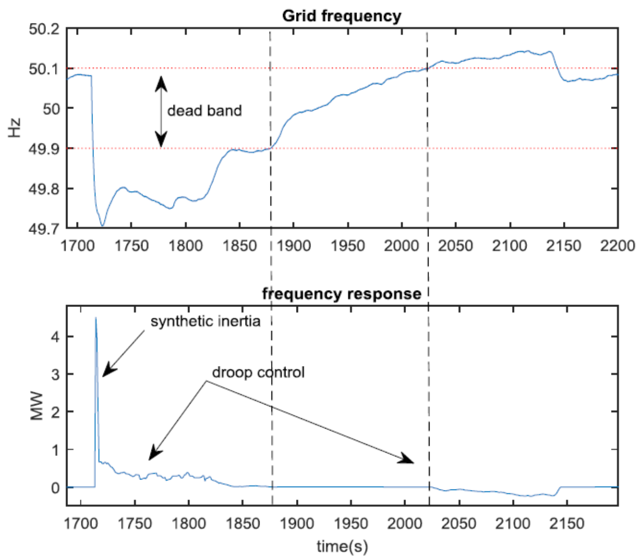

Figure 38: Illustration of a grid event and the accompanying power output that provides frequency stability

If the wind farm were to operate optimally from an energy capture perspective for all times excluding those when grid events occur, it is possible that the provision of droop control could only be sustained for a short period of time for reasons previously discussed.

One alternative solution would be to operate the wind turbines in a curtailed mode, thereby providing a reserve for prolonged events such as droop control. Of course, in so doing there will be a loss of energy capture. Thus, the wind farm operator would need to evaluate the costs and benefits associated with losing energy capture but being able to provide important ancillary services to a power system.

As such, two sets of simulations were carried out. In the first, the wind turbines were not curtailed in any way. At approximately 1720s, an event occurs. Initially, synthetic inertia is provided, which can be identified by the sharp feature in Figure 39; afterwards, the power output of the wind farm is held above what would otherwise have been achieved during normal operation. Referring to, it can be seen that each turbines contributes a different amount of power, with each individual turbine's output being fundamentally constrained by the PAC rules.

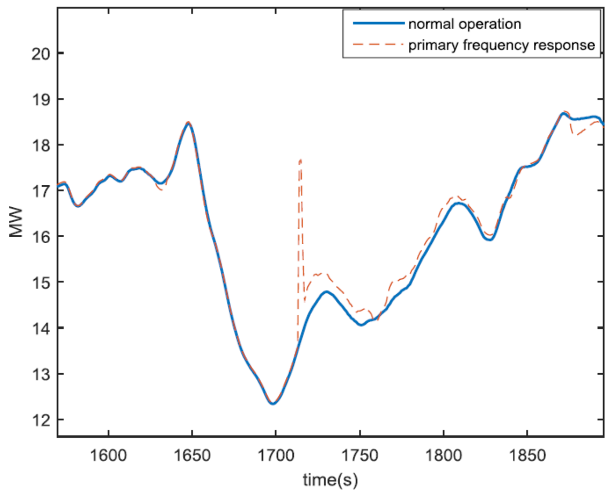

Figure 39: Comparison of the power output of the wind farm with and without the grid event. No grid curtailment has been applied in this simulation

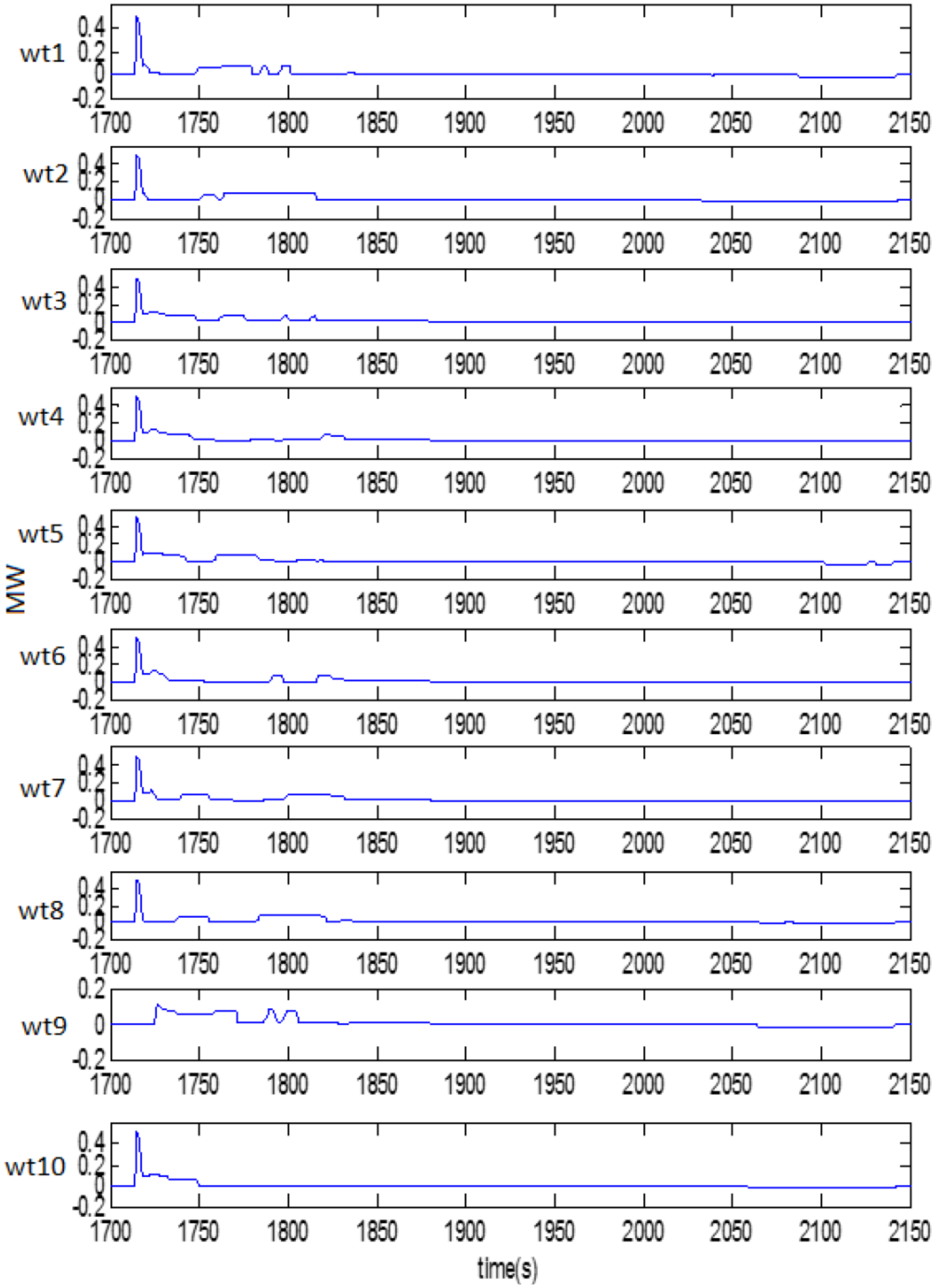

Figure 40: Power outputs from the individual turbines in the wind farm following the event in Figure 35

Figure 41 shows such constraints being imposed. It can be seen that wind turbine nine experiences level three, at which point output from that wind turbine is curtailed.

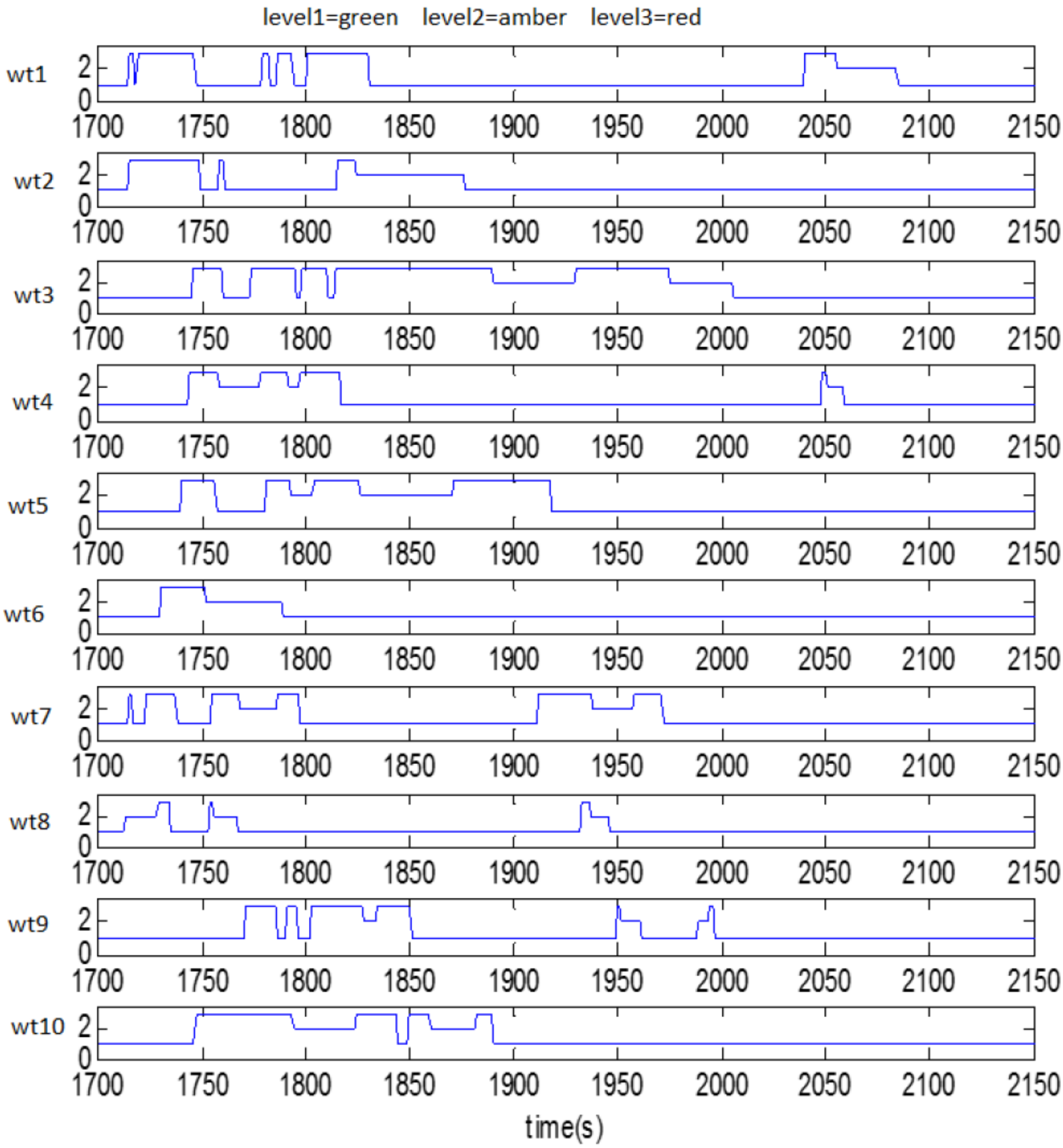

Figure 41: Illustration of the states of the wind turbines as defined by the PAC

Alternatively, Figure 41 may be visualised through the torque-speed plane. It can be seen that the PAC flags relay information to the wind farm controller preventing any of the turbines from operating outside an acceptable range of conditions.

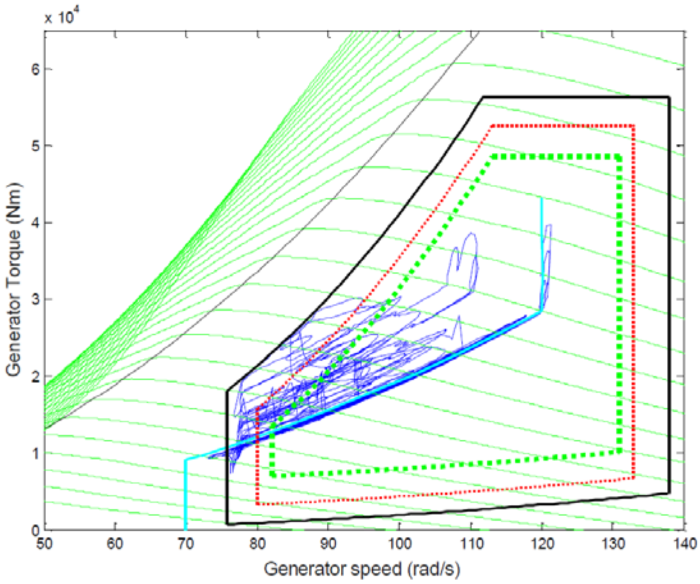

Figure 42: Illustration of the behaviour of the wind turbines in the torque/speed plane

By comparison, if the power is curtailed, the wind farm has additional power that it can take from the wind. As a result, droop control is superior at around 1760s when compared to the first approach (no curtailment).

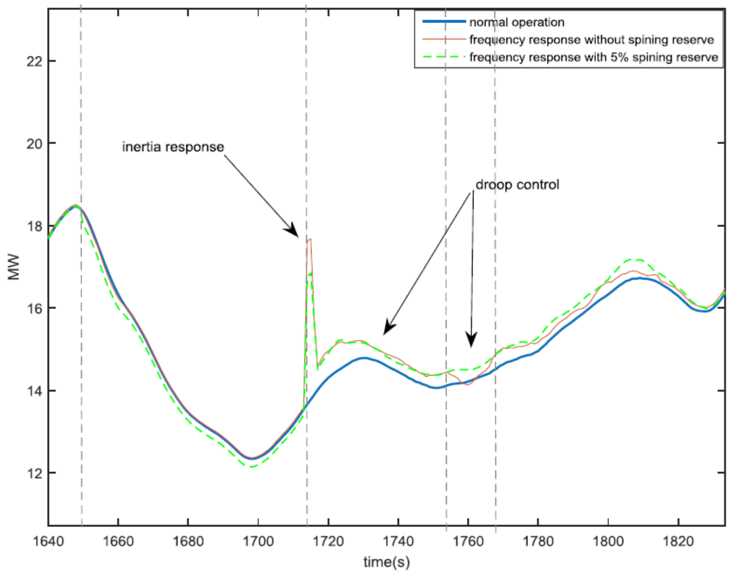

Figure 43: Comparison of the two control strategies: curtailment, giving spinning reserve; and no curtailmnet, atempting to maximimse energy capture outside of grid events.

Figure 44 illustrates the how the turbines cross-compensate for one another. The envelope over all the plots is the overall response scaled down to the turbine. The changing status of each turbine's flags switching in and out is indicated by the vertical lines switching between the horizontal axes and the envelope. Clearly, there is cross-compensation between turbines, an advantage of wind farm control over individual turbine delivery of frequency support. The PAC flags prevent all wind turbines from changing their power outputs at the same time when creating the spinning reserve. Once the event occurs, each turbine is constrained by the PAC flags; hence, once a given wind turbine reaches a hard limit, the power output of the wind turbine is reduced. This can be seen to be occurring for all turbines, though at different times during the droop control.

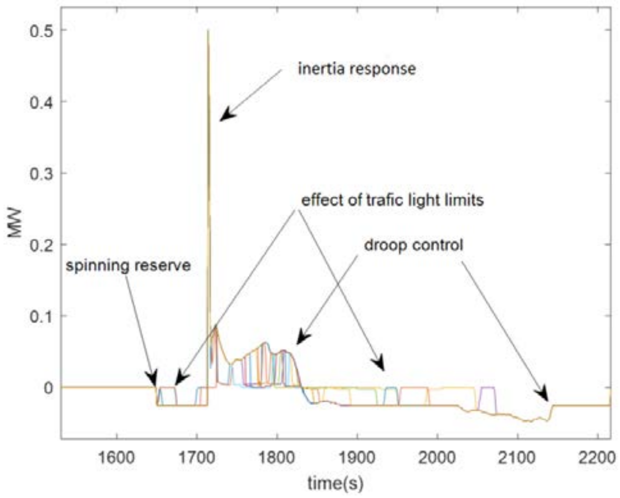

Figure 44: Change of power outputs of individual turbines when curtailment is applied

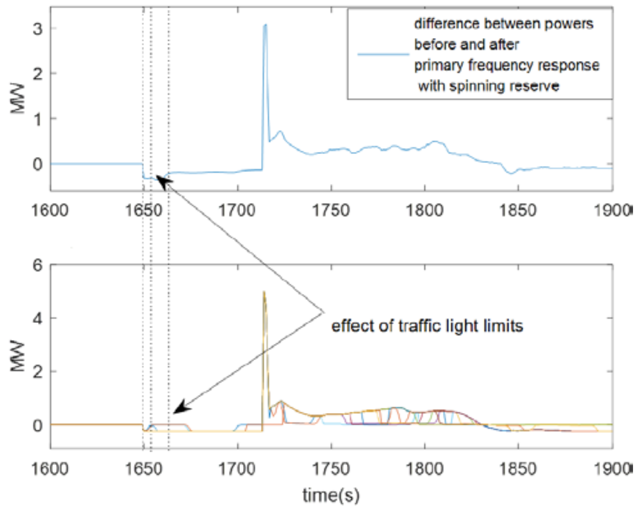

Figure 45: Droop control

As can be seen from Figure 45, by curtailing the power output, when droop control is required of the wind farm, far fewer wind turbines hit the outer limits set by the PAC.

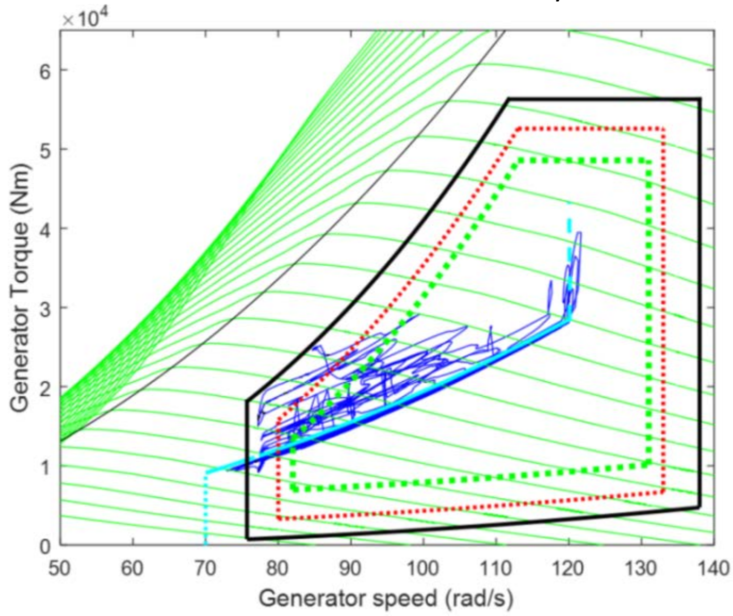

Figure 46: Torque/speed plane illustrating the behaviour of the wind turbines when the wind farm was subjected to curtailment prior to the event shown in Figure 38

5.4 Assessing the effect of the proposed wind farm controller on fatigue

While providing grid support may be beneficial, it is also important to consider the mechanical loading to which the turbines are subjected to when the aforementioned wind farm control system is implemented. In this work, results are presented for mechanical loading with and without the application of curtailment. This is, therefore, not an attempt to optimize the mechanical loading; rather, the intention is to show that providing grid support does not significantly increase mechanical loading, and with it the cost of the wind farm.

In this section, a wind farm comprising 20 Supergen 5MW wind turbines, arranged in a regular four-by-five lattice structure, is used.

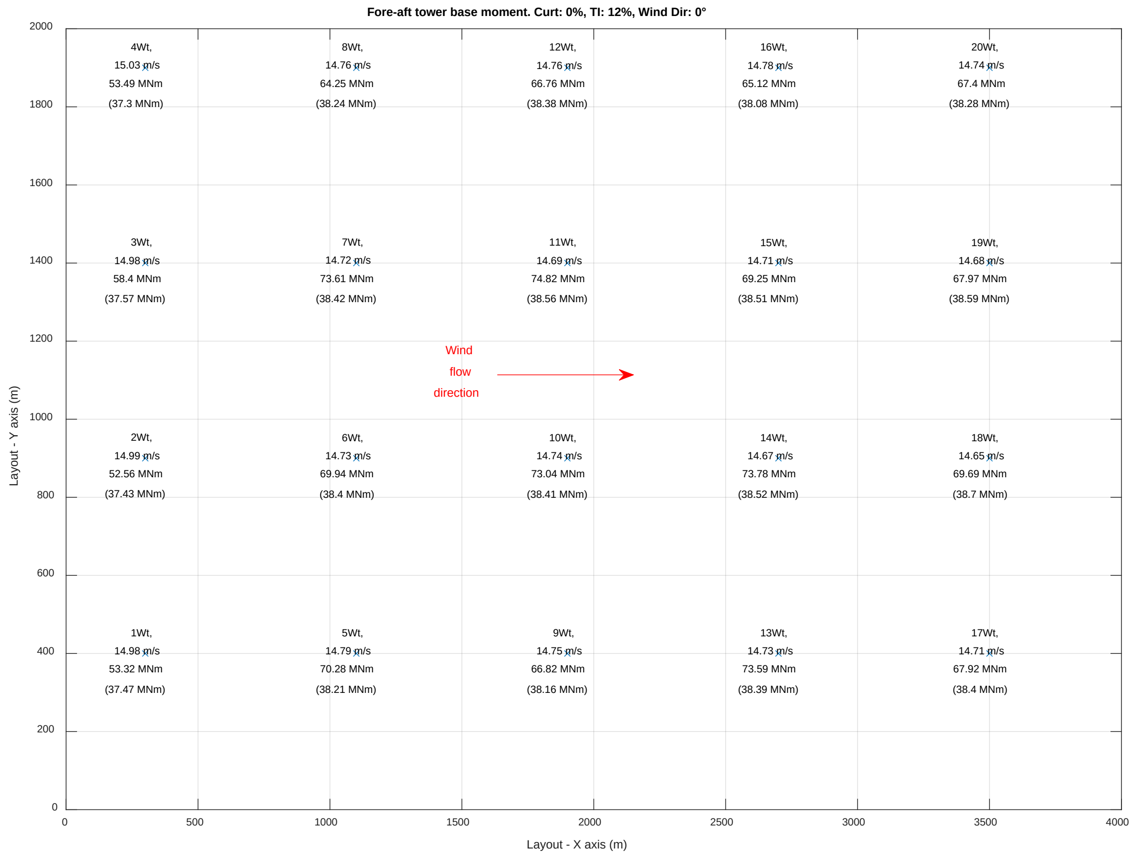

Figure 47: Fore-aft tower base moment DELs for the wind turbines when the wind is aligned with the X axis and curtailment is not applied

Figure 46 shows the fore-aft tower base moments for the wind turbines in the wind farm when no curtailment is applied and the wind direction is parallel to the X axis. The mean wind speed experienced is provided along with the DEL and mean moment over a ten-minute interval (given in brackets). As expected, the DELs for the front row of turbines in the farm are the lowest, with average DEL values being below 80MNm. The general trend is that the further downstream the turbine, the higher the DELs. The exception occurs in the middle of the farm, which is presumably due to a combination of wake mixing and random turbulence. A similar pattern can be observed with the average fore-aft moments for each turbine over a ten-minute interval (numbers in brackets).

When the wind direction is rotated by ninety degrees, such that turbines 4, 8, 12, 16 and 20 form the front row; as such, both the DELs and mean fore-aft tower base moments for the aforementioned turbines are the smallest out of the turbines in the farm. Interestingly, the DEL and mean fore-aft base moment is notably higher for wind turbine 15 than it is for turbine 19. This could be due to a random gust appearing during the ten minute simulation. It should be noted, however, that the average fore-aft tower base moment follows the pattern as seen in Figure 47; that is, the front row of turbines experience low roughly equal average fore-aft tower base moments, with successive rows exhibiting similar properties albeit with progressively higher averages.

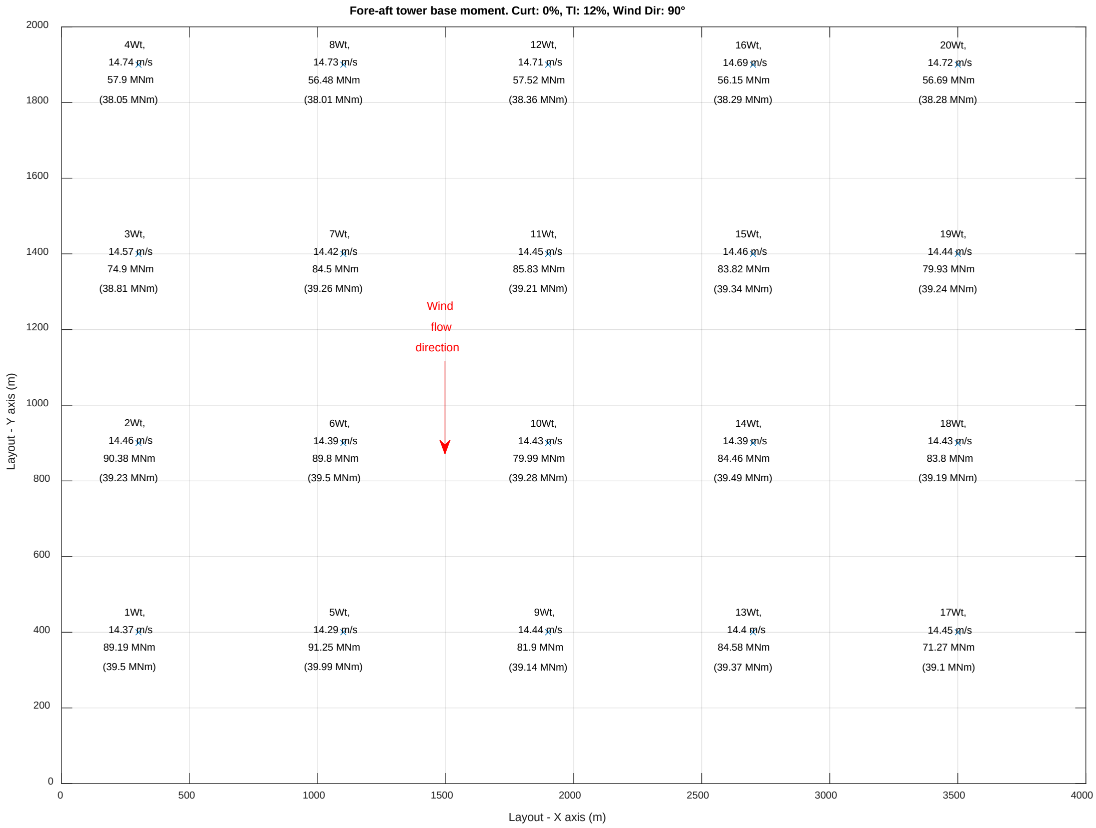

Figure 48: Fore-aft tower base moment DELs for the wind turbines when the wind is aligned with the Y axis and curtailment is not applied

Results for a selection of wind directions are also herein presented:

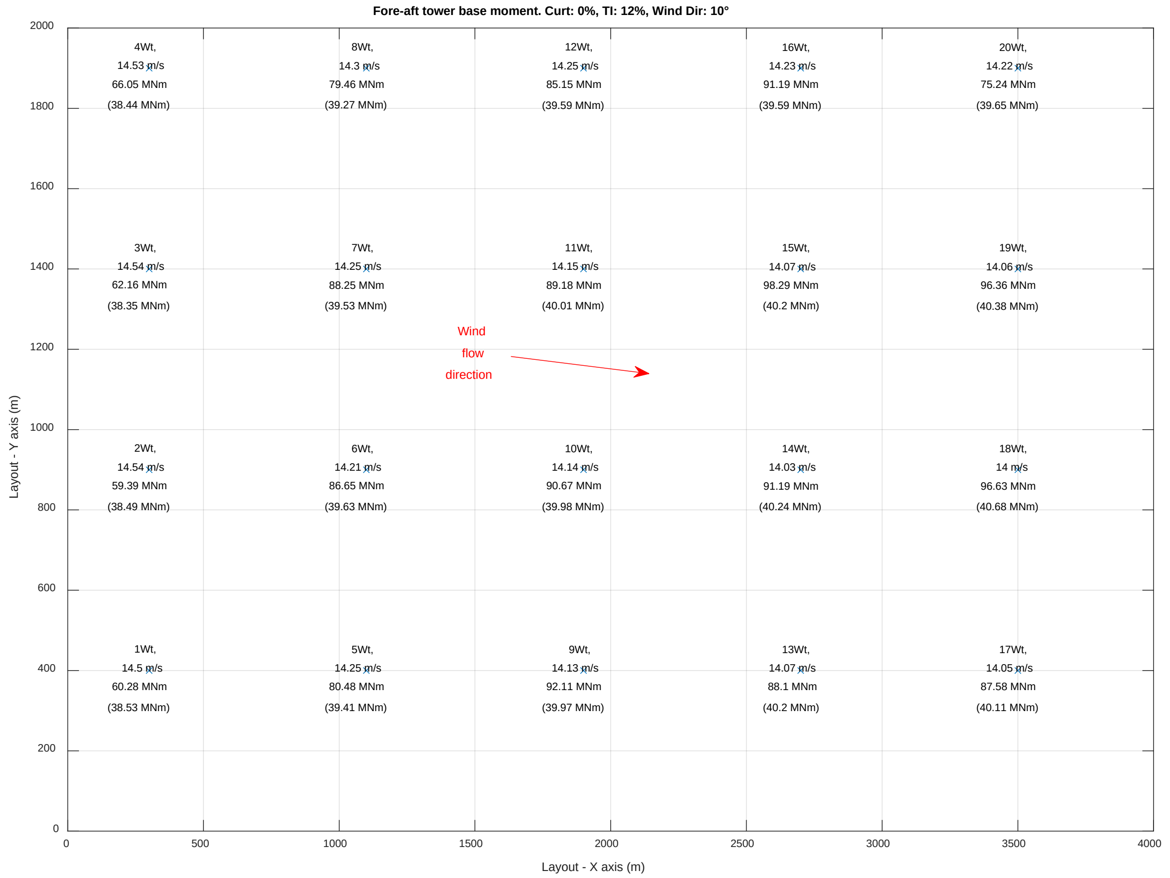

Figure 49: Fore-aft tower base moment DELs for the wind turbines when the wind is 10 degrees to the nominal

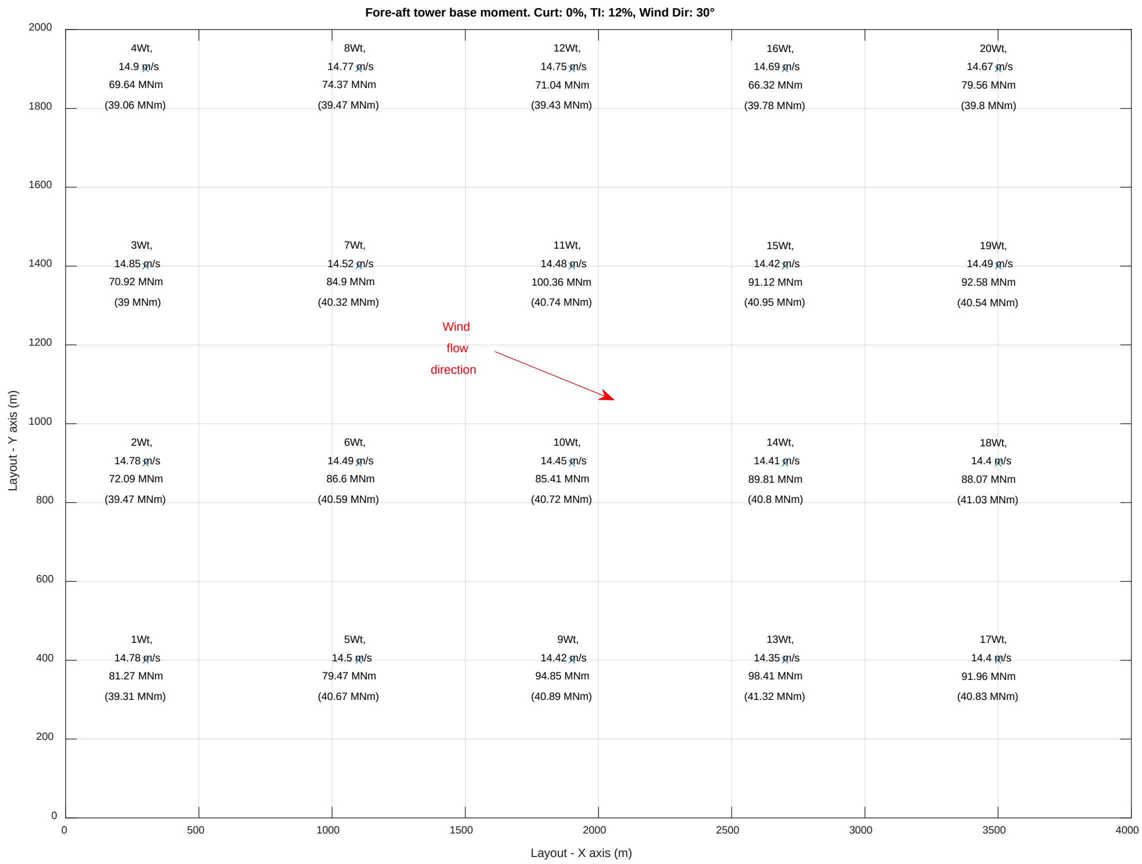

Figure 50: Fore-aft tower base moment DELs for the wind turbines when the wind is 30 degrees to the nominal

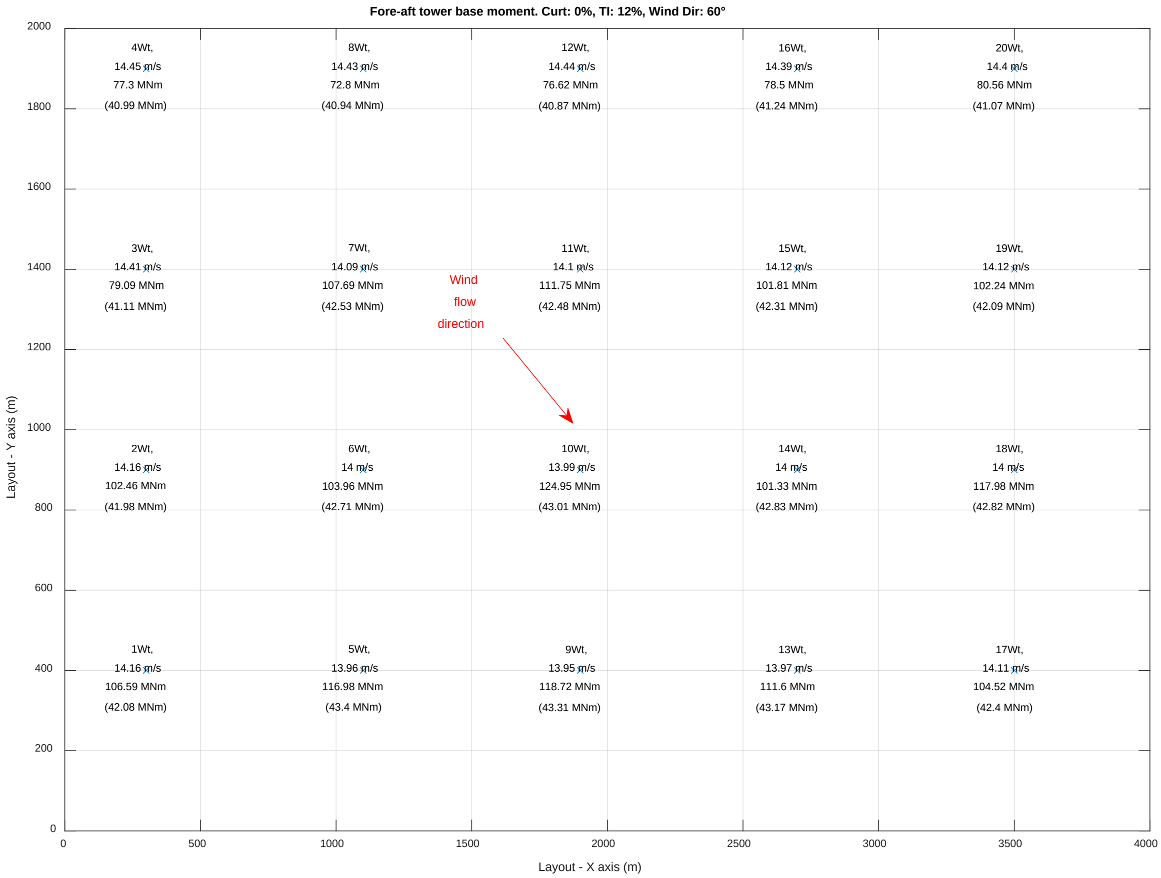

Figure 51: Fore-aft tower base moment DELs for the wind turbines when the wind is 60 degrees to the nominal

When curtailment is applied, it can be seen that the mechanical stress due to fore-aft motion in the tower is reduced for all turbines. This can be seen both when the wind direction is parallel to the X axis and when it is parallel to the Y axis.

The greatest reduction in DELs when the wind direction is zero degrees is observed in the back row of turbines; DELs have been reduced from in excess of 100MNm to values close to 50MNm. The reduction in average forces is less significant; however, DELs have a more critical role in fatigue analysis than average forces and so the reduction gains should not be understated by focusing too much attention on average forces.

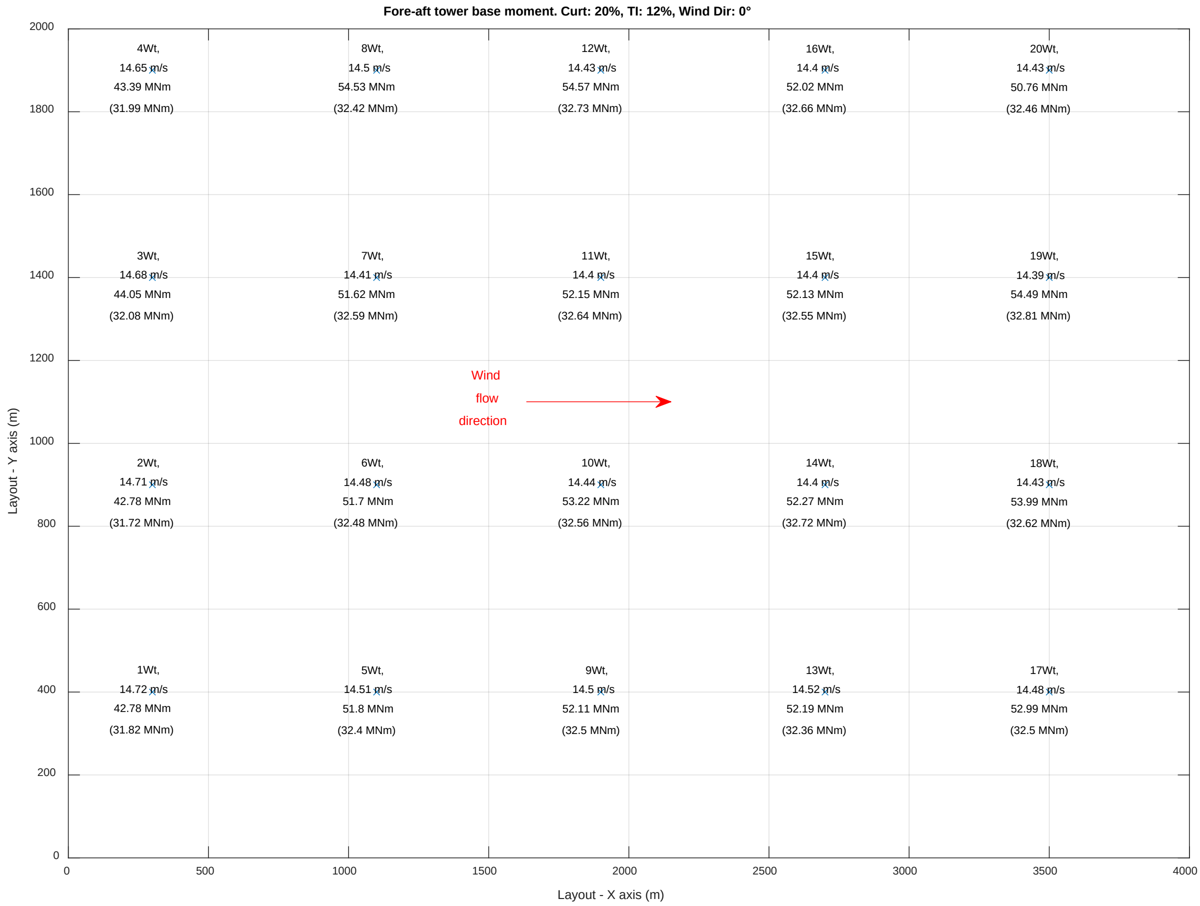

Figure 52: Fore-aft tower base moment DELs for the wind turbines when the wind is aligned with the X axis and curtailment is applied

Similar trends can be observed when the wind direction is 90 degrees, albeit with turbines 1, 5, 9, 13 and 17 forming the rear row.

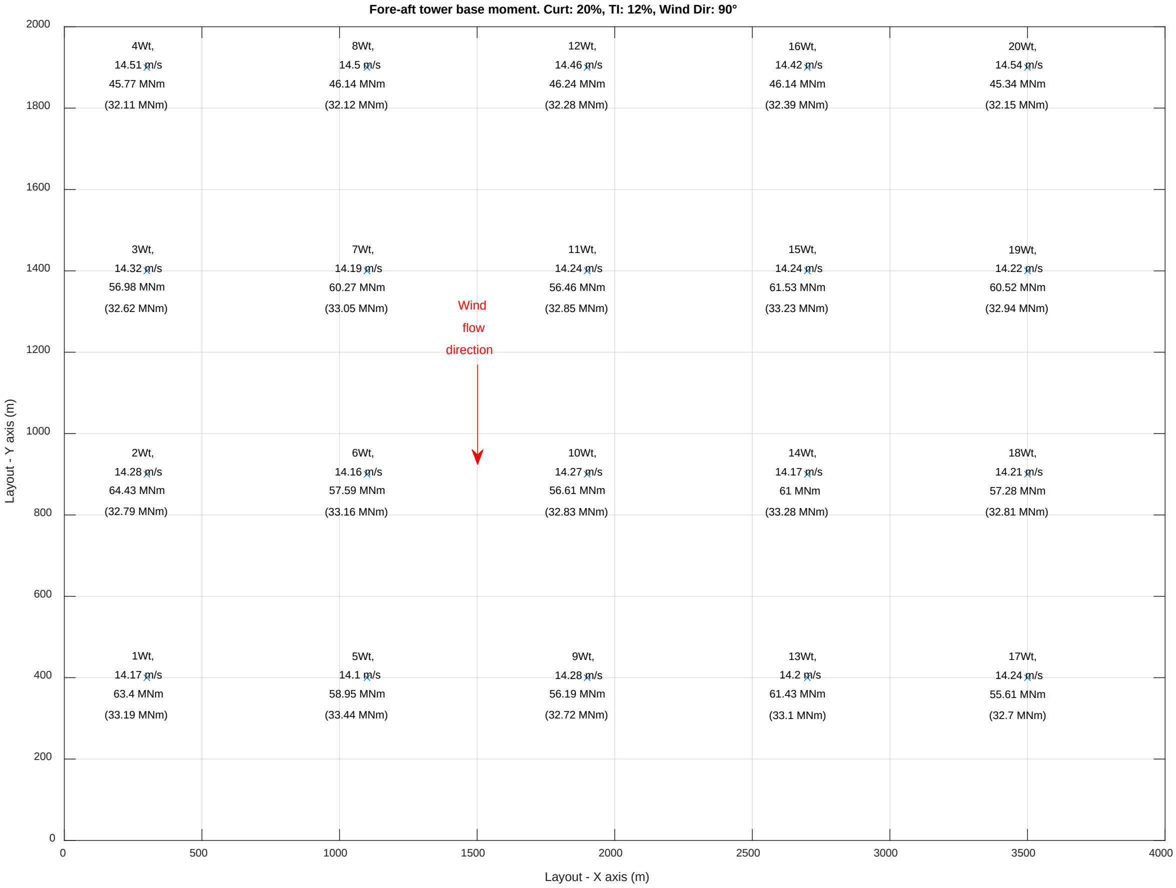

Figure 53: Fore-aft tower base moment DELs for the wind turbines when the wind is aligned with X axis and curtailment is applied

Results for a selection of wind directions are also herein presented:

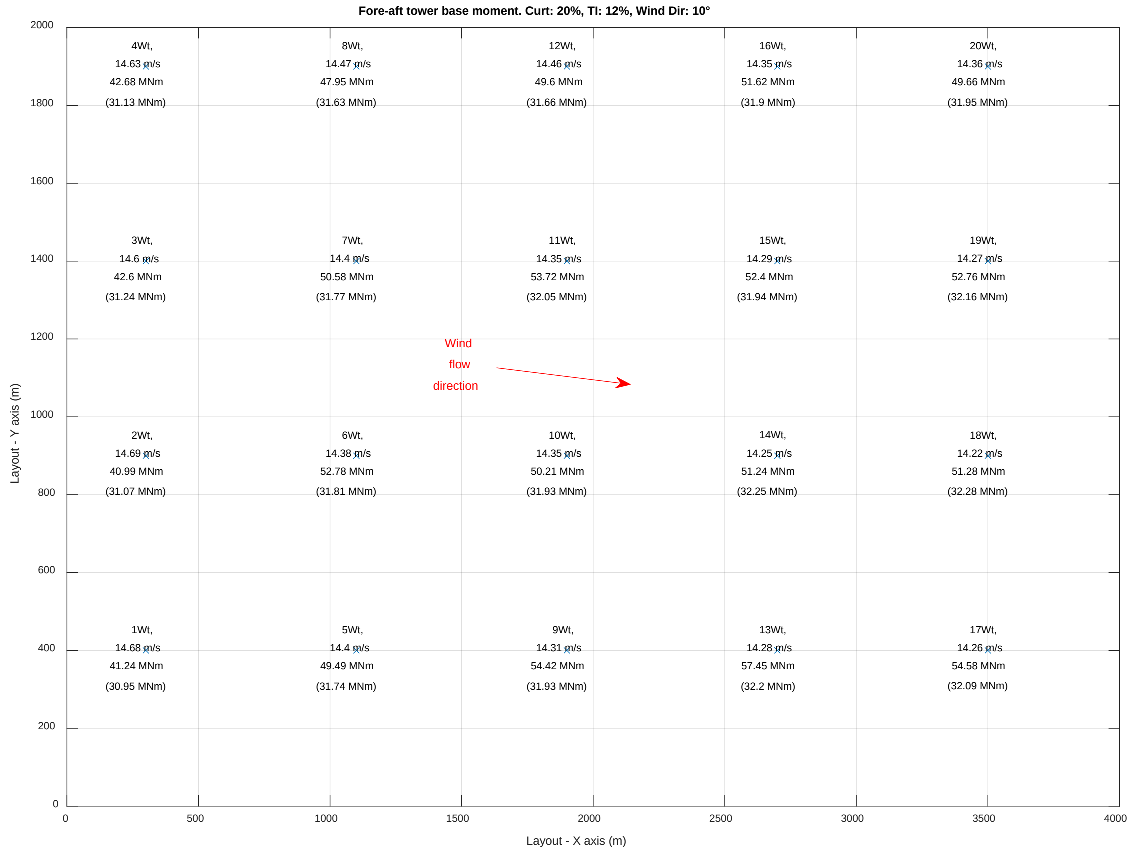

Figure 54: Fore-aft tower base moment DELs for the wind turbines when the wind is 10 degrees to the nominal and curtailment is applied

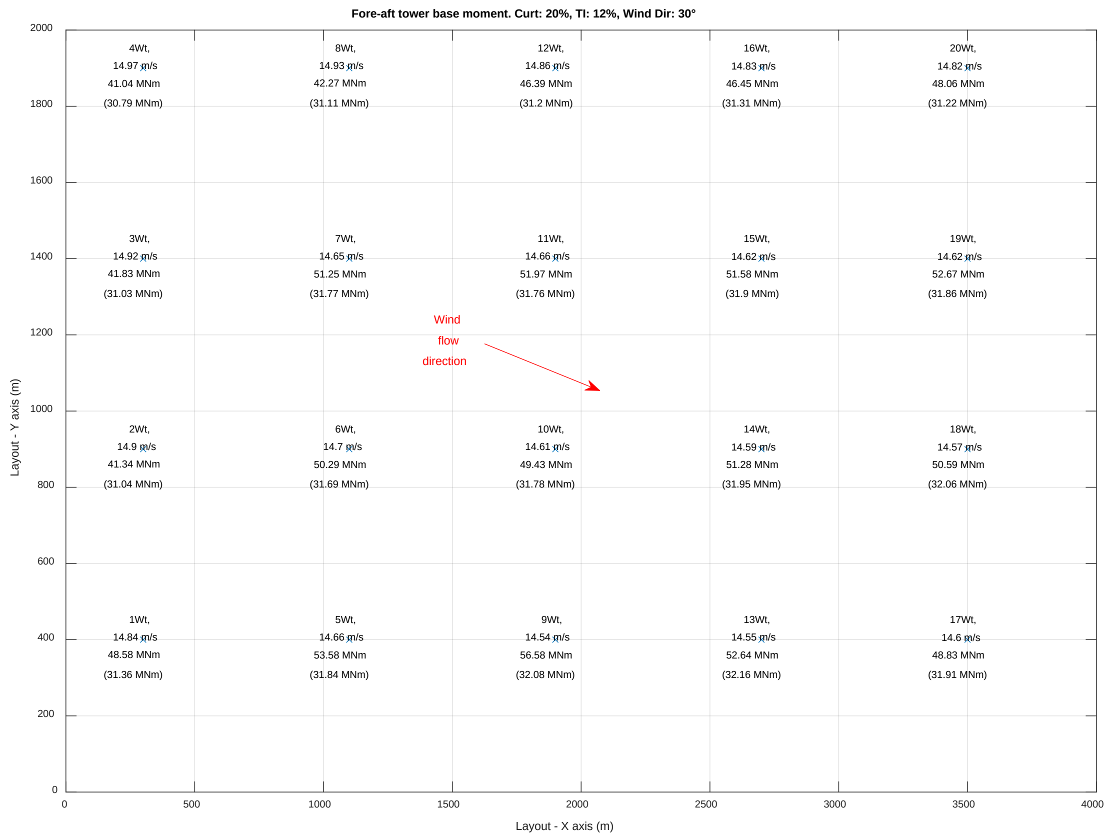

Figure 55: Fore-aft tower base moment DELs for the wind turbines when the wind is 30 degrees to the nominal and curtailment is applied

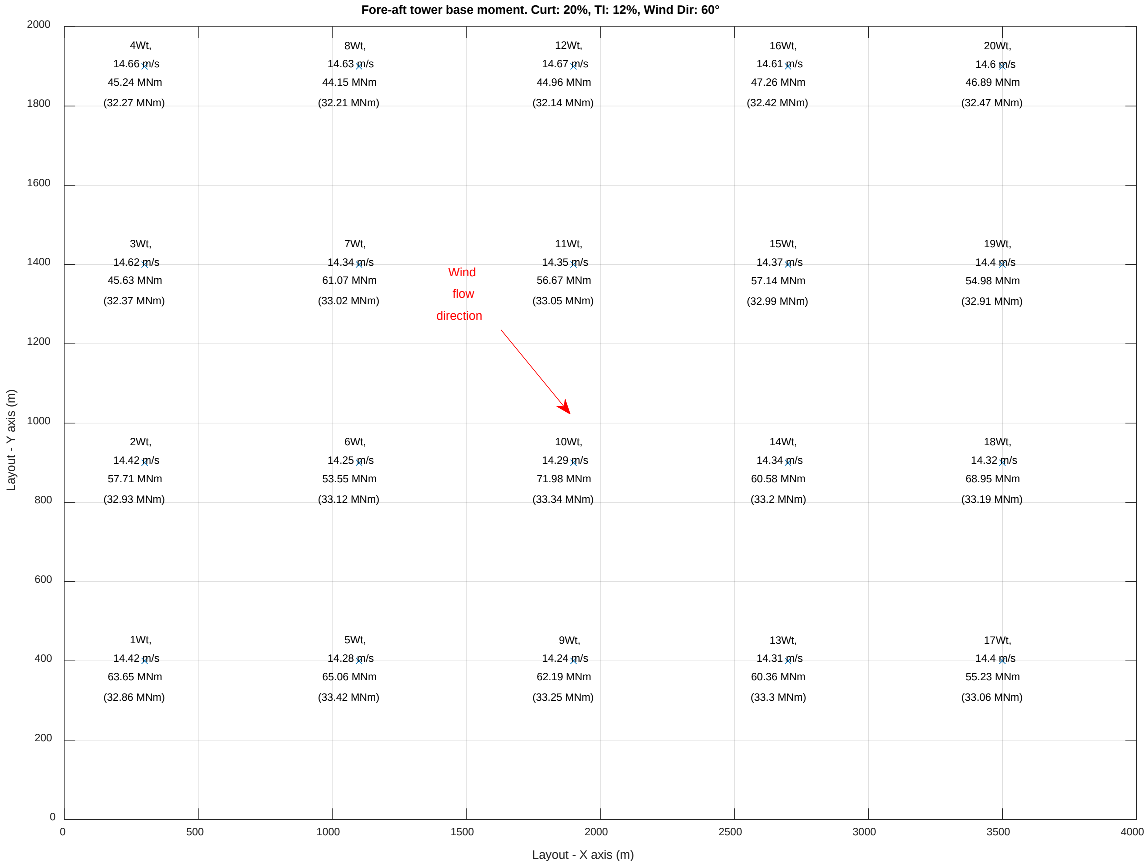

Figure 56: Fore-aft tower base moment DELs for the wind turbines when the wind is 60 degrees to the nominal and curtailment is applied

Similar trends can also be observed in the side-to-side tower motion analysis; that is, wind turbine that are immersed in the wakes of other turbines are subjected to greating mechanical loading, and curtailing the global power output through a farm controller does significantly reduce the loading. Figure 57 shows the side-to-side tower base moment DELs for the wind turbines when the wind direction is 0 degrees and no curtailment is applied. Figure 58 shows the side-to-side tower base moment DELs for the wind turbines when the wind direction is 90 degrees and no curtailment is applied. Figure 62 shows the side-to-side tower base moment DELs for the wind turbines when the wind direction is 0 degrees and the wind farm power output has been curtailed by 20%. Figure 63 shows the side-to-side tower base moment DELs for the wind turbines when the wind direction is 90 degrees and the wind farm power output has been curtailed by 20%.

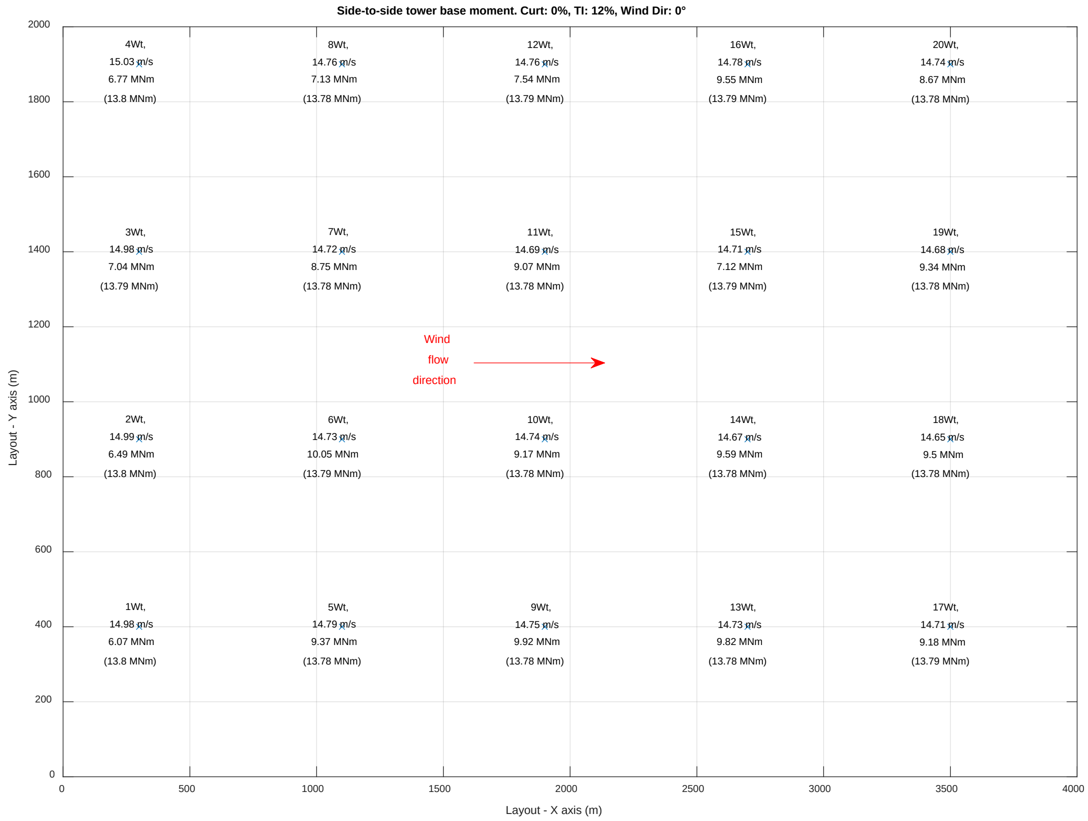

Figure 57: Side-to-side tower base moment DELs for the wind turbines when the wind is aligned with the X axis and curtailment is not applied

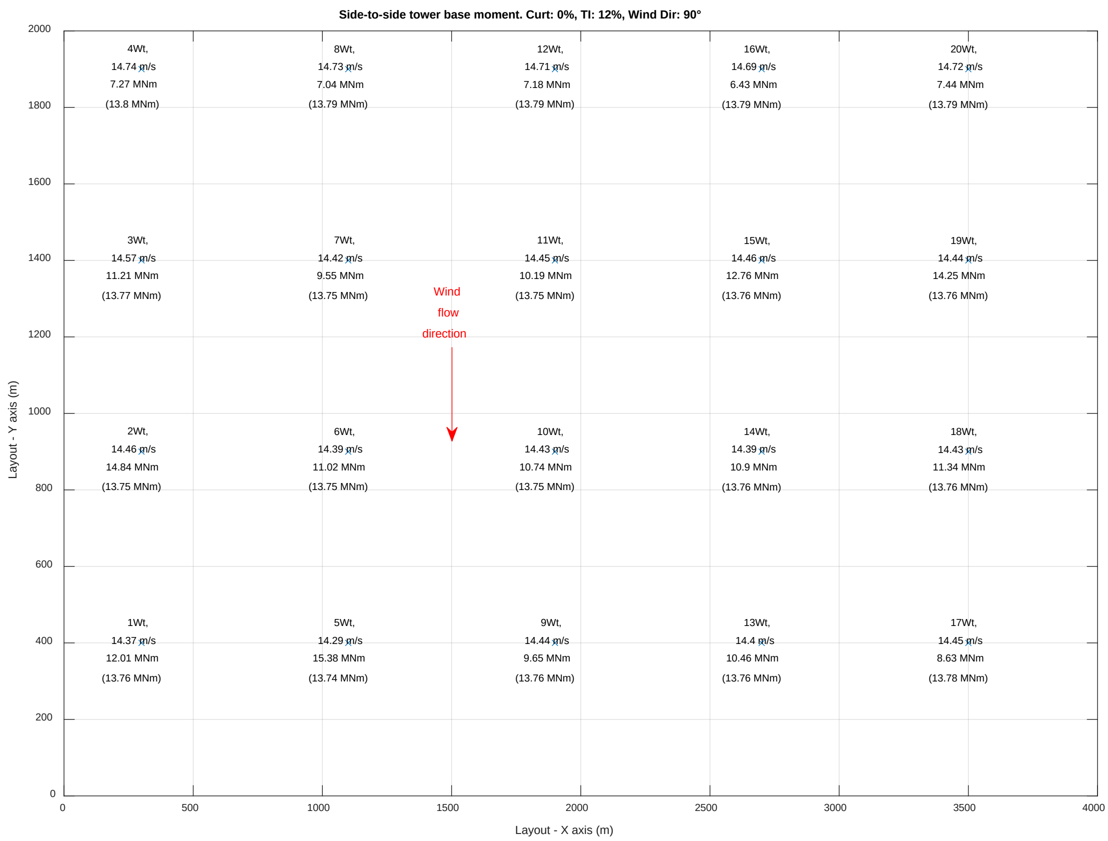

Figure 58: Side-to-side tower base moment DELs for the wind turbines when the wind is aligned with Y axis and curtailment is not applied

Results for a selection of wind directions are also herein presented:

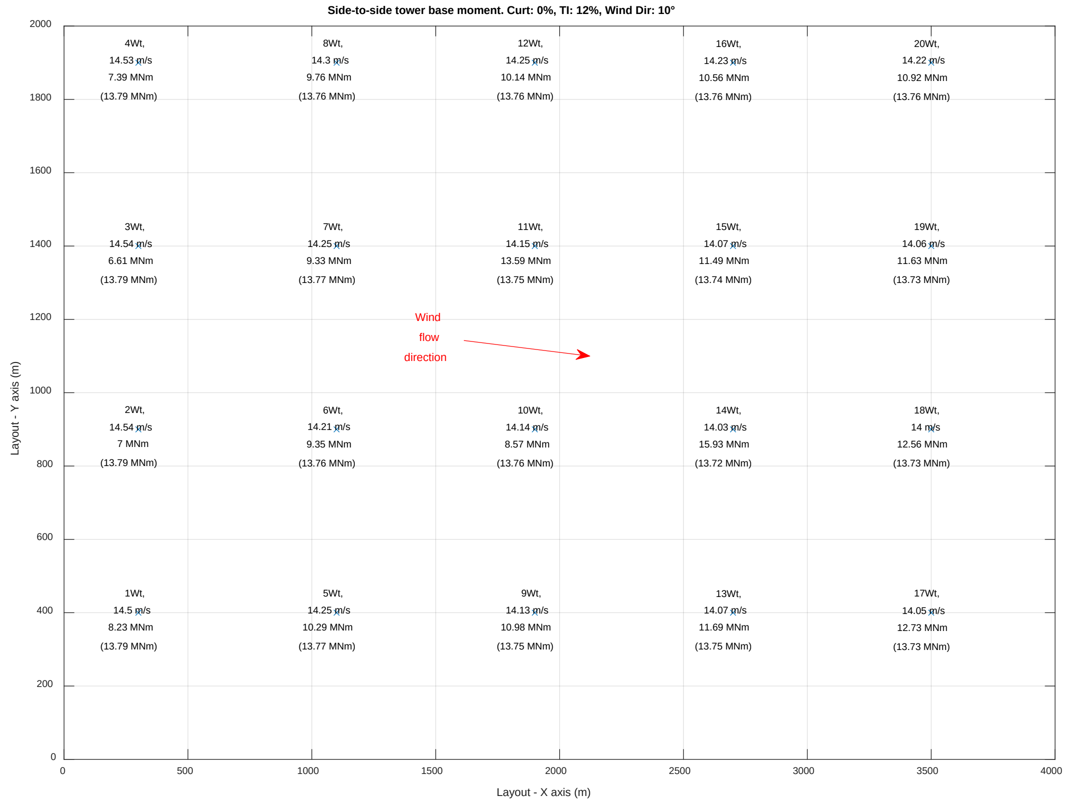

Figure 59: Fore-aft tower base moment DELs for the wind turbines when the wind is 10 degrees to the nominal

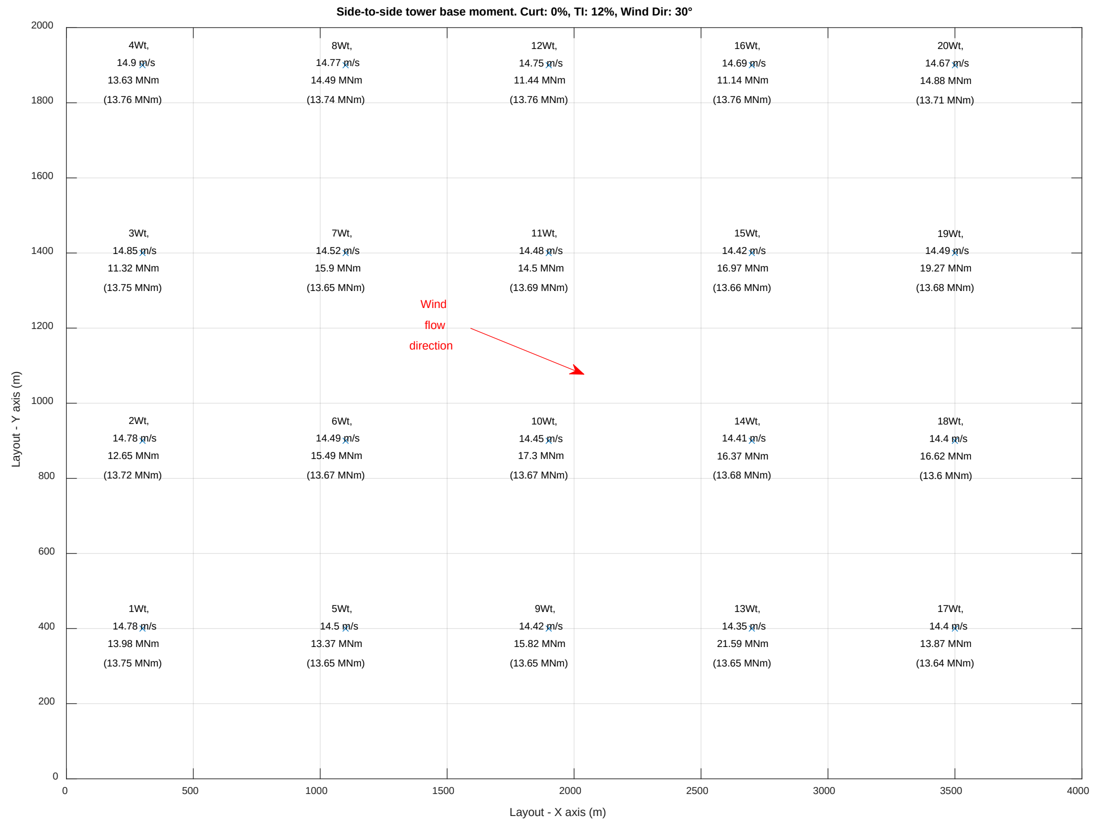

Figure 60: Fore-aft tower base moment DELs for the wind turbines when the wind is 30 degrees to the nominal

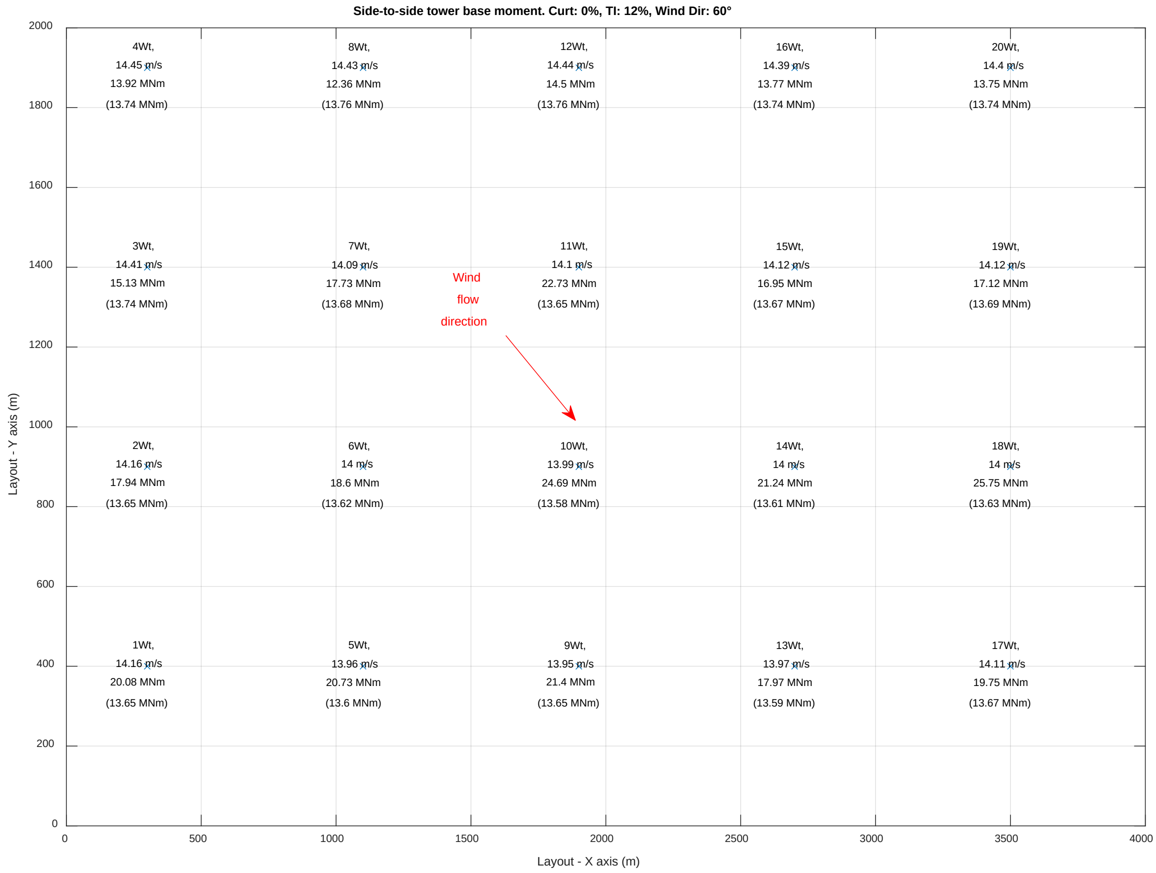

Figure 61: Fore-aft tower base moment DELs for the wind turbines when the wind is 60 degrees to the nominal

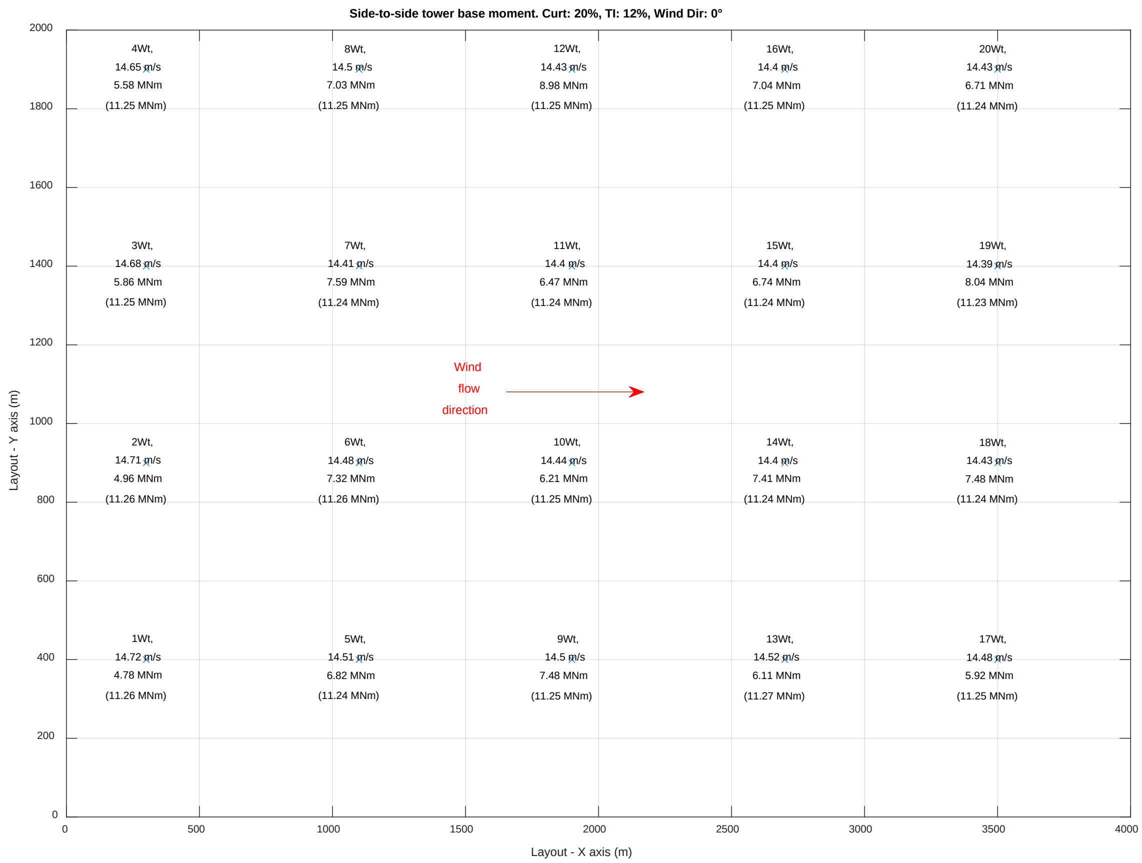

Figure 62: Side-to-side tower base moment DELs for the wind turbines when the wind is aligned with the X axis and curtailment is applied

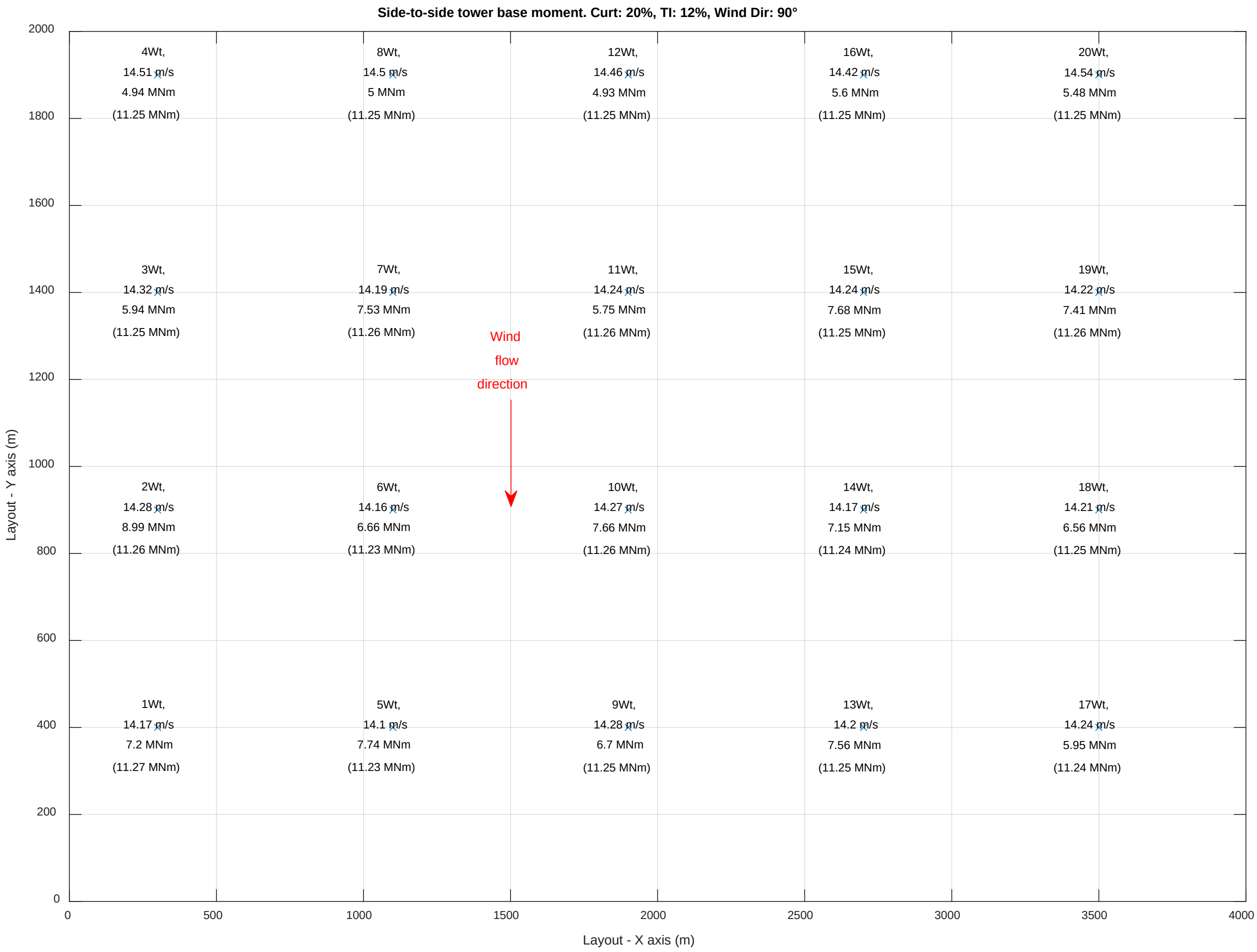

Figure 63: Side-to-side tower base moment DELs for the wind turbines when the wind is aligned with the Y axis and curtailment is applied

Results for a selection of wind directions are also herein presented:

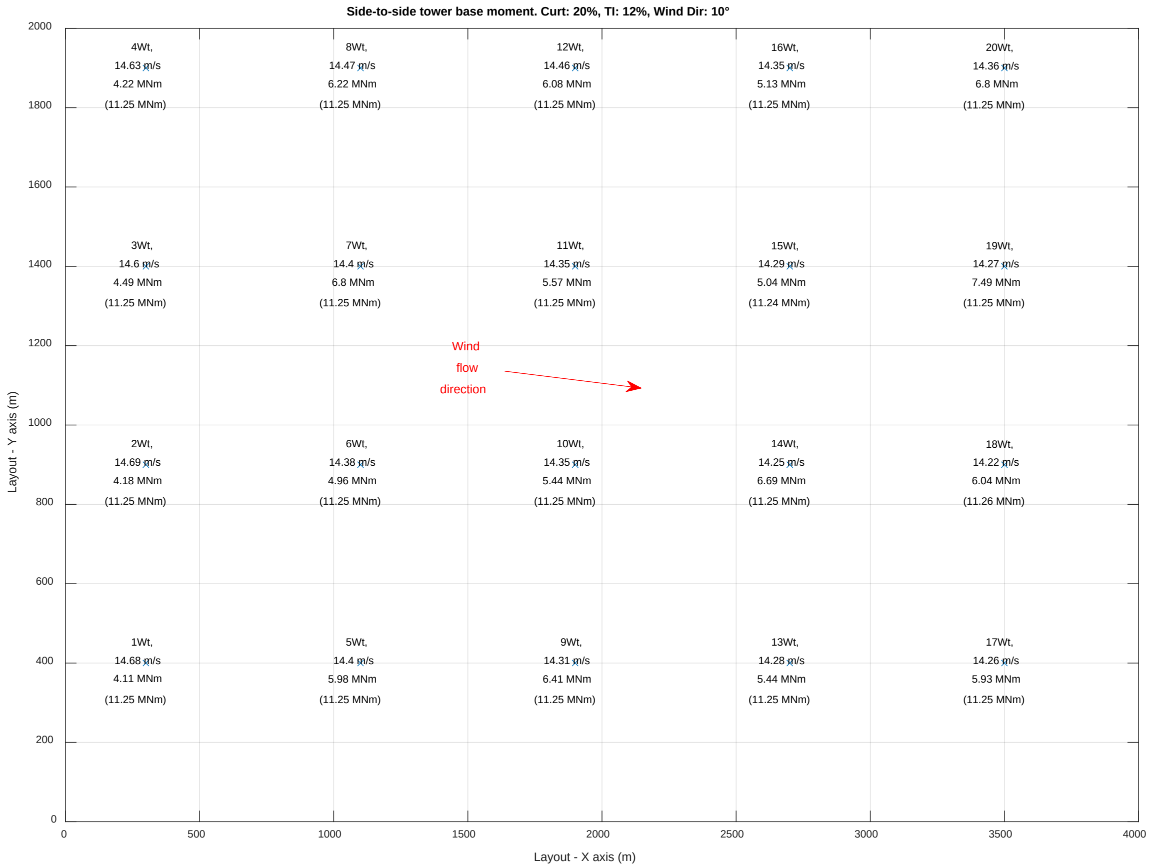

Figure 64: Side-to-side tower base moment DELs for the wind turbines when the wind is 10 degrees to the nominal and curtailment is applied

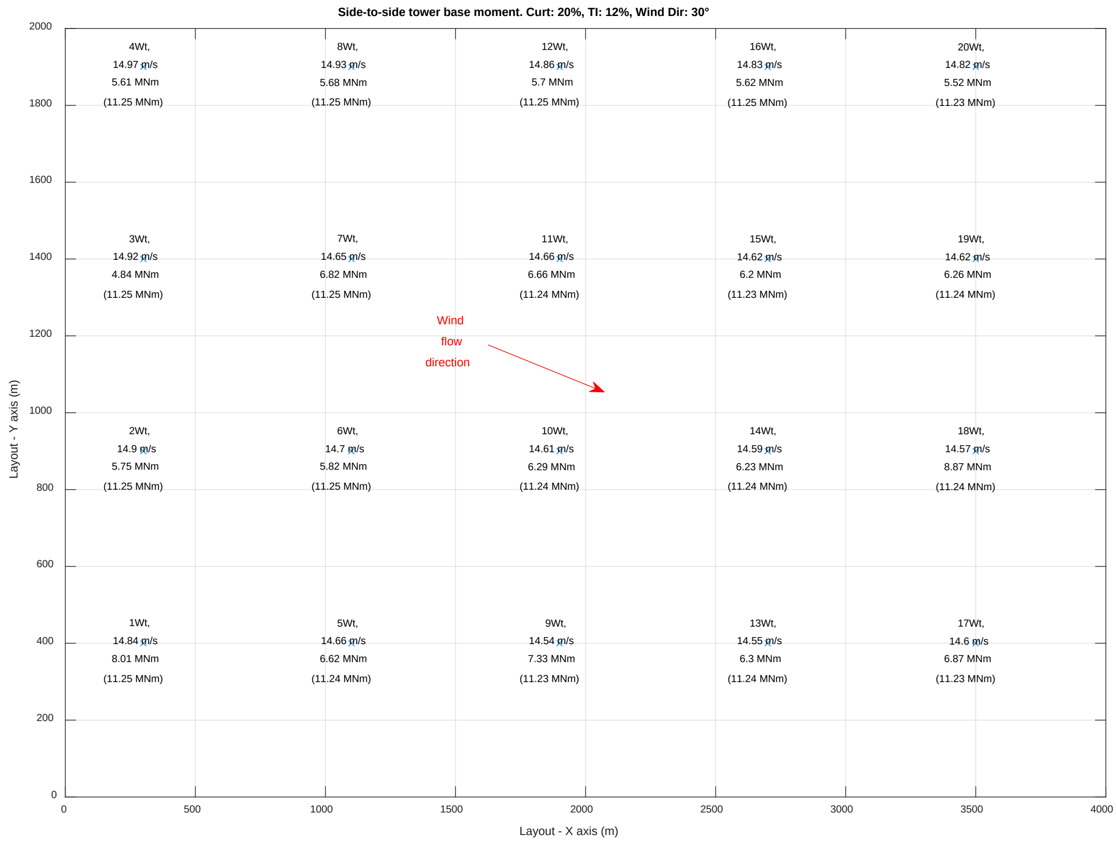

Figure 65: Side-to-side tower base moment DELs for the wind turbines when the wind is 30 degrees to the nominal and curtailment is applied

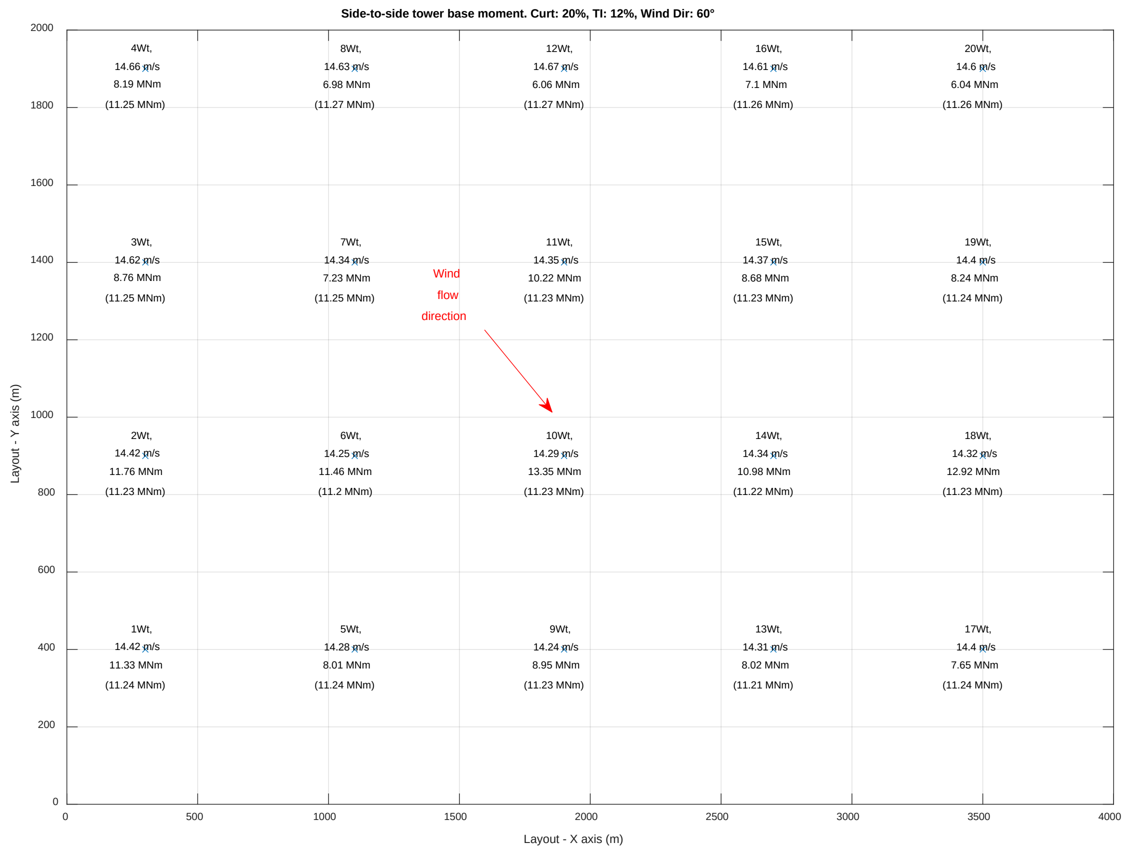

Figure 66: Side-to-side tower base moment DELs for the wind turbines when the wind is 60 degrees to the nominal and curtailment is applied

Figure 67 shows the in-plane blade root moment DELs for the wind turbines when the wind direction is 0 degrees and no curtailment is applied. Figure 68 shows the in-plane blade root moment DELs for the wind turbines when the wind direction is 90 degrees and no curtailment is applied. Figure 72 shows the in-plane blade root moment DELs for the wind turbines when the wind direction is 0 degrees and the wind farm power output has been curtailed by 20%. Figure 73 shows the in-plane blade root moment DELs for the wind turbines when the wind direction is 90 degrees and the wind farm power output has been curtailed by 20%. It can be observed that the curtailment does not have any real influence on the in-plane DELs; this is because the in-plane DEL is predominantly due to gravitational loading.

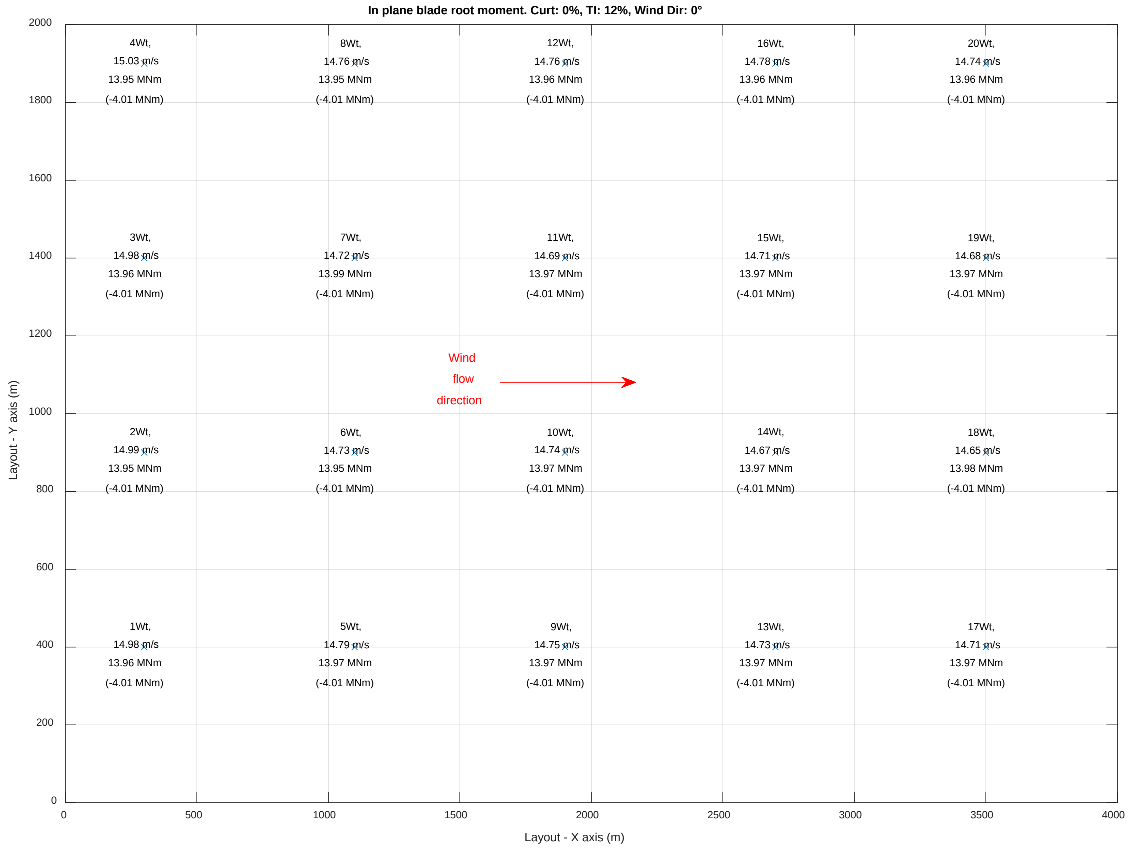

Figure 67: In-plane blade root moment DELs for the wind turbines when the wind is aligned with the X axis and no curtailment is applied.

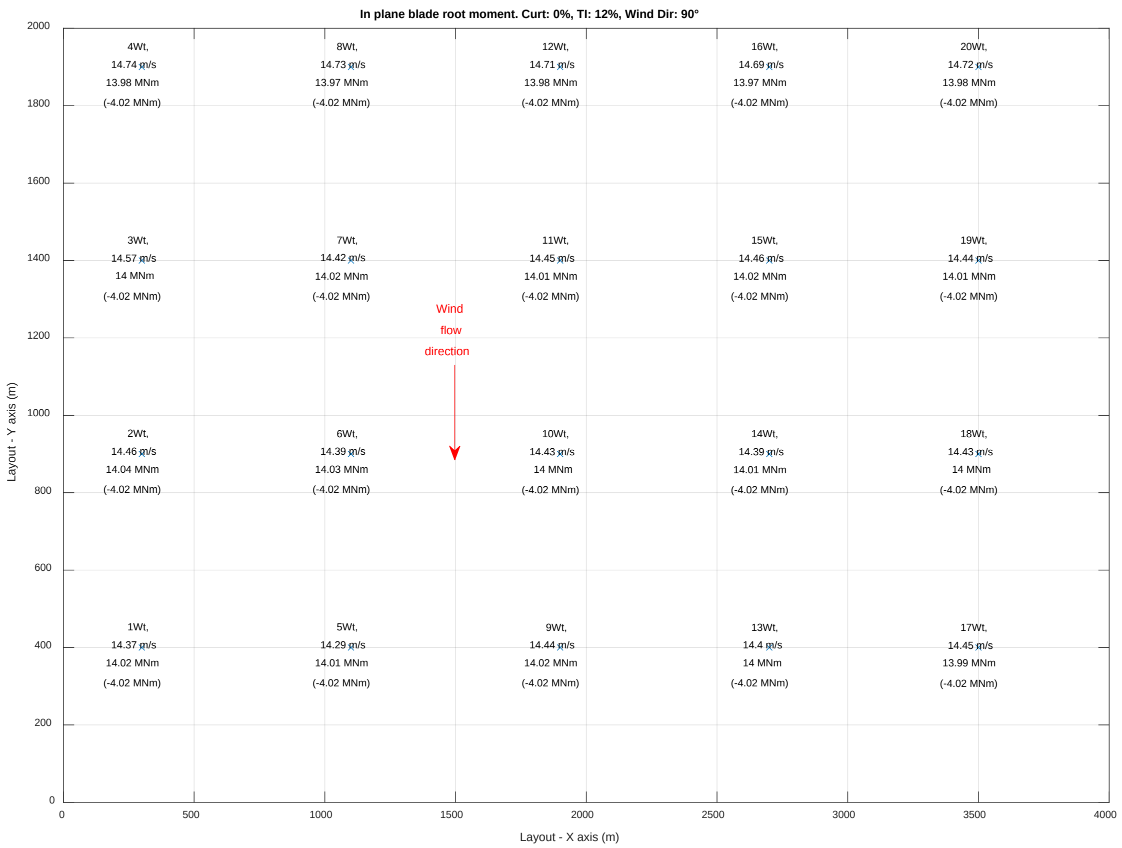

Figure 68: In-plane blade moment DELs for the wind turbines when the wind is alined with the Y axis and no curtailment is applied

Results for a selection of wind directions are also herein presented:

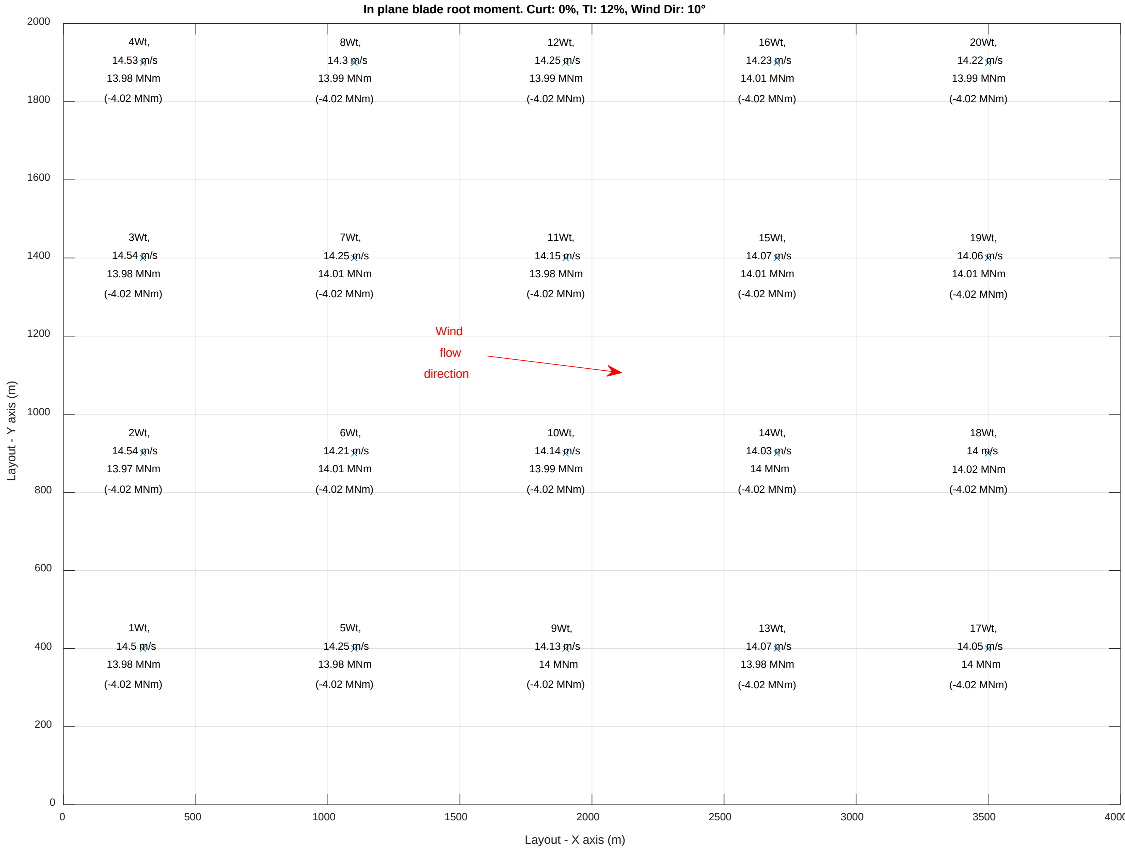

Figure 69: In-plane moment DELs for the wind turbines when the wind is 10 degrees to the nominal

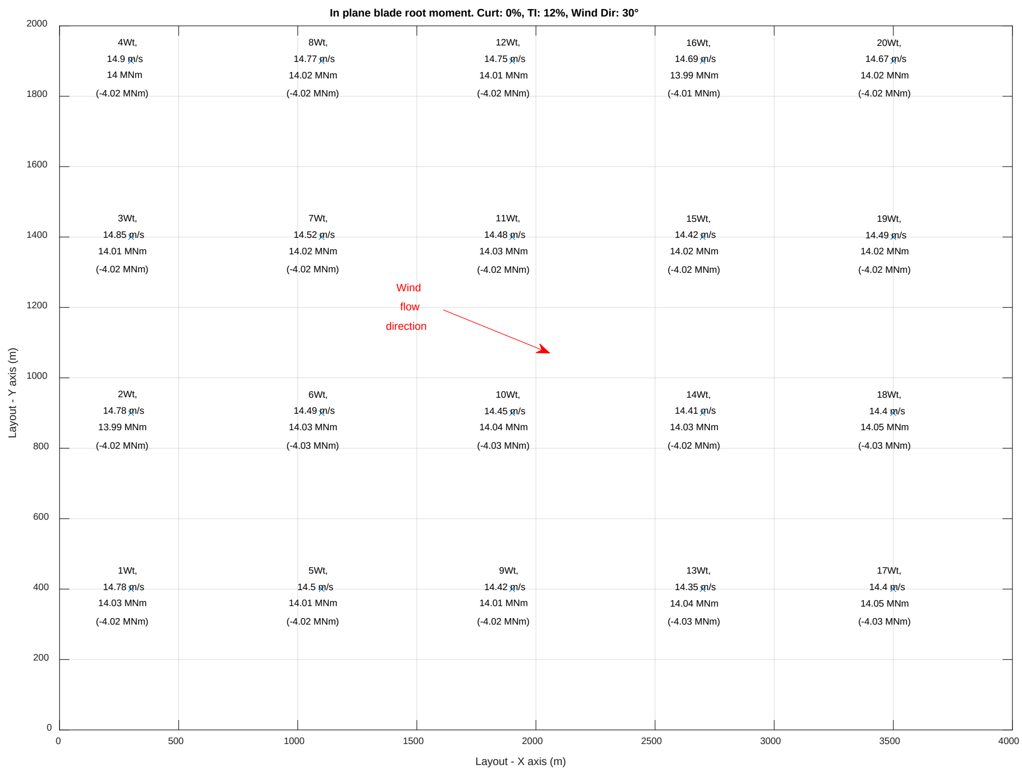

Figure 70: In-plane moment DELs for the wind turbines when the wind is 30 degrees to the nominal

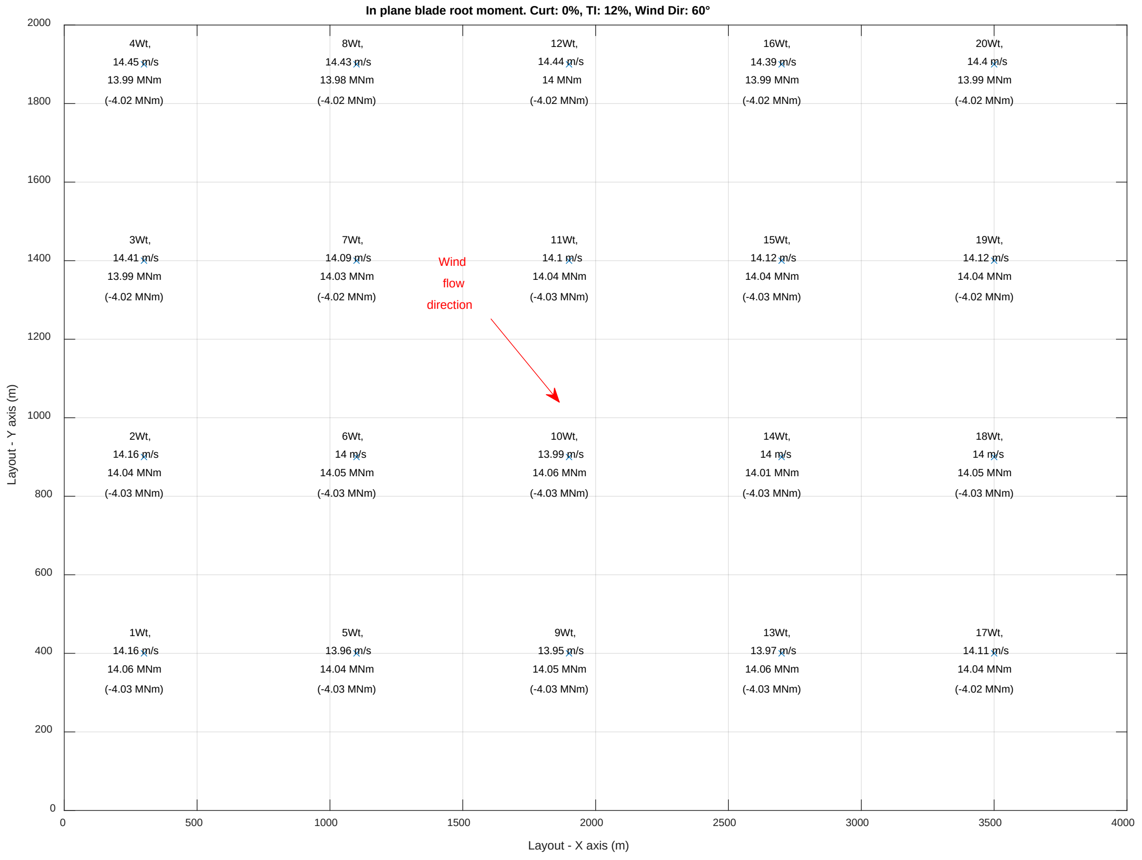

Figure 71: In-plane moment DELs for the wind turbines when the wind is 60 degrees to the nominal

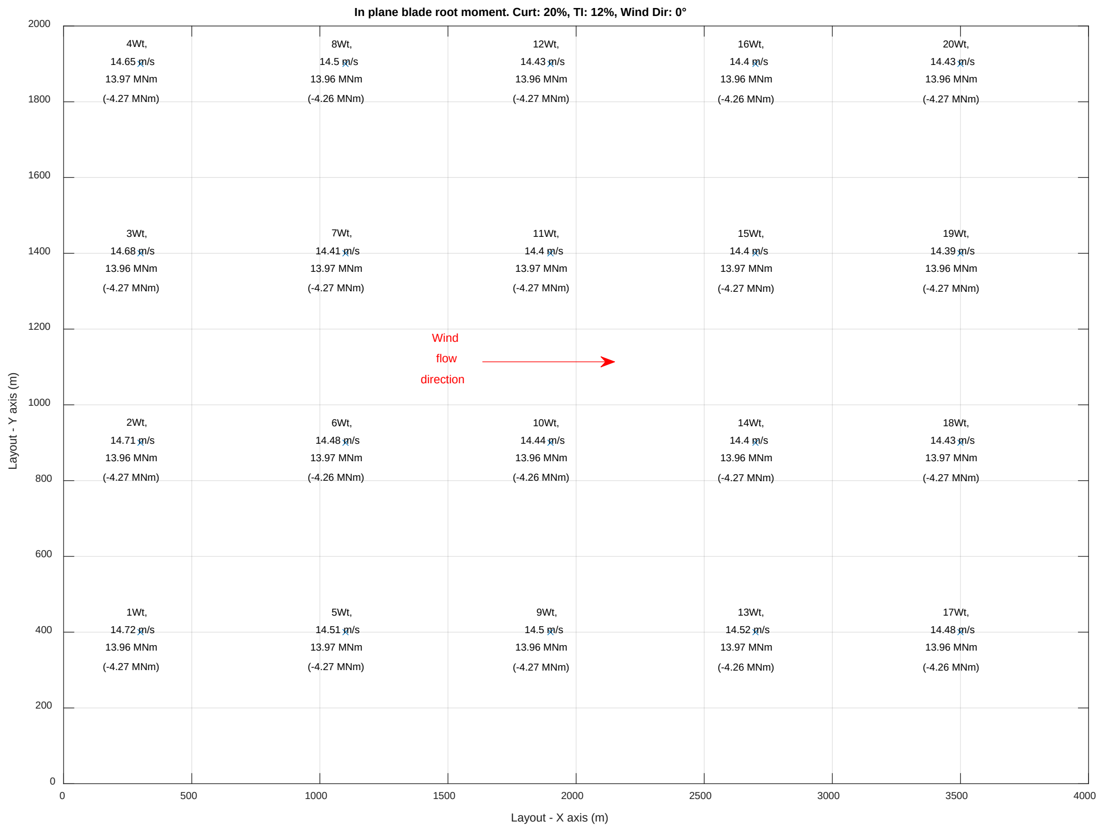

Figure 72: In-plane blade moment DELs for the wind turbines when the wind is aligned with the X axis and curtailment is applied

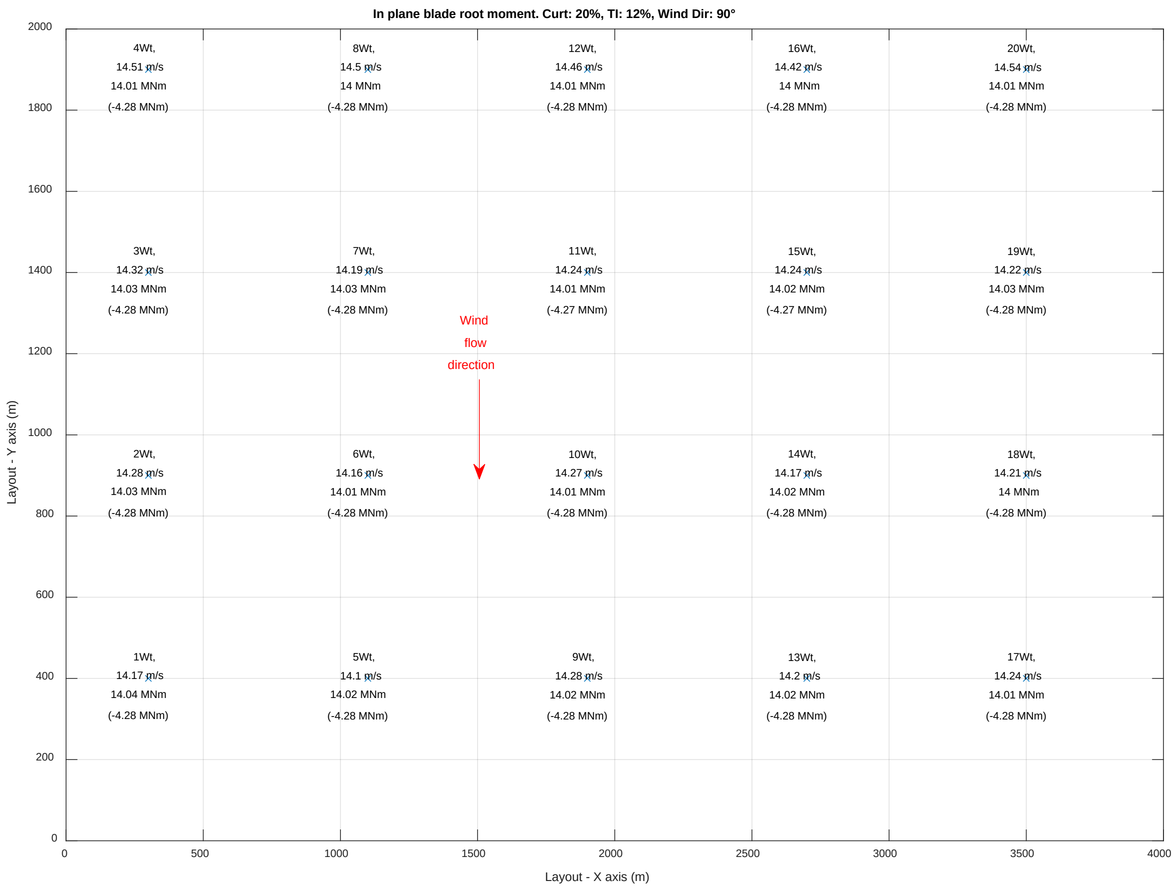

Figure 73: In-plane blade moment DELs for the wind turbines when the wind is aligned with the Y axis and curtailment is applied

Results for a selection of wind directions are also herein presented:

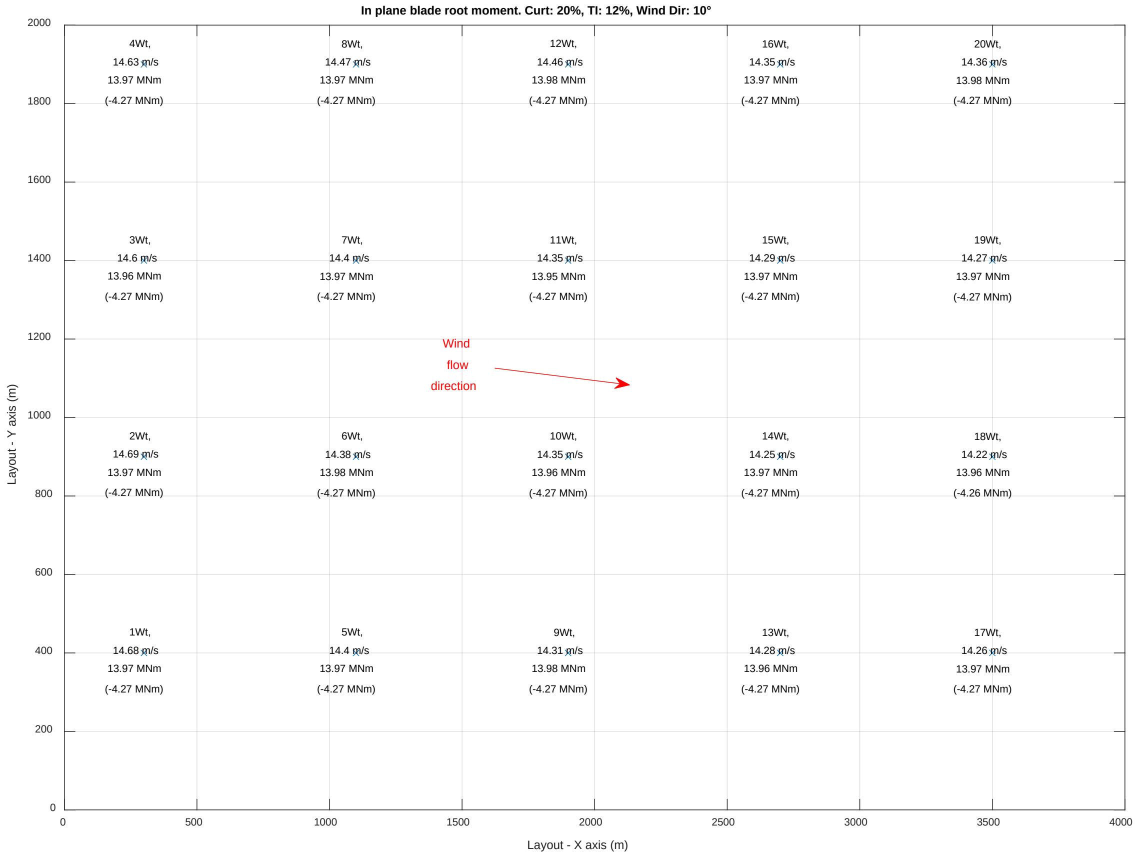

Figure 74: In-plane moment DELs for the wind turbines when the wind is 10 degrees to the nominal and curtailment is applied

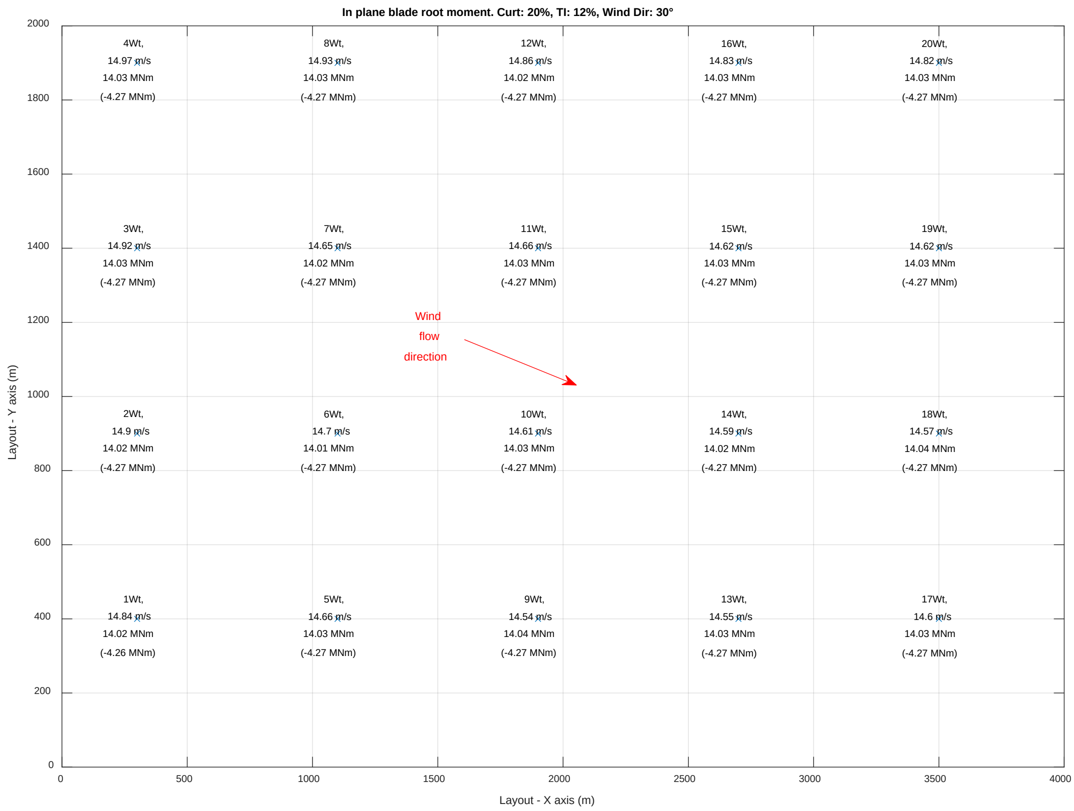

Figure 75: In-plane moment DELs for the wind turbines when the wind is 30 degrees to the nominal and curtailment is applied

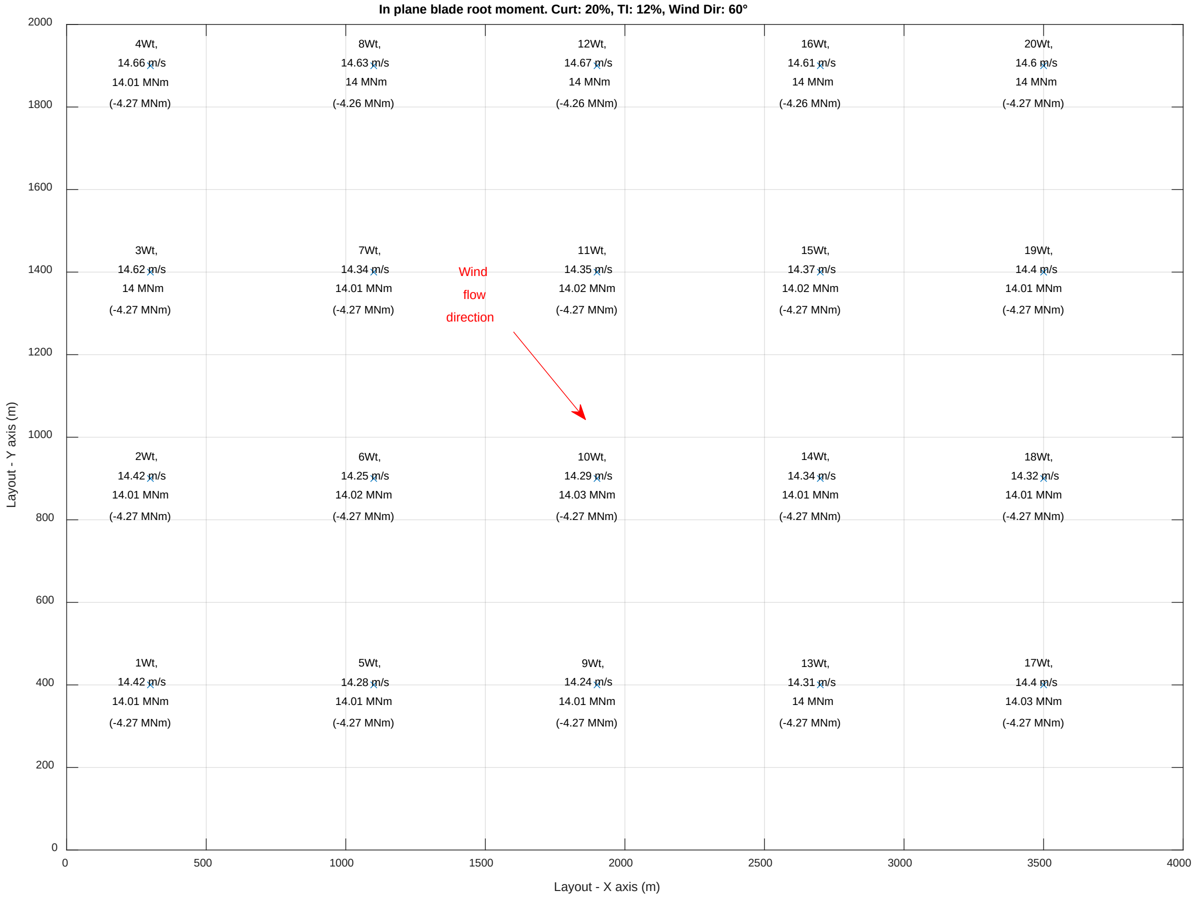

Figure 76: In-plane moment DELs for the wind turbines when the wind is 60 degrees to the nominal and curtailment is applied

Figure 77 shows the out-of-plane blade root moment DELs for the wind turbines when the wind direction is 0 degrees and no curtailment is applied. Figure 78 shows the out-of-plane blade root moment DELs for the wind turbines when the wind direction is 90 degrees when no curtailment is applied. Figure 82 shows the out-of-plane blade root moment DELs for the wind turbines when the wind direction is 0 degrees when the wind farm power output has been curtailed by 20%. Figure 83 shows the out-of-plane blade root moment DELs for the wind turbines when the wind direction is 90 degrees when the wind farm power output has been curtailed by 20%.

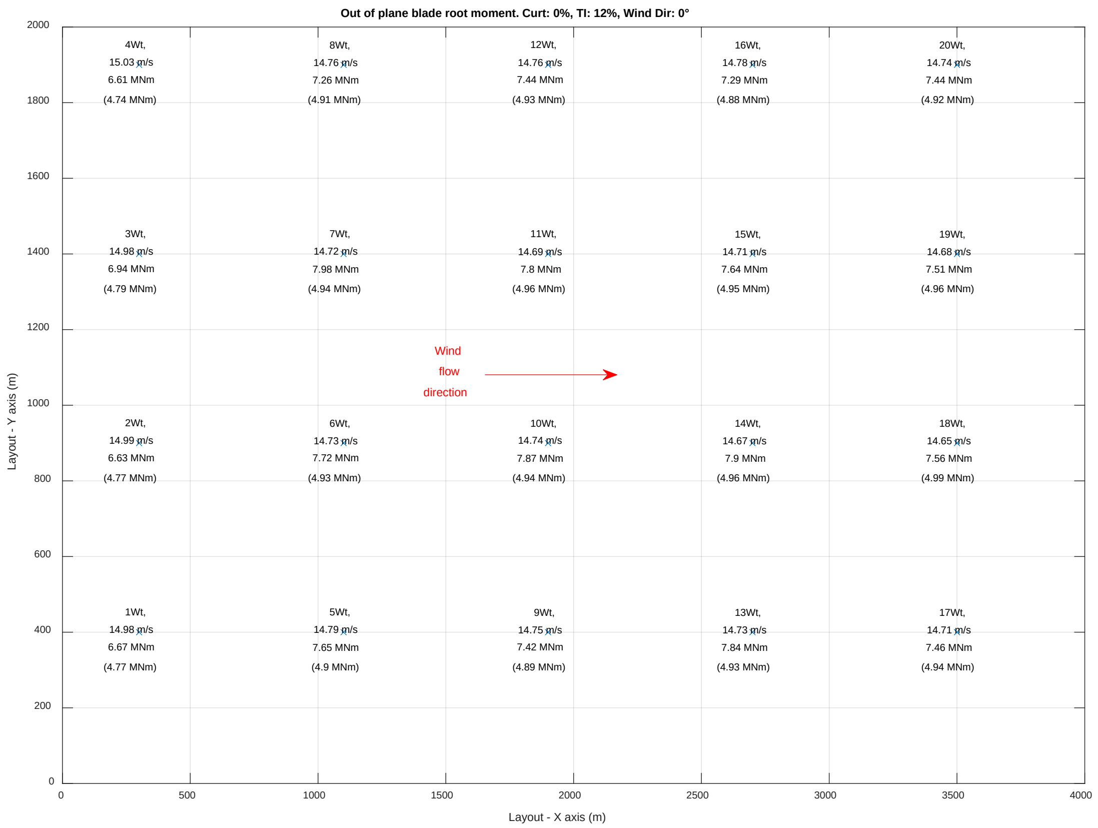

Figure 77: Out-of-plane blade root moment DELs for the wind turbines when the wind is aligned with the X axis and no curtailment is applied

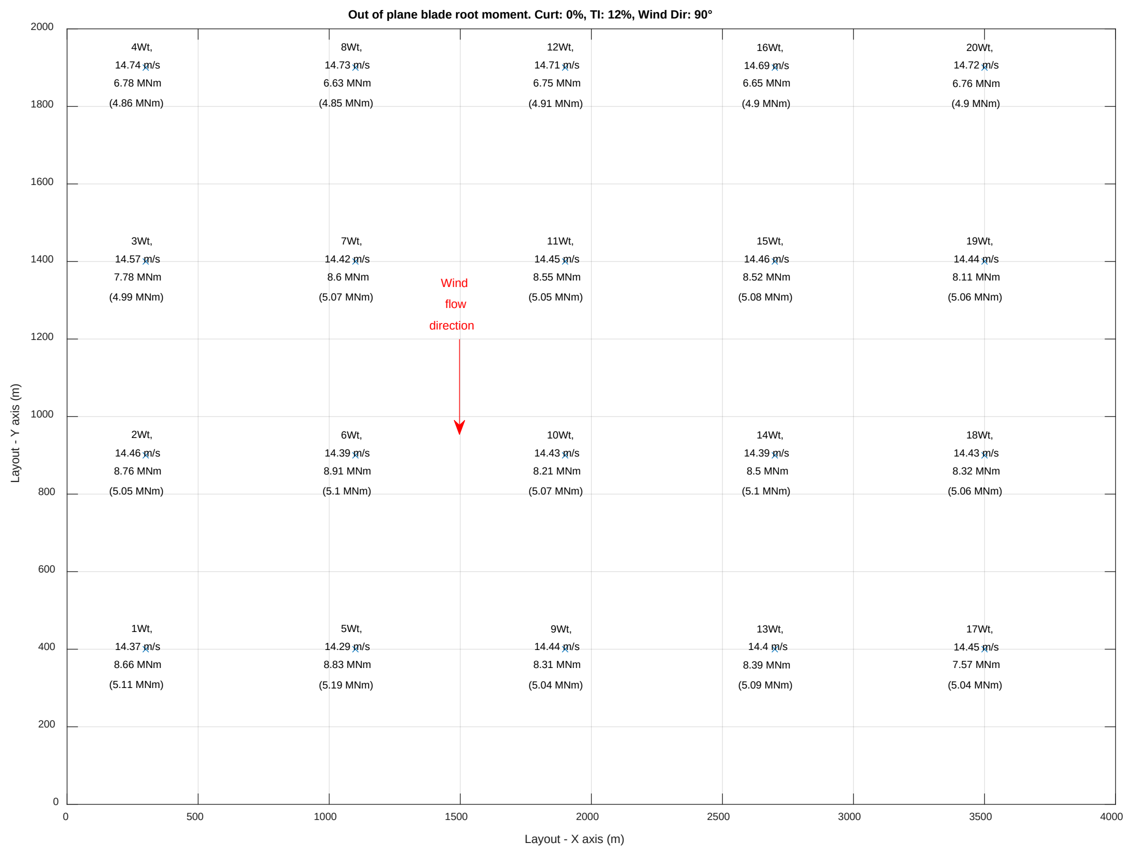

Figure 78: Out-of-plane blade root moment DELs for the wind turbines when the wind is aligned with the Y axis and no curtailment is applied

Results for a selection of wind directions are also herein presented:

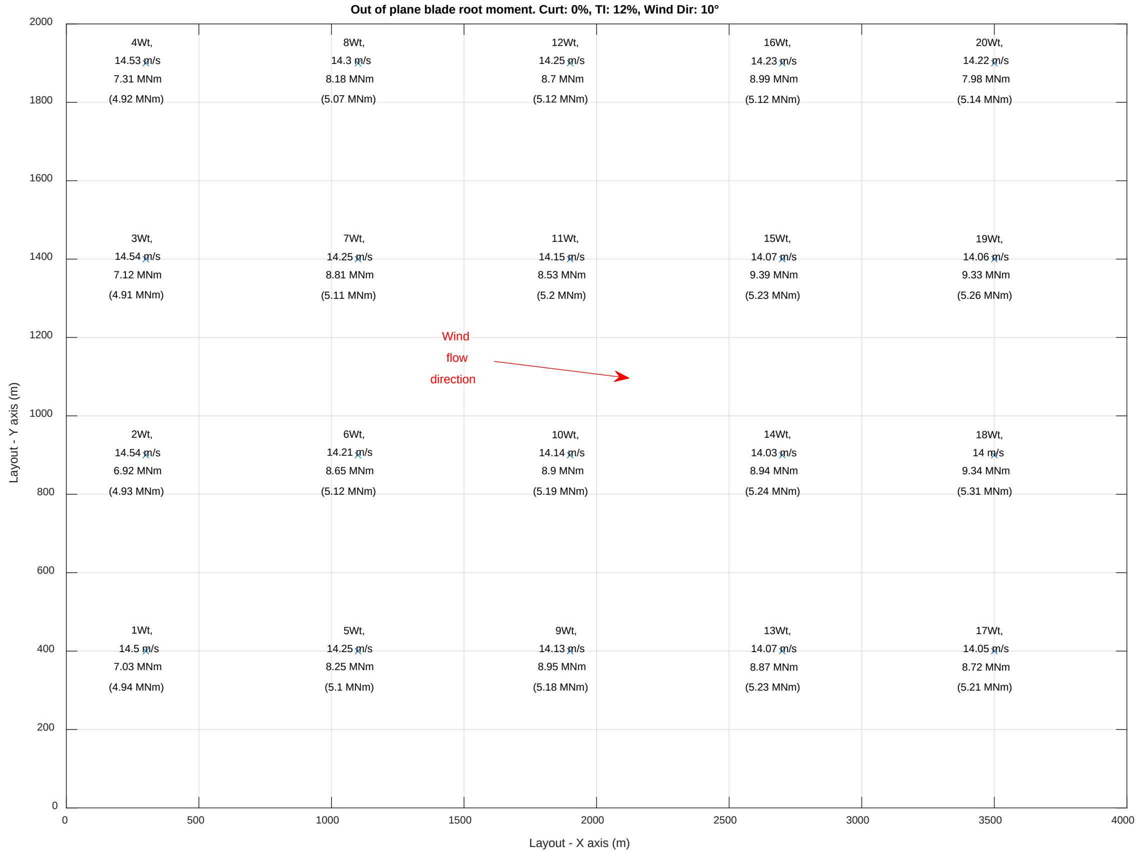

Figure 79: Out-of-plane moment DELs for the wind turbines when the wind is 10 degrees to the nominal

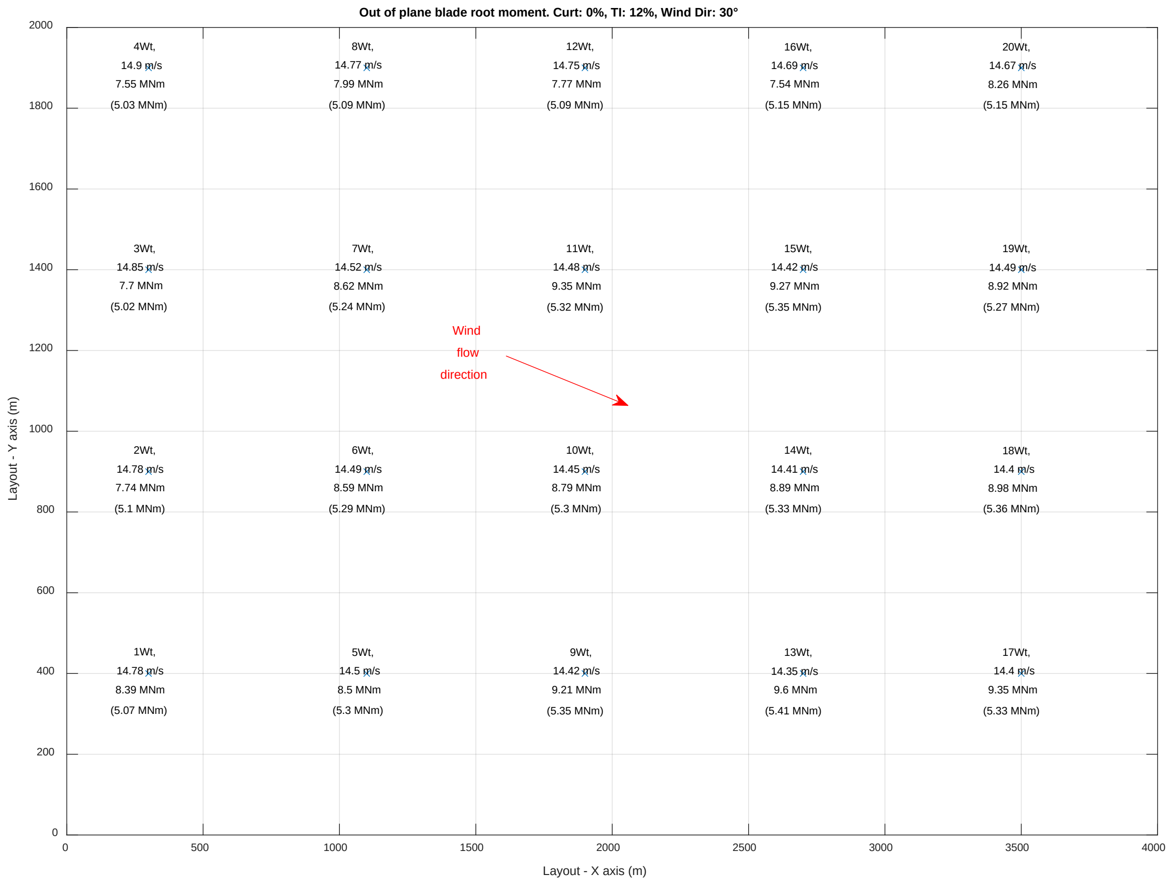

Figure 80: Out-of-plane moment DELs for the wind turbines when the wind is 30 degrees to the nominal

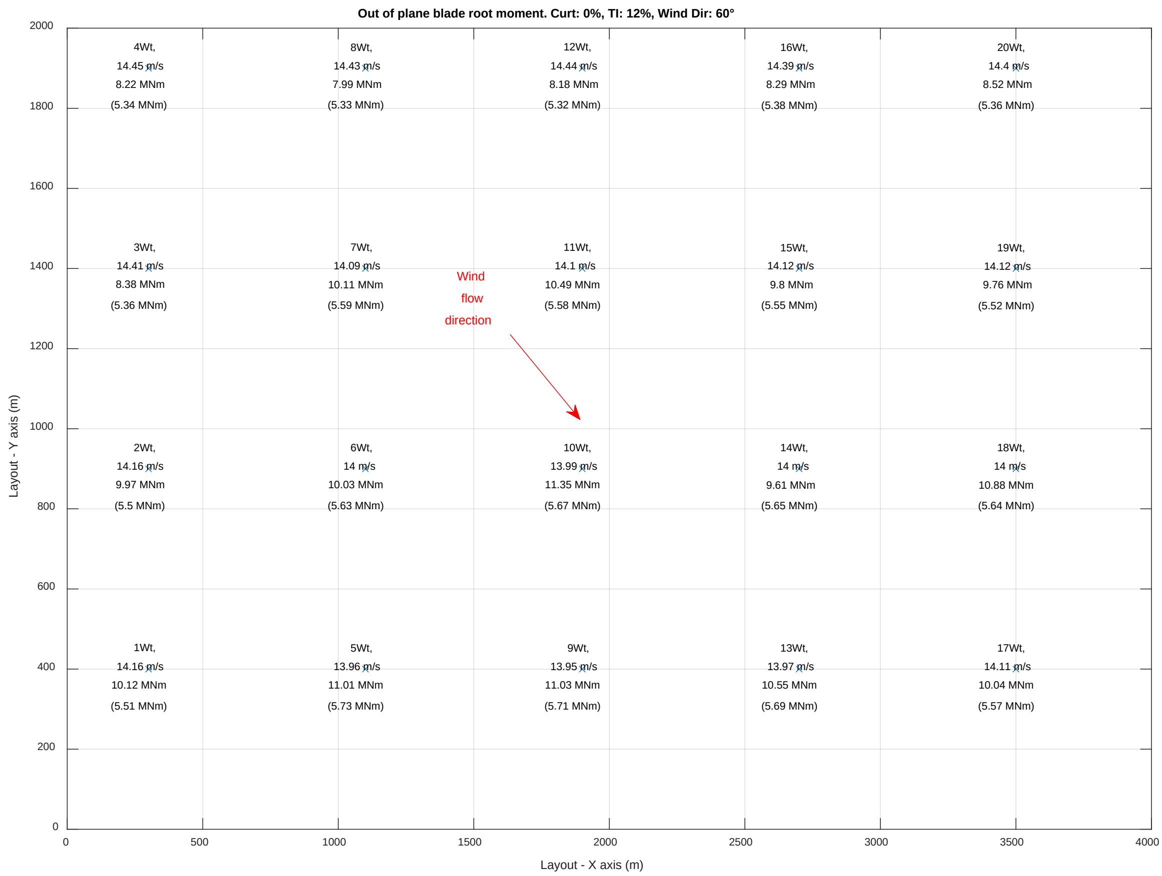

Figure 81: Out-of-plane moment DELs for the wind turbines when the wind is 60 degrees to the nominal

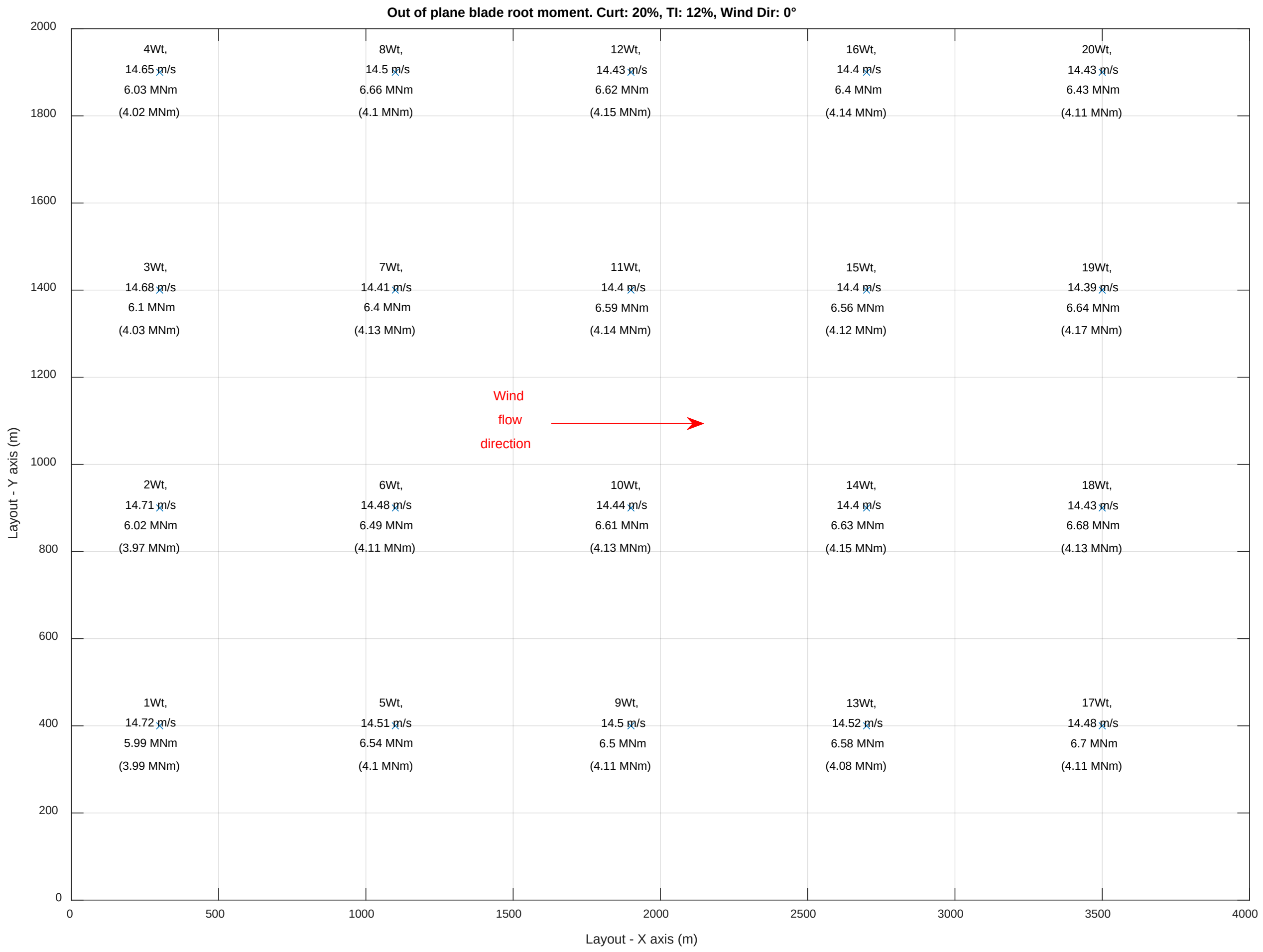

Figure 82: Out-of-plane blade root moment DELs for the wind turbines when the wind is aligned with the X axis and curtailment is applied

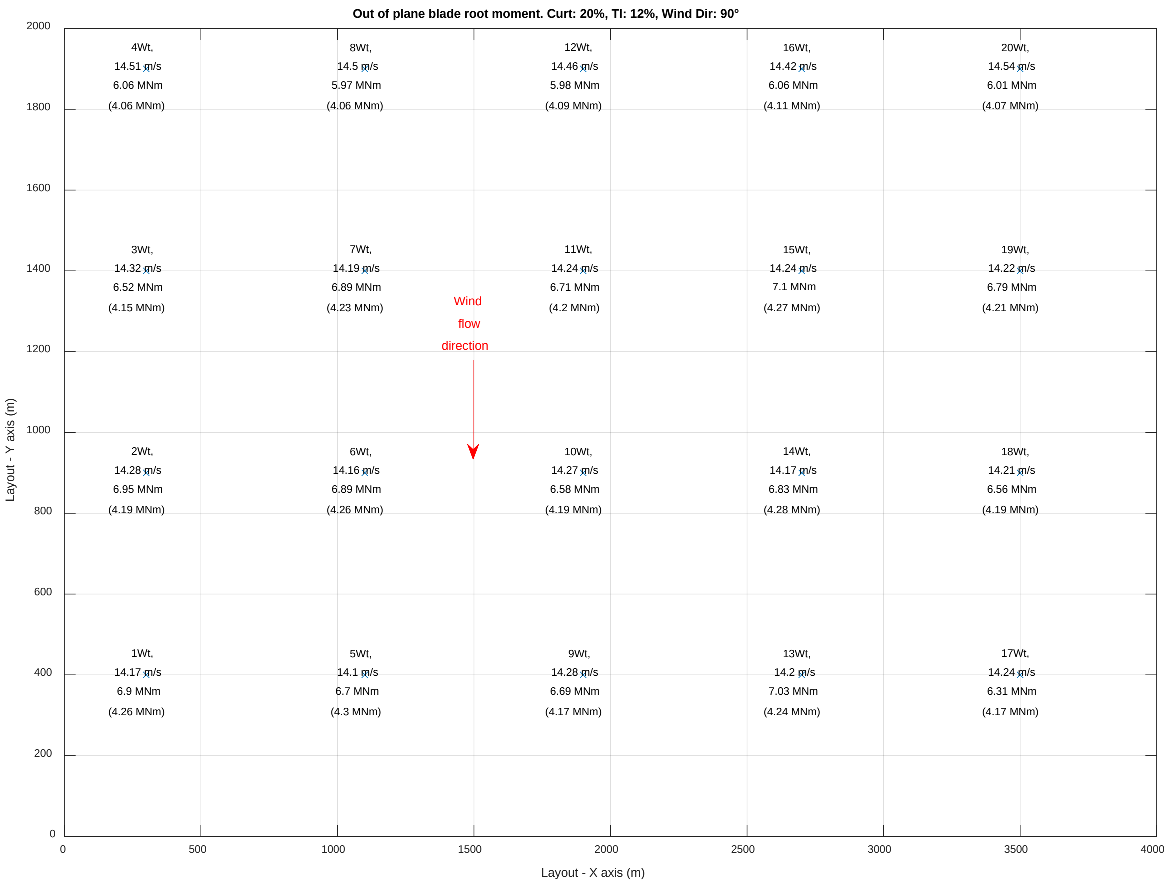

Figure 83: Out-of-plane blade root moment DELs for the wind turbines when the wind is aligned with the Y axis and curtailment is applied

Results for a selection of wind directions are also herein presented:

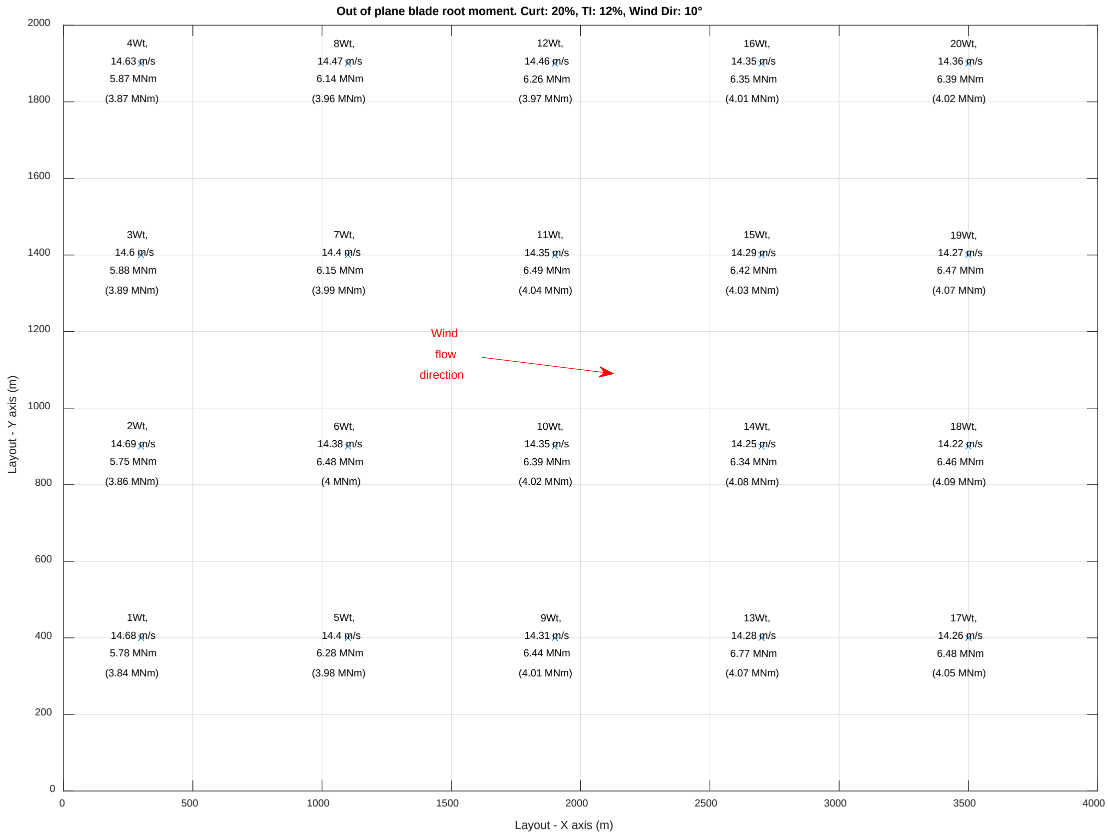

Figure 84: Out-of-plane moment DELs for the wind turbines when the wind is 10 degrees to the nominal and curtailment is applied

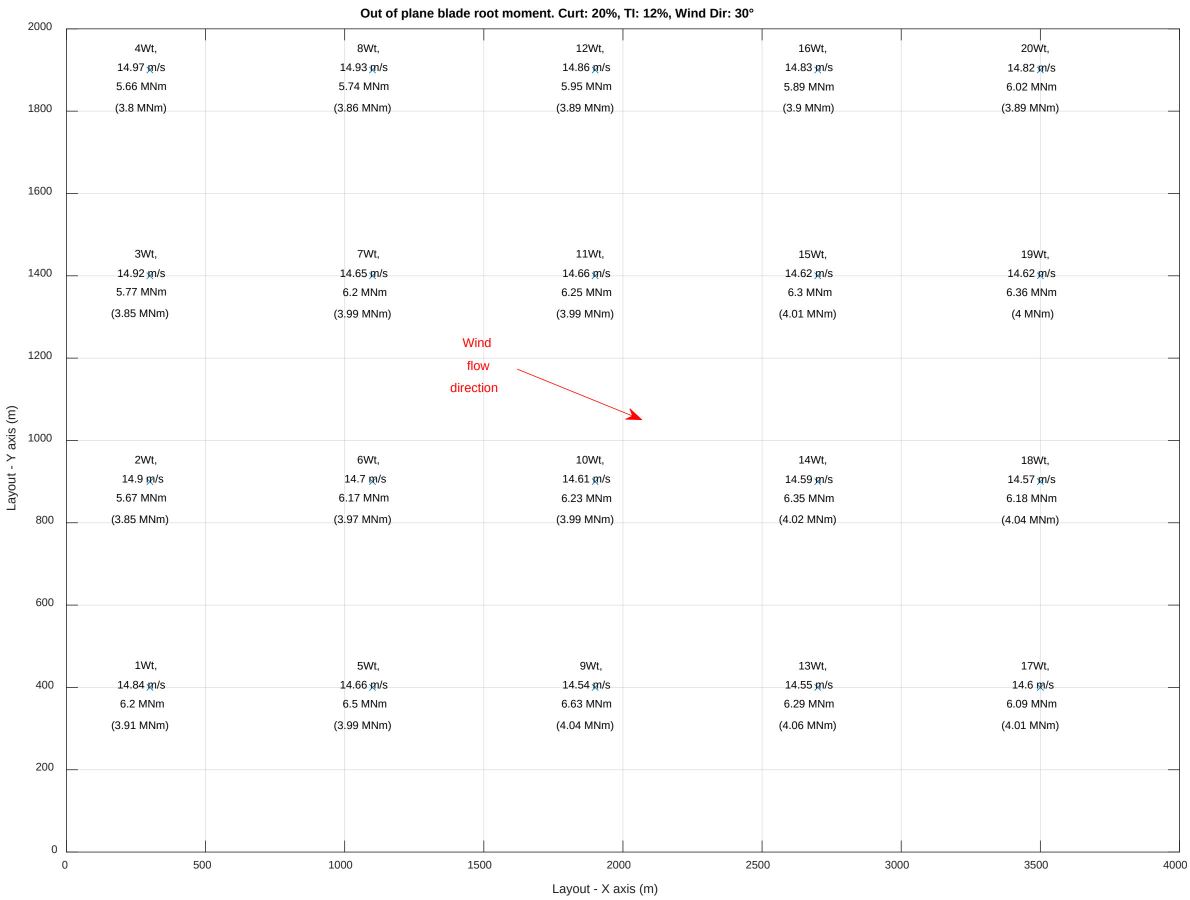

Figure 85: Out-of-plane moment DELs for the wind turbines when the wind is 30 degrees to the nominal and curtailment is applied

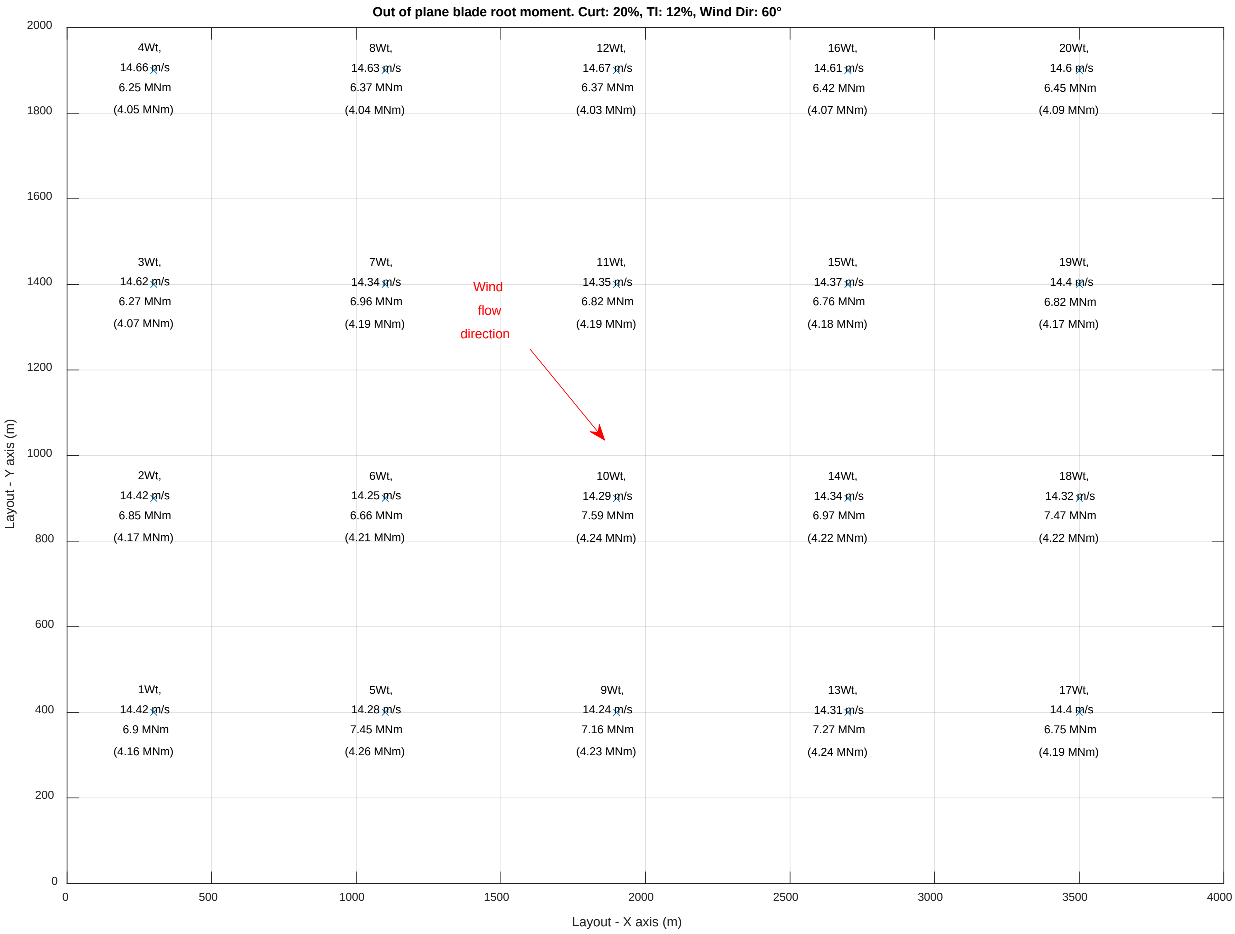

Figure 86: Out-of-plane moment DELs for the wind turbines when the wind is 60 degrees to the nominal and curtailment is applied

While the controller developed by the University of Strathclyde has, thus far, only been designed to enable a wind farm to provide ancillary services, it can be observed that curtailing the wind farm's power output comes with the added benefit of reducing mechanical loading. This suggests that the architecture used in this study could be modified without too much difficulty such that mechanical loading can be reduced. It is noted that while wind farm control may facilitate load reduction in general, it is expected that only marginal reductions will be achievable for the in-plane root bending moment, particularly as turbines increase in size. This is because the dominant source of loading will be gravity. Turbine-level control (using the pitch mechanism) would be most appropriate to reduce the gravitational loading.

5.5 Effect of the Provision of Ancillary Services on Cost of Energy

Two issues have been of particular interest to transmission system operators in the last decade: the loss of inertia directly linked to the power system, thereby reducing frequency stability; and the loss of voltage stiffness, which compromises the performance of converters connecting to the grid. Voltage stability may be addressed by modification of the grid-side converter controllers in isolation of the rotor-side converter controller and the mechanical systems. Research suggests that industry has already been involved in the mitigation of voltage stability, and developed the appropriate control solutions. Thus, the focus turns to frequency stability.

If a wind farm operator were to curtail the output of the wind farm to provide spinning reserve, there is the opportunity to reduce the thrust force acting on the rotor, which, by extension, would lead to a reduction in the mechanical loading on both the drivetrain and the tower. This can be observed in Figure 77 and Figure 82. However, the curtailment will result in a loss of energy capture. This would delay the payback time for the investors in the wind farm, which may result in higher interest being paid. Accordingly, some compensation would need to be awarded to the owners of the wind farm if they were to provide frequency support. It should be noted, however, that the amount of curtailment needed to provide spinning reserve is relatively small, as shown in Figure 44 and Figure 45.

As an example, at present, National Grid envisions an additional annual cost of £3000-4000m to provide stability in the wake of the displacement of conventional generation in favour of converter-interface generation, including wind power, by the year 2030 [54]. Given that the projected energy consumption for Great Britain in 2030 is 350TWh [55], this equates to an additional cost, without any action being taken by wind farms, of £8.57-11.42 per MWh, which will ultimately be passed onto the consumer.

It is difficult to quantify the overall cost that a wind farm owner would bear by curtailing the output of the wind farm. This would be a function of the following items: lifetime extension that would result from reduced loads, which itself will depend on the exact turbine being employed; the additional interest that may be paid by delaying the payback time; and the site conditions, particularly to what extent will curtailment demands be imposed during high wind speed intervals. It is anticipated that given the high projected additional cost that transmission system operators will have to bear if renewable energy devices contribute very little to the provision of ancillary services, both the transmission system operator and wind farm owners will be able to benefit from having wind farms participate in the provision of ancillary services should the appropriate control systems be adopted.

5.6 Conclusions

In this chapter, the wind farm controller introduced in chapter 3 has been used to demonstrate how a wind farm can provide ancillary services. Investigations covered both wind speeds above rated and wind speeds below rated. Furthermore, the effect of delays have been assessed, with it being shown that the wind farm control system can still provide adequate control over the power output even when there are cumulative delays as large as 12 seconds. Finally, it has been shown that the fatigue to which a turbine is subjected is affected by curtailment. This does suggest that farm level control could be applied for load minimisation.

6 CONCLUSIONS

This report has outlined the key features of a new wind farm simulation tool: StrathFarm. It has been shown that the predictive capabilities are comparable to a commercial product.

Using StrathFarm, it has been demonstrated that the combination of a wind farm controller and power adjusting controllers (one for each turbine in the farm) yields a system which can provide ancillary services crucial to the smooth operation of a power system. The proposed solution has the following major advantages:

1. The Power Adjusting Controller and wind farm controller have both been tested in turbulent wind fields, unlike many of the wind farm control solutions that have been published thus far. Initial results have been very promising. This success is in part due to the formulation of the Power Adjusting Controller.
2. The impact of control systems has been shown to be favourable from the perspective of damage equivalent loads.
3. Introduction of the Power Adjusting Controller should not create any changes in the system such that the full envelope controller needs to be redesigned. This is preferable since it means it can be applied to commercial wind turbines from any manufacturer with relative ease.
4. Introduction of the wind farm controller does not introduce sufficient feedback for the turbine control systems to need modification. Thus, as with the Power Adjusting Controller, the wind farm controller can be applied to commercial wind turbines from any manufacturer with relative ease.
5. Given the high costs transmission system operators expect to encounter as conventional generation is displaced, taking with it ancillary services that were previously taken for granted, there is an opportunity for a wind farm to receive compensation for curtailing its output, thereby making it available to provide frequency support.

7 ACKNOWLEDGEMENTS

The University of Strathclyde would like to acknowledge contributions made by the following people: Adam Stock, Saman Poushpas, Lindsey Amos, Sung-ho Hur, Romans Kazacoks, Velissarios Kourkoulis, Victoria Neilson, Lourdes Gala Santos, Giorgio Zorzi. Alexander Giles would like to personally thank Tim Rubert and Luis Recalde for their useful feedback. Additionally, the following funding is gratefully acknowledged: EPSRC EP/G037728/1 DTC Wind Energy Systems, EPSRC EP/L016680/1 DTC Wind and Marine Energy Systems, EPSRC EP/H018662/1 Supergen Wind Phase 2, EPSRC EP/L014106/1 Supergen Wind Hub, and EPSRC EP/N006224/1 MAXFARM.

The University of Strathclyde would like to acknowledge IRPWind for funding from the European Union Seventh Framework Programme under the agreement GA-2013-609795.

8 REFERENCES

[1] A. Suzuki, *Application of dynamic inflow theory to wind turbine rotors*. 2000.

[2] W. Z. Shen, R. Mikkelsen, J. N. Sørensen, and C. Bak, “Tip loss corrections for wind turbine computations,” *Wind Energy*, vol. 8, no. 4, pp. 457–475, 2005.

[3] E. A. Bossanyi, “GH bladed theory manual,” *GH Partners Ltd*, 2003.

[4] J. M. Jonkman and M. L. Buhl Jr, “FAST User’s Guide-Updated August 2005,” 2005.

[5] J. Lee, E. Son, B. Hwang, and S. Lee, “Blade pitch angle control for aerodynamic performance optimization of a wind farm,” *Renew. energy*, vol. 54, pp. 124–130, 2013.

[6] V. Akhmatov, H. Knudsen, A. H. Nielsen, J. K. Pedersen, and N. K. Poulsen, “Modelling and transient stability of large wind farms,” *Int. J. Electr. Power Energy Syst.*, vol. 25, no. 2, pp. 123–144, 2003.

[7] J. D. Grunnet, M. Soltani, T. Knudsen, M. N. Kragelund, and T. Bak, “Aeolus toolbox for dynamics wind farm model, simulation and control,” in *The European Wind Energy Conference & Exhibition, EWEC 2010*, 2010.

[8] S. Poushpas, “Wind farm simulation modelling and control,” University of Strathclyde, 2016.

[9] S. Frandsen, R. Barthelmie, S. Pryor, O. Rathmann, S. Larsen, J. Højstrup, and M. Thøgersen, “Analytical modelling of wind speed deficit in large offshore wind farms,” *Wind energy*, vol. 9, no. 1–2, pp. 39–53, 2006.

[10] I. Katic, J. Højstrup, and N. O. Jensen, “A simple model for cluster efficiency,” in *European wind energy association conference and exhibition*, 1986, pp. 407–410.

[11] A. Niayifar and F. Porté-Agel, “Analytical modeling of wind farms: A new approach for power prediction,” *Energies*, vol. 9, no. 9, p. 741, 2016.

[12] P. M. O. Gebraad, P. A. Fleming, and J.-W. van Wingerden, “Wind turbine wake estimation and control using FLORIDyn, a control-oriented dynamic wind plant model,” in *American Control Conference (ACC), 2015*, 2015, pp. 1702–1708.

[13] P. M. O. Gebraad, F. W. Teeuwisse, J. W. Wingerden, P. A. Fleming, S. D. Ruben, J. R. Marden, and L. Y. Pao, “Wind plant power optimization through yaw control using a parametric model for wake effects—a CFD simulation study,” *Wind Energy*, vol. 19, no. 1, pp. 95–114, 2016.

[14] A. Peña, P.-E. Réthoré, and M. P. Laan, “On the application of the Jensen wake model using a turbulence-dependent wake decay coefficient: the Sexbierum case,” *Wind Energy*, vol. 19, no. 4, pp. 763–776, 2016.

[15] M. Gaumond, P.-E. Réthoré, S. Ott, A. Pena, A. Bechmann, and K. S. Hansen, “Evaluation of the wind direction uncertainty and its impact on wake modeling at the Horns Rev offshore wind farm,” *Wind Energy*, vol. 17, no. 8, pp. 1169–1178, 2014.

[16] A. Crespo, J. Hernandez, and S. Frandsen, “Survey of modelling methods for wind turbine wakes and wind farms,” *Wind energy*, vol. 2, no. 1, pp. 1–24, 1999.

[17] O. Rathmann, S. T. Frandsen, and R. J. Barthelmie, “Wake modelling for intermediate and large wind farms,” in *2007 European wind energy conference and exhibition*, 2007.

[18] M. J. Churchfield, S. Lee, J. Michalakes, and P. J. Moriarty, “A numerical study of the effects of atmospheric and wake turbulence on wind turbine dynamics,” *J. Turbul.*, no. 13, p. N14, 2012.

[19] L. A. Martinez-Tossas, M. J. Churchfield, and S. Leonardi, “Large eddy simulations of the flow past wind turbines: actuator line and disk modeling,” *Wind Energy*, vol. 18, no. 6, pp. 1047–1060, 2015.

[20] M. Calaf, C. Meneveau, and J. Meyers, “Large eddy simulation study of fully developed wind-turbine array boundary layers,” *Phys. fluids*, vol. 22, no. 1, p. 15110, 2010.

[21] B. Witha, G. Steinfeld, and D. Heinemann, “Advanced turbine parameterizations in offshore

LES wake simulations," in *Extended abstract of the 6th International Symposium on Computational Wind Engineering (CWE)*, 2014.
[22] J. N. Sørensen and C. W. Kock, "A model for unsteady rotor aerodynamics," *J. Wind Eng. Ind. Aerodyn.*, vol. 58, no. 3, pp. 259–275, 1995.
[23] S. Boersma, B. M. Doekemeijer, P. M. O. Gebraad, P. A. Fleming, J. Annoni, A. K. Scholbrock, J. A. Frederik, and J. W. van Wingerden, "A tutorial on control-oriented modeling and control of wind farms," in *American Control Conference (ACC), 2017*, 2017, pp. 1–18.
[24] J. Katz and A. Plotkin, *Low-speed aerodynamics*, vol. 13. Cambridge university press, 2001.
[25] D. Marten, J. Wendler, G. Pechlivanoglou, C. N. Nayeri, and C. O. Paschereit, "QBlade: An open source tool for design and simulation of horizontal and vertical axis wind turbines," *IJETAE*, vol. 3, no. 3, pp. 264–269, 2013.
[26] D. Marten, M. Lennie, G. Pechlivanoglou, C. O. Paschereit, N. V Dy, I. Paraschivoiu, and F. Saeed, "Validation and comparison of a newly developed aeroelastic design code for VAWT," in *35th Wind Energy Symposium*, 2017, p. 452.
[27] E. Branlard, G. Papadakis, M. Gaunaa, G. Winckelmans, and T. J. Larsen, "Aeroelastic large eddy simulations using vortex methods: unfrozen turbulent and sheared inflow," in *Journal of Physics: Conference Series*, 2015, vol. 625, no. 1, p. 12019.
[28] A. J. Rosenberg, "A computational analysis of wind turbine and wind farm aerodynamics with a focus on dual rotor wind turbines," Iowa State University, 2016.
[29] E. S. P. Branlard and A. R. Meyer Forsting, "Using a cylindrical vortex model to assess the induction zone infront of aligned and yawed rotors," in *EWEA Offshore 2015 Conference*, 2015.
[30] E. Branlard, "Velocity Field Upstream of Aligned and Yawed Rotors: Wind Turbine and Wind Farm Induction Zone," in *Wind Turbine Aerodynamics and Vorticity-Based Methods*, Springer, 2017, pp. 321–332.
[31] B. Biegel, D. Madjidian, V. Spudic, A. Rantzer, and J. Stoustrup, "Distributed low-complexity controller for wind power plant in derated operation," in *Control Applications (CCA), 2013 IEEE International Conference on*, 2013, pp. 146–151.
[32] T. Knudsen, T. Bak, and M. Svenstrup, "Survey of wind farm control—power and fatigue optimization," *Wind Energy*, vol. 18, no. 8, pp. 1333–1351, 2015.
[33] T. Horvat, V. Spudić, and M. Baotić, "Quasi-stationary optimal control for wind farm with closely spaced turbines," in *MIPRO, 2012 Proceedings of the 35th International Convention*, 2012, pp. 829–834.
[34] K. E. Johnson and G. Fritsch, "Assessment of extremum seeking control for wind farm energy production," *Wind Eng.*, vol. 36, no. 6, pp. 701–715, 2012.
[35] L. Vollmer, G. Steinfeld, D. Heinemann, and M. Kühn, "Estimating the wake deflection downstream of a wind turbine in different atmospheric stabilities: an LES study," *Wind Energy Sci.*, vol. 1, no. 2, pp. 129–141, 2016.
[36] S. Raach, D. Schlipf, and P. W. Cheng, "Lidar-based wake tracking for closed-loop wind farm control," in *Journal of Physics: Conference Series*, 2016, vol. 753, no. 5, p. 52009.
[37] S. Raach, D. Schlipf, F. Borisade, and P. W. Cheng, "Wake redirecting using feedback control to improve the power output of wind farms," in *American Control Conference (ACC), 2016*, 2016, pp. 1387–1392.
[38] S. Raach, J.-W. van Wingerden, S. Boersma, D. Schlipf, and P. W. Cheng, "$\mathcal{H}\infty$ controller design for closed-loop wake redirection," in *American Control Conference (ACC), 2017*, 2017, pp. 703–708.
[39] Z. Dar, K. Kar, O. Sahni, and J. H. Chow, "Windfarm Power Optimization Using Yaw Angle Control," *IEEE Trans. Sustain. Energy*, vol. 8, no. 1, pp. 104–116, 2017.
[40] P. A. Fleming, P. M. O. Gebraad, S. Lee, J.-W. van Wingerden, K. Johnson, M. Churchfield, J.

Michalakes, P. Spalart, and P. Moriarty, “Evaluating techniques for redirecting turbine wakes using SOWFA,” *Renew. Energy*, vol. 70, pp. 211–218, 2014.
[41] J. R. Kristoffersen and P. Christiansen, “Horns Rev offshore windfarm: its main controller and remote control system,” *Wind Eng.*, vol. 27, no. 5, pp. 351–359, 2003.
[42] E. Bossanyi and T. Jorge, “Optimisation of wind plant sector management for energy and loads,” in *Control Conference (ECC), 2016 European*, 2016, pp. 922–927.
[43] G. Electric, “General Electric - Wind Plant Wake Management Fact Sheet,” *2014*. [Online]. Available: https://www.gerenewableenergy.com/content/dam/gepower-renewables/global/en_US/downloads/brochures/wind-turbine-plant-wake-management-gea31217.pdf. [Accessed: 27-Jun-2017].
[44] Siemens, “Windsight 360.” [Online]. Available: https://www.siemens.com/global/en/home/markets/wind/turbines-and-services/technology/winsight360.html. [Accessed: 18-Jan-2018].
[45] Envision, “Envision - Pioneering Wind Power: smart turbines for every environment.” [Online]. Available: http://www.envision-energy.com/wind-power/. [Accessed: 18-Jan-2018].
[46] K. W. Solutions, “Reliable and robust embedded wind park controller,” 2016. [Online]. Available: http://www.kkwindsolutions.com/Files//Files/Product_and_Service_Sheets/20160322_Wind-Park-Controller.pdf. [Accessed: 18-Jan-2018].
[47] Kongsberg, “Wind farm control.” [Online]. Available: https://www.kongsberg.com/en/kongsberg-digital/renewables and utilities/wind-farm-management-prod/wind farm control/. [Accessed: 18-Jan-2018].
[48] DEIF, “Park control.” [Online]. Available: https://www.deif.fr/wind-power/solutions/park-control. [Accessed: 18-Jan-2018].
[49] S. Hogg and C. Crabtree, *UK Wind Energy Technologies*. Routledge, 2016.
[50] A. Stock, B. Leithead, and H. Yue, “Augmented control for flexible operation of wind turbines,” University of Strathclyde, 2015.
[51] and V. Altin, M., Anaya-Lara, O., Eguinoa, I., Foussekis, D., Göksu, Ö., Astrain Juangarcia, D., Kühn, M., Lampropoulos, N., Merz, K., Petrović, V., Recalde Camacho, L., Rossis, K., Stefanatos, N., “D63.3 Offshore wind turbine control,” 2018.
[52] P. S. Veers, “Three-dimensional wind simulation,” 1988.
[53] V. W. Neilson, “Individual blade control for fatigue load reduction of large-scaled wind turbines: theory and modelling,” *no. March*, pp. 40–54, 2010.
[54] ENTSO-E, “High Penetration of Power Electronic Interfaced Power Sources,” 2017.
[55] Various, “Pathways for the GB Electricity Sector to 2030,” 2016.
inflow,” in *American Control Conference (ACC), 2013*, 2013, pp. 640–646.

Dynamic Wind Power Plant Control for System Integration – Final Report

Dr David Campos Gaona

August 2019

1. Introduction

This report presents the activities carried out in the Supergen Wind Hub Flexible Fund project Dynamic Wind Power Plant Control for System Integration started in August 2016 and Finished in July 2018.

The project had as general objective to strengthen wind farm control capabilities by changing the conventional philosophy of controlling individual turbines to a holistic wind farm control approach through the implementation of more advanced control strategies that will realize the grid-friendly offshore power plant. In order to do so, this project used a holistic and hierarchical control approach, built upon the Power Adjusting Control (PAC) concept to provide the full range of ancillary services including synthetic inertia at the wind farm level rather than single turbine level. Figure 1 show the PAC concept applied to a wind turbine where an additional controller is added to the full envelop controller of the wind turbine to regulate its power output. At wind farm level the power output of each turbine is regulated by a wind farm controller to provide an aggregated response.

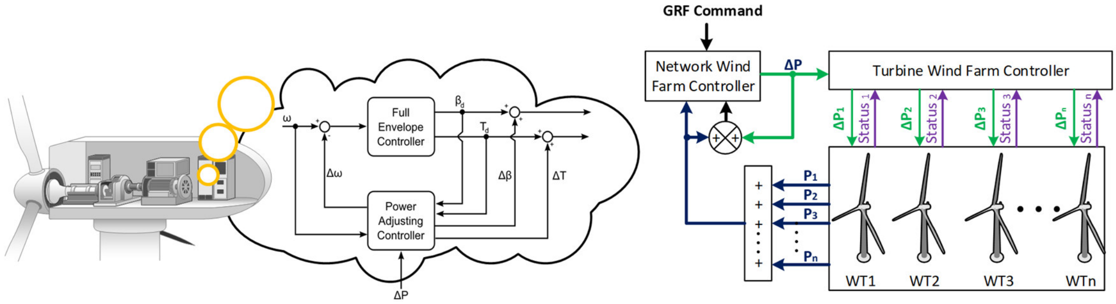

Figure 1 The power adjusting control concept at turbine and wind farm level

In order to detect a system frequency event and coordinate the action of a PAC-controlled offshore wind farm, this project uses a fully instrumented small/medium synchronous generator at the wind power plant point of connection. Additionally, by slaving the wind farm (or more accurately the wind farm controller) to the generator, the wind farm also provides ancillary services similar to the generator but greatly scaled up. This methodology is referred in this report as the Generator Response Following (GRF) concept. A schematic diagram of the GRF concept is presented in Figure 2. The GRF controller uses feed forward systems to provide immediate dynamic response from an HVDC-connected wind farm when communication delays prevent an immediate response from a distant offshore wind farm.

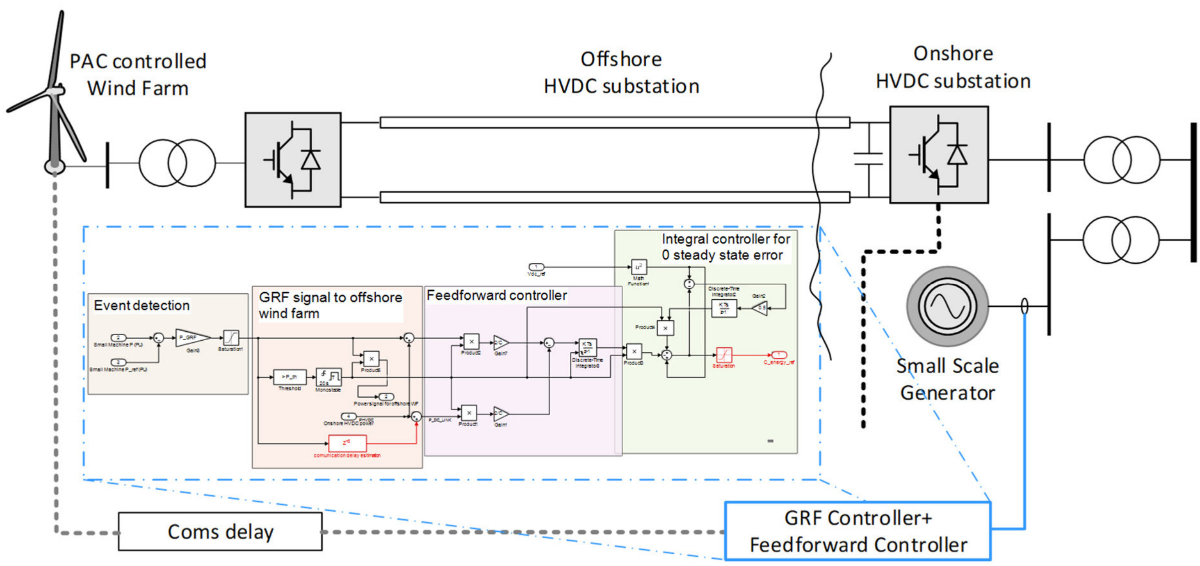

Figure 2 The Generator Response Following concept in a HVDC connected offshore wind farm

2. Model development

2.1 Development of a multi-machine system for frequency excursions.

A complex multi-machine system consisting of 4 Generators, governors, transformers, transmission lines and VSC-HVDC converters was developed to create a network for testing the Generator-Response Following concept. The multi machine model consist of three high power generators and one medium size generator. The power output of the medium size generator is used to command a PAC emulator at the offshore wind farm for synthetic inertia using the Generator-Response Following concept. The PAC-Based wind farm emulator is connected to in-house-developed fully featured VSC-HVDC transmission system controlled by two degrees of freedom internal model controllers. The wind farm is composed of an aggregated model of a type-4 PMSG wind turbine. The multi-machine model initial parameters and steady state power flow have been calculated and implemented in the model. This reduces the time of simulations since there is no initial transient states. Figure 3 shows a picture of the developed Simulink model.

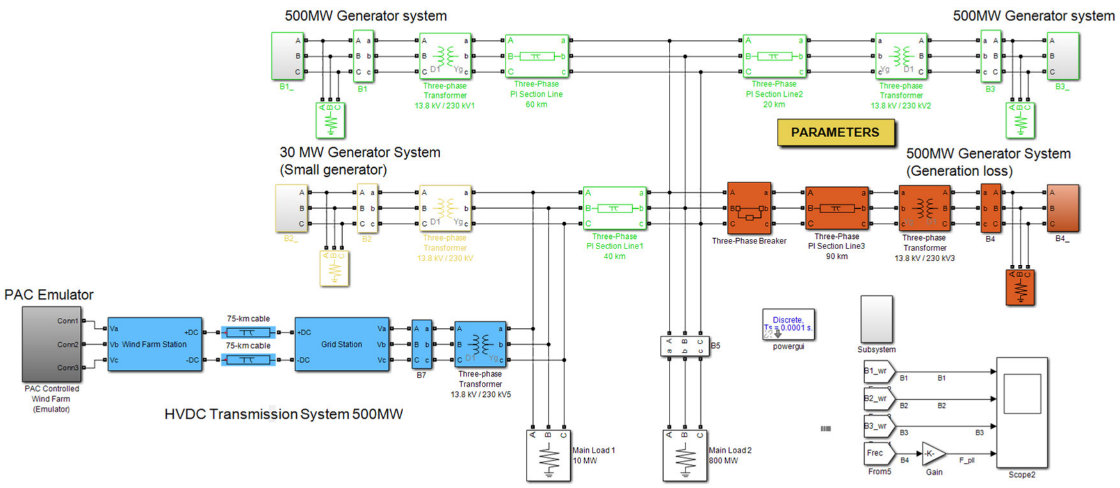

Figure 3 Multi-machine model for Generator-Response Following concept testing.

The multi machine AC grid runs from an initial state condition where all the machines are in steady state providing a significant fraction of its power to the grid loads. The initial condition for the multi-machine system was obtained by running power flow analysis. During the power flow analysis, the HVDC system was substituted with a generic 500MW machine to obtain its steady stage power injection. Once the steady state conditions were obtained, these were embedded within the B2B system resulting in a full steady state operative condition for the simulated grid. The excitation of each machine system was calculated to provide 1 PU of AC Voltage at the terminal of the generator.

The initial steady state power reference for each machine and the HVDC converter is shown in Table 1.

Table 1 Steady state power reference of generators and HVDC system in the simulated in the AC grid

Machine	Rated Power	Steady state power reference in PU
Hydro Generator	500MVA	0.889858
Turbo Generator 1	500MVA	0.698066
Generic Generator (loss of generation)	400MVA	0.669803
HVDC converter	500MVA	0.916192

2.2 Development of the HVDC system

The HVDC converter consist of two voltage-source converters (VSC) interconnected via a common DC link using transmission cables. Each VSC consist of a 2-level three-phase converter. For a proper functioning of a VSC-HVDC system the grid side converter (GSC) and offshore converter should work in a coordinated manner where whatever energy injected to the offshore wind converter by the offshore wind farm should be the same energy that the GSC converter delivers to the AC grid.
The HVDC converter is capable to produce an AC voltage simultaneously at the offshore converter and at GSC by the action of the power electronic switches. The AC current can flow in any direction (i.e. positive or negative) with respect of the voltages of the converter. The magnitude and direction of the currents with respect of the voltage of the GSC will define if the VSC converters are working in a rectifiers/inverter configuration or vice versa.
In the case of an offshore wind farm system, the offshore station will usually work as a rectifier, i.e. the AC power from the wind farm will be rectified as DC power that is transmitted to the GSC via the DC cables. The GSC will usually work as an inverter where the DC power in the DC link will be converted to AC power and delivered to the grid.
Figure 4 shows the different controllers and subsystems that were deployed in the HVDC converter system.

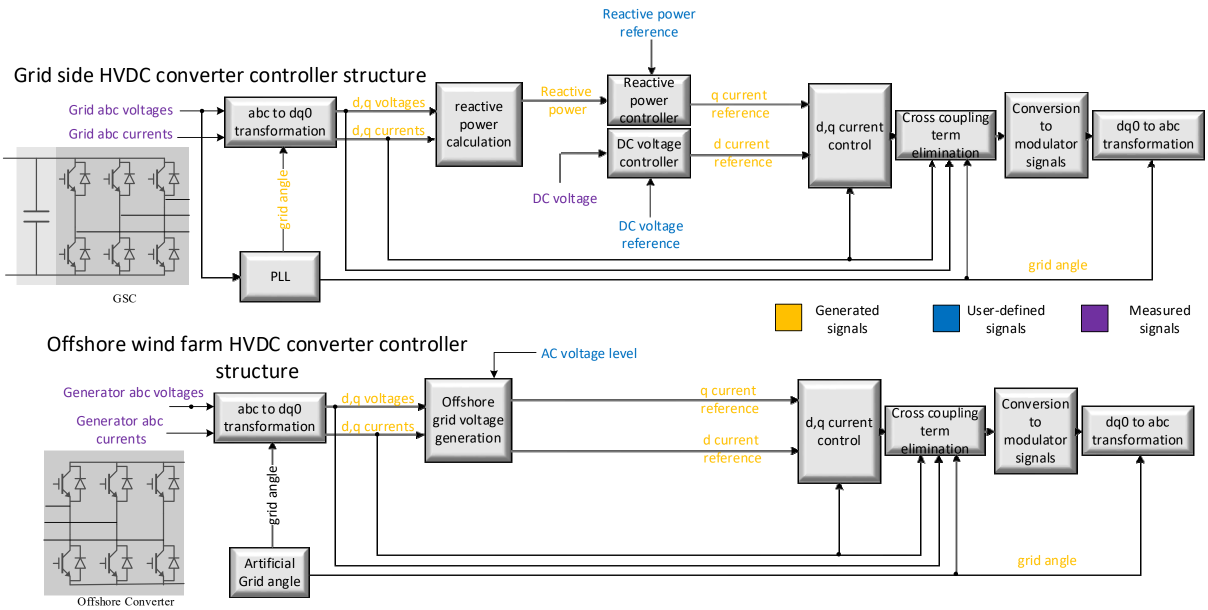

Figure 4 Controller structure of the offshore converter and GSC converters of the HVDC system

Figure 5 shows the Simulink implementation of the GSC along with its main controllers and its user interface. As seen in the figure the Simulink model consists of a 2-Level VSC interconnected to the grid via a LR filter. The VSC works in average model of operation, meaning the voltages at its terminals are not produced by the switching of power electronics, rather they are a multiplication of the modulator signals with the DC voltage. By using average mode of operation of the VSC, the simulations of the whole grid can be carried out using sampling times of 50-100 microseconds, which are suitable to analyze power system phenomena. The average simulation of a VSC reproduces faithfully the fundamental frequency dynamics of a VSC without the need of smaller sampling times to include the switching of the power electronic devices. Since this developed AC networks has the purpose of studying electromagnetic and electromechanic transients, but not high frequency harmonics product of power electronic switching, the average simulation of the VSCs is considered enough for the simulation needs of this project.

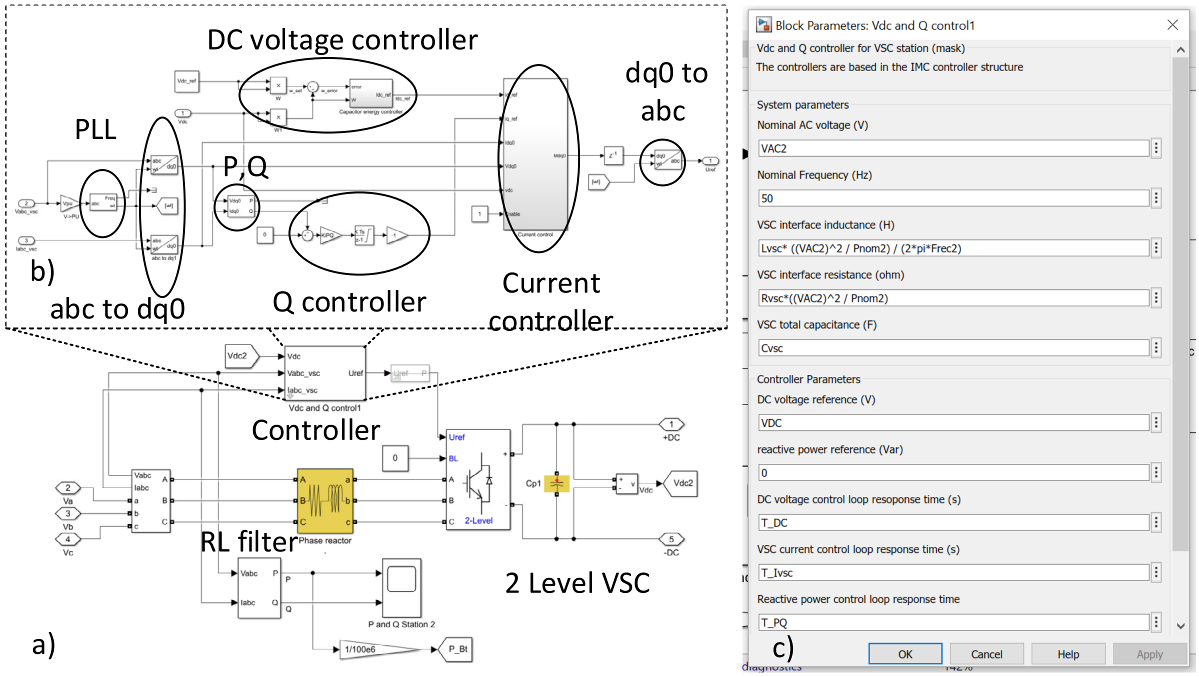

Figure 5 Simulink implementation of the GSC. a) Simulink Model, b) Controller structure, c) controller user interface

Figure 5 b) shows the internal structure of the GSC controller, this structure follows the layout presented in Figure 4. Figure 5 c) shows the user interface of the GSC controller. This user interface requests from the user parameters of nominal voltage and frequency of the grid, as well as the value of in inductance and resistance of the RL filter and the value in capacitance of the DC circuit. Latter on, the interface requests the references for the DC voltage and reactive power controllers. Finally, the response-time of the control-closed loops of the DC voltage, reactive power and GSC currents is requested. The response time selection allows the user to define how fast the closed loop controller will track a set point change. For example, a response time of 0.01ms for the DC voltage loop implies that the gains of the controllers are adjusted to deliver a control action that will change the DC voltage from a previous reference into a new reference in 0.01 ms (more specifically the response time defines the "rise time" required by the response to rise from 10% to 90% of its final value).

2.3 Use of 2DF IMC for improved disturbance rejection in the HVDC DC voltage controller.

The use of feedforward controllers to provide immediate response in case of frequency excursions requires the use of energy stored in the DC capacitors of the HVDC link. To do so in a fast and accurate manner, an additional control loop has to be added to the DC voltage controller. This additional control loop commands the DC voltage to follow a specific "shape" which is then translated in a release of stored energy from the HVDC capacitors. This energy follows the natural power output of a synchronous generator during a frequency excursion for a period of hundreds of milliseconds until the delayed action of the offshore wind farm takes place. Nevertheless, having precise control of the DC voltage during this event is not a trivial task because of the poor disturbance rejection characteristics of the DC plant (i.e. a plant with a pole in the origin). This is because the delayed action of the offshore wind farm is reflected as a sudden disturbance in the control loop regulating the DC voltage, which if not dealt with properly, affects the capability of the onshore HVDC station to mimic the response of the medium-size generator. To deal with this problem the robust control technique of two degrees of freedom internal model control is used.

The internal model control (IMC) technique relies on the "internal model" principle whose philosophy states that a control action over a plant can be achieved only if the control system includes, either implicitly or explicitly, some representation of the process to be controlled [9, 10]. Figure 6 show the structure of the IMC.

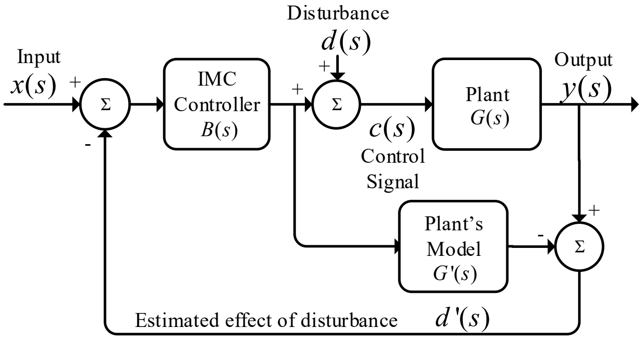

Figure 6: IMC Controller Structure.

As seen in Figure 6, the model of the plant to be controlled ($G'(s)$) is to be an exact representation of the plant itself ($G(s)$) and considering that no disturbance is present, then the estimated effect of disturbance $d'(s)$, resulting from the difference between the plant output and the plant model output, turns zero and the close loop system turns equal to the open loop system. On this condition, an IMC controller of the type $B(s) = G'^{-1}(s)$ implies a perfect theoretical control then. However, such ideal control cannot be implemented by two main reasons,

a) The need of use pure differentiators, (in case the model of the plant is proper)

b) Infinitely large excursions of the manipulative variable for infinitely small high frequency disturbances (which cannot be implemented realistically in any digital or analog controller).

For a realizable control, the IMC structure introduces a low pass filter $L(s)$ in cascade to the IMC controller. The filter is designed to add poles to $G(s)$ in order to turn the controller transfer function proper. The filter $L(s)$ is usually of the type

$$L(s) = \left(\frac{\alpha}{s+\alpha}\right)^n \quad (1)$$

Where the order of the filter, n, is chosen accordingly to the order of $G(s)$, and α is regarded as the closed loop bandwidth of the filter, for a first order filter.

The IMC controller has the advantage of having the controller parameters related in a unique, straightforward manner to the model parameters with α being the only controller variable to be adjusted.

2.3.1 The need of an additional degree of freedom for poorly damped processes.

When there is a set-point change in a closed loop control system, the mathematical inertia of the controller combines with the physical inertia of the process; this combination damps the process's response to a set-point change. However, if an unexpected load ever disturb the process abruptly, a set point tracking controller will tend to overreact and cause the process variable to oscillate unnecessarily. This is because a set point tracking controller does not plays a significate role in determining how the process reacts to a disturbance, as such, the load disturbance rejection of the closed loop system, even with the use of a fast IMC or PID controller, is still determined by the process (see Figure 7).

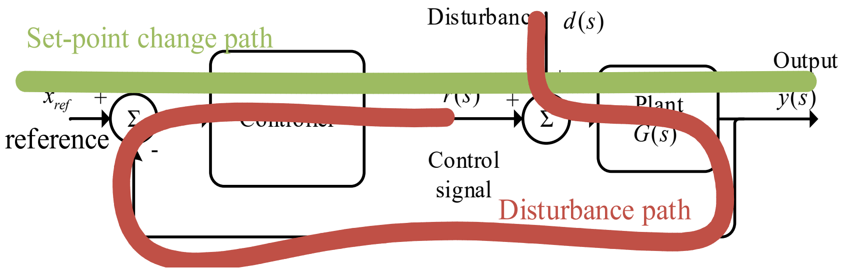

Figure 7 Set-point and Disturbance Paths in a Closed Loop Controller

To further improve the performance of the IMC controller, an inner feedback loop to R can be added to provide an additional degree of control freedom to speed up the load disturbance rejection a poorly damped plant. This additional control loop is used to speed up the natural response of the plant by moving the pole of the plant away from the origin within the negative side of the real axis. The configuration of the additional control loop is shown in Figure 8.
By adding a feedback loop the transfer function of the improved plant $M_{dc}(s)$ turns to be

$$M(s) = \frac{G(s)}{1+G(s)R} = \frac{1}{G^{-1}(s)+R} \tag{2}$$

where $M(s)$ is the new transfer function of the plant augmented with an inner feedback loop gain R.

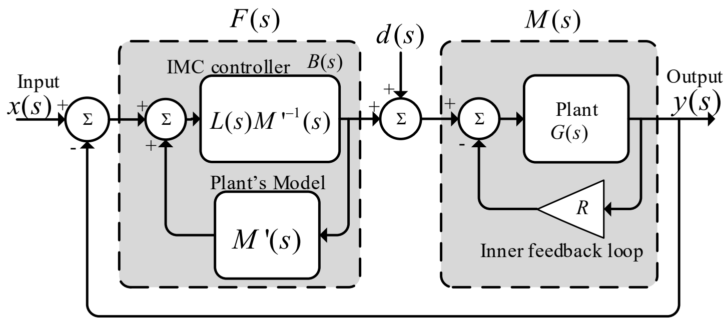

Figure 8: The Two Degrees of Freedom IMC Configured as a PI Controller

This IMC with two degrees of freedom is especially useful for the poorly damped systems of the HVDC system such as the DC circuit.
The processes to be controlled using the two degrees of freedom IMC controller are the $d\,q$ currents and the DC voltage. The transfer functions of these processes are given by a first order transfer function, implying a first-degree filter for their respective IMC controller. Under this consideration the transfer function of the IMC control $F(s)$ (considering that $M'(s)$ is the model of $M(s)$) is shown in equation(3)

$$F(s) = \frac{B(s)}{1-B(s)M'(s)} = \frac{L(s)M'^{-1}(s)}{1-L(s)M'^{-1}(s)M'(s)} = \frac{\alpha}{s}M'^{-1}(s) \tag{3}$$

The additional degree of freedom is chosen, in each case controller case, to make the process dynamics as fast as the controller dynamics. This allows the load disturbance rejection to be as fast as the controllers closed loop dynamics. To achieve this, the pole R is set in the inner feedback loop to match the pole of the IMC controller in the transfer function from the disturbance $d(s)$ to output signal of the plant $y(s)$, which is:

$$\frac{y(s)}{d(s)} = \frac{M(s)}{1+F(s)M(s)} = \frac{M(s)}{1+(\alpha/s)M'^{-1}(s)M(s)} = \left(\frac{s}{s+\alpha}\right)\frac{1}{G^{-1}(s)+R} \tag{4}$$

If R is chosen appropriately, equation (4) can be reduced to

$$\frac{y(s)}{d(s)}=\left[\left(\frac{s}{s+\alpha}\right)\frac{K}{s+\alpha}\right]=K\left[\frac{s}{(s+\alpha)^2}\right] \tag{5}$$

where K is a constant.

As can be notice in equation (5), the load disturbance $d(s)$ is damped with the same time constant as the closed loop control.

The IMC controller closed loop bandwidth α is chosen accordingly the rise time t_r needed for the output signal $y(s)$.

To illustrate the advantages of using the two degrees of freedom IMC Figure 9 shows a simulation result where a first order plant is controlled by a PI using technical optimum (pole-zero matching) and the same plant is controlled using an IMC controller. Both controllers are exposed at a set-point change at t=0.1 and then to a disturbance at t=0.2. As seen in Figure 9 both the PI controller and the IMC controller respond with the same dynamics for a set point change, however a much better transient response (in terms of overshoot and settling time) is provided by the 2 degrees of freedom IMC during a disturbance.

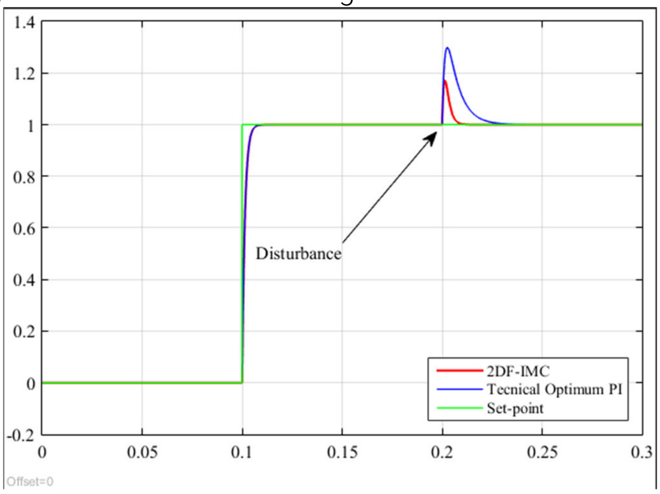

Figure 9: IMC and PI Controller Transient Response Comparison for a First Order Plant

2.4 Development of wind turbine electric models.

Two high-order models of wind turbines (Type-3 and Type-4) where designed in Matlab Simulink for Averaged and Commuted simulation. Both systems are controlled using the two degrees of freedom Internal Model Controllers for all their internal control loops. Since the control constant of the system are in function of the parameters of the turbines, (because of the use of the Internal Model control procedure) the user of the models requires only providing the parameters of the electrical system of the turbine and the closed loop response time of the controllers. This feature has proven beneficial for the ad-hoc use of the models in different electric grid configuration and for different electrical characteristics and power ratings. The speed of simulation and stability of the developed type-3 model (for both averaged and commuted simulation) is higher with respect of the generic type-3 models provided by Simulink (23% faster). The type-4 model developed also share the same characteristics of stability and speed-of-simulation of the type-3 model, however it cannot, yet, be compared with a generic model from Simulink, since this type of model is not yet available in the Simulink libraries.

Figure 10 shows the developed Type-3 Wind Turbine Model, additionally Table 1 Summarizes the advantages of the developed Type-3 wind turbine model when compared with the DFIG model provided in the Simulink demos.

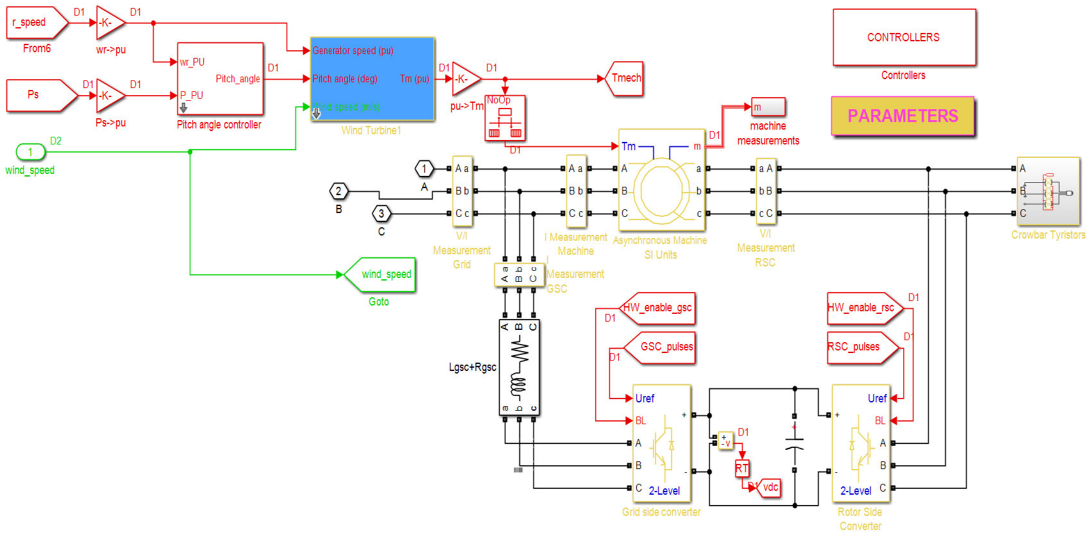

Figure 10 Developed Simulink Model of a Type-3 (DFI) wind turbine

Table 2 Comparison Table between the developed DFIG model and the Matlab model provided in Simulink

MODEL	CONTROLLERS	SIMULATION SPEED	MODERN FEATURES	EASINESS TO MIGRATE TO CUSTOM MODELS
Developed DFIG Model	• Based in the IMC controllers • All control parameters are calculated automatically based in the parameters of the system. User only specifies desired speed of response (bandwidth) of the controller	23% Faster than Simulink Model (using Simulink Profiler)	• Crowbar protection • Fault tolerant Robust controllers with active damping	• High portability • Parameters are embedded, no need of initialization variables.
Matlab	• PI controllers • Unknown tuning rules, • No documentation, • Change in parameters of the machine renders the system inoperable	Nominal Simulation Speed	• No crowbar protection • No fault tolerant controllers.	• Very reduced portability • requires internal initialization files (not available for the users) and initial conditions

Figure 11 Shows the developed Type-4 Wind Turbine Model, additionally Table 2 Summarizes the advantages of the developed Type-4 wind turbine model when compared with a similar (but less advanced in its power electronic topology) model provided in the Simulink demos.

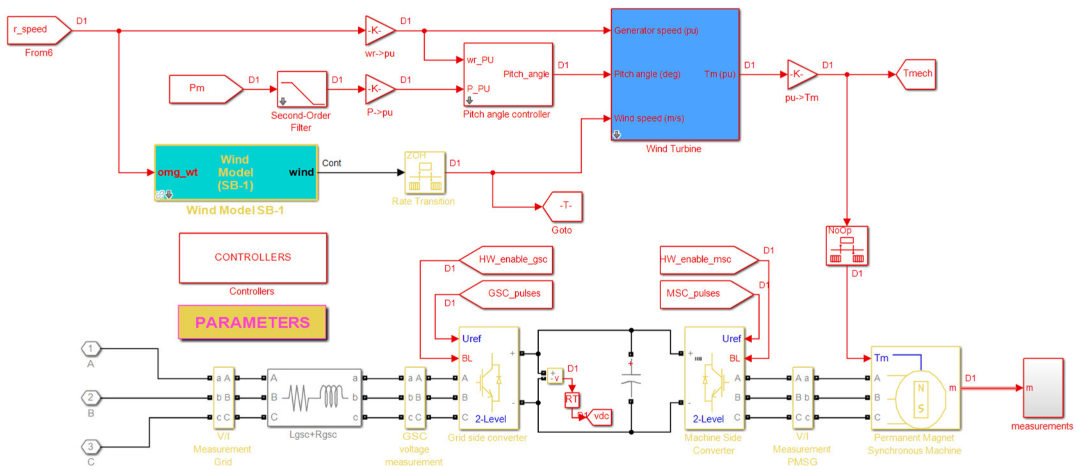

Figure 11 Developed Simulink Model of a Type-4 (FRC) wind turbine

Table 3 Features of the Developed FRC model when compared with a similar model of Matlab.

MODEL	Power Electronics architecture	CONTROLLERS	MODERN FEATURES	EASINESS TO MIGRATE TO CUSTOM MODELS
Developed FRC Model	• Based in Back to Back Voltage Source Converter	• Based in the IMC controllers • All control parameters are calculated automatically based in the parameters of the system. User only specifies desired speed of response (bandwidth) of the controller	• DC Chopper • Fault tolerant Robust controllers with active damping	• High portability • Parameters are embedded, no need of initialization variables.
Matlab (Less advanced power electronic topology)	• Based in uncontrolled rectifier in the machine side converter and Voltage Source Converter in the Grid side Converter	• PI controllers • Unknown tuning rules, • No documentation, • Change in parameters of the machine renders the system inoperable	• No DC Chopper • No fault tolerant controllers.	• Very reduced portability • requires internal initialization files (not available for the users) and initial conditions

The result of using an in-house controller for the DFIG wind turbines allowed a much finer tuning of the controllers involved in the maximum power tracking of the wind turbine (such as the Electrical Torque and the current controllers). The result is a higher power production for the same model of wind turbine (same mechanical and electrical characteristics) provided by the Matlab model. To evidence this, Figure 12 shows a comparison of the performance of a 1.5MW DFIG wind turbine when controlled with the in-house developed controllers (purple color) and the Matlab demo controllers (blue color). As seen in Figure 12, the in-house developed controllers enable a higher production of mechanical and electric torque; this is because the speed of the wind turbine is able to track more efficiently the maximum power curves. The result is an overall increased active power production for the same wind turbine with the same wind input characteristics.

Additionally, the developed models include the latest fault-ride-through measurement implemented in modern wind turbines such as crowbar protection fault tolerant controllers that are not implemented in the generic Matlab Models.

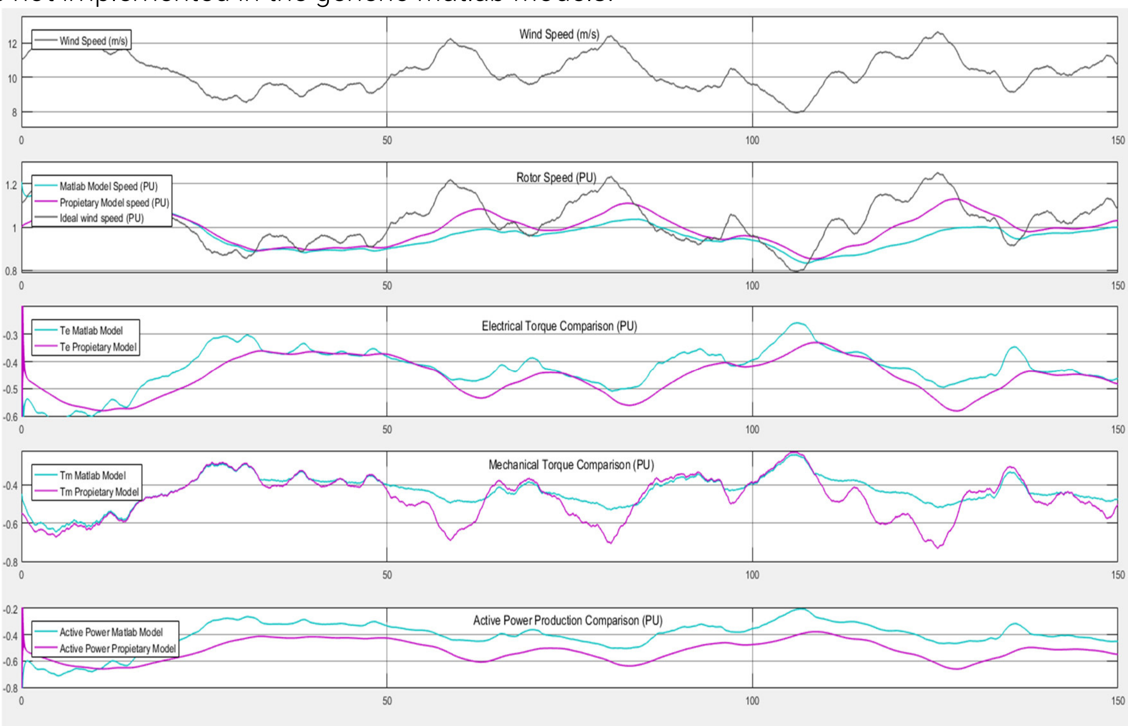

Figure 12 Performance Comparison of Matlab and Developed DFIG model.

Regarding the modeling of power electronic converters, the developed model have the capability of simulating the power electronic switching (for studies of harmonics or power electronic losses) or use ideal averaged representation of the power electronic converters (for faster simulation and electromechanical transient studies). The dynamics of the controllers are not affected by using the model in averaged or switched power electronic configurations.

3. Evaluation of the Generator Response Following Concept

3.1 Evaluation of the Generator Response Following Concept assuming constant wind speed and no communication delay.

Figure 13 shows the performance of the multi-machine test model when a sudden loss of a generator at t=10s affects the frequency of the system. Figure 13 includes the behavior of the test model when the Generator-Response Following (GRF) is disabled (purple plots) and when the GRF is enable (green plots). As seen in Figure 13 a) the frequency rate of change and drop of system frequency is reduced when GRF is enabled. Figure 13 b) shows the power output of the medium size generator during the frequency excursion. As seen in Figure 13 b) the natural inertia response of small machine generates a peak of extra power above the power reference of the machine (blue line). When the FRF is enable, the magnitude and shape of extra power generated by the small generator is magnified 16 times by the VSC-HVDC station, as seen in Figure 13 c). Figure 13 d) shows a comparison in PU of the inertial power of the small generator against the power output in PU of the VSC-HVDC system. As seen in Figure 13 d) the magnitude and shape of the inertial power of the small generator is replicated with minimum change by the VSC-HVDC when the GRF is enable. These simulations assume zero delay in the transmission of the power command to the PAC-Controlled Wind Farm.

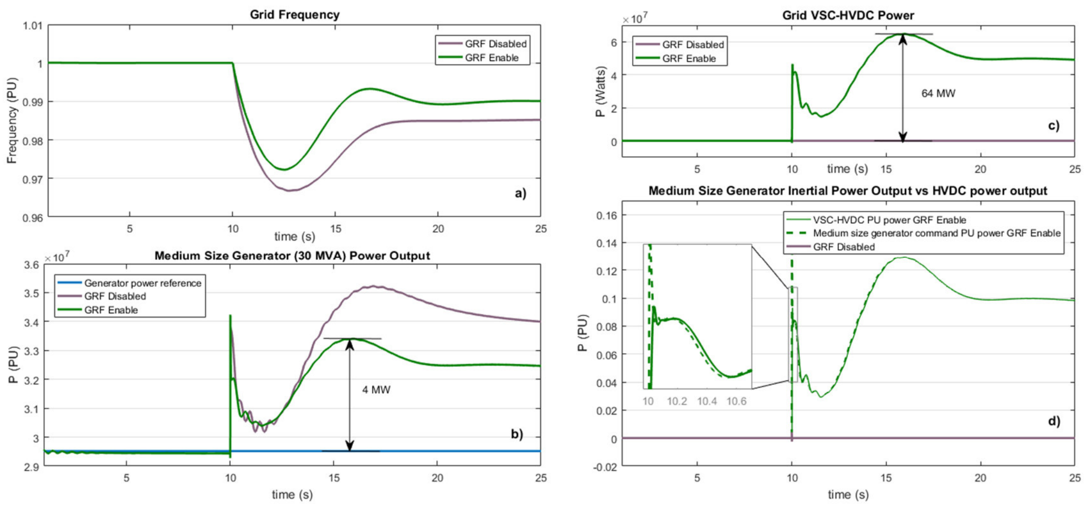

Figure 13 Behavior of the Multi-machine model for Generator-Response Following concept control assuming no communication delay

3.2 Effects of time delay in the PAC-Controlled wind Farm

If time delay is included in the simulation, and no instantaneous energy extraction from the DC capacitor takes place, then the delayed response of the wind farm to a frequency excursion event produces an instability mode with the medium size generator connected at the point of common coupling of the offshore wind farm as seen in Figure 14. This shows the need to compensate the delay in communications using a feed forward loop in the onshore HVDC system to provide immediate artificial inertial response in a frequency event.

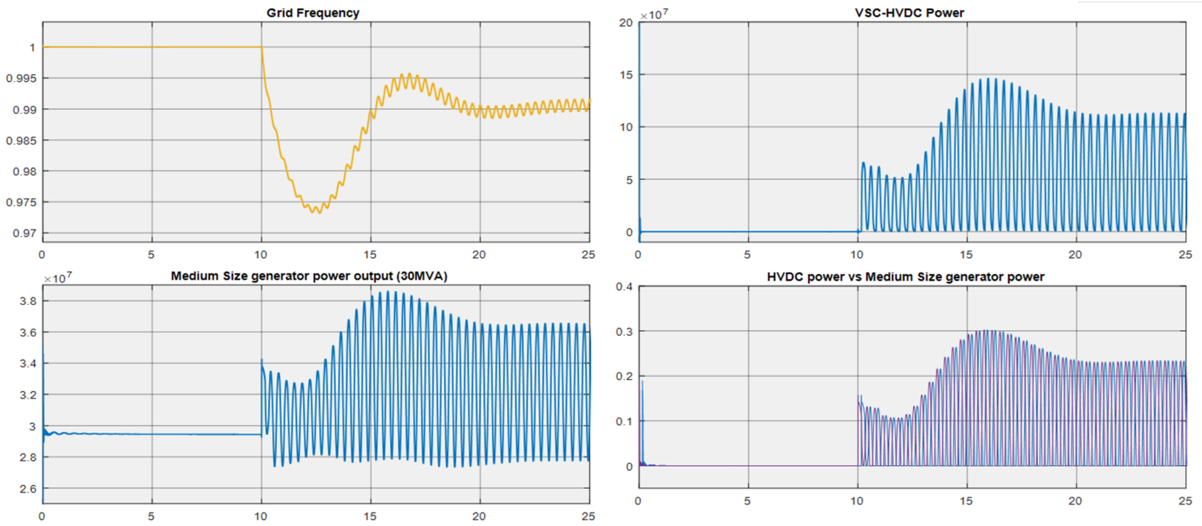

Figure 14 Effects of a 150ms delay in the PAC controlled wind farm using the GRF concept.

3.3 The feed forward controller for the GRF concept.

The feed forward controller is composed of several stages to implement the GRF concept in the offshore wind farm. These stages are described next.

<u>Event detection</u>

This stage compares the power output of the medium scale generator against its power output set point. Whenever the output power of the generator is higher than its set point this could be an indication than a frequency event has happened, however in order to differentiate between a steady state governor action and a frequency excursion, a threshold to activate the GRF signal is incorporated in the detection mechanism. This threshold is user selectable and should be defined based in the droop constants of the medium scale generator. A small droop constant makes the generator governor more sensible to steady state frequency variations. A large droop constant makes governor less sensible to frequency variations which in turn implies less steady state deviation from its power set point.

<u>The GRF signal to offshore wind farm stage.</u>

After a positive detection of a frequency excursion the signal to the offshore wind farm to produce extra power (following the behaviour of the medium scale generator) is sent to the master PAC controller of the offshore wind generators. The duration of the GRF signal (i.e. the time the offshore wind farm power output should follow the behaviour of the medium scale generator) is a user-configurable variable. This duration is selected based in the reasonable synthetic power output capabilities of the offshore wind farm.

<u>The feedforward controller</u>

The feedforward controllers discharges the DC voltage of the HVDC link Capacitors to provide immediate synthetic inertia response following the “shape” of the power output of the medium size generator. The feedforward controller modifies the set point of capacitor energy controller (the voltage controller) in order to reproduce the requested power output of the GRF signal. The feedforward controllers relies in the robust controllers deployed in the HVDC DC system to faithfully represent the power dynamics needed. As explained previously, the DC voltage controller of the HVDC has increased load disturbance rejection capabilities thanks to the use of the 2DF-IMC controllers. The feedforward controller also takes into account the delayed energy provision from the Wind Farm in order to reduce the effects of such energy in the instantaneous value of the DC voltage. Any misshape of the DC voltage implies an inaccurate representation of the instantaneous synthetic inertia provision from the HVDC.

Integral controller for zero steady state error.

The integral controller has as objective to bring back the DC voltage to its set point level after the GRF action. The speed of response of this controller is much slower than the feedforward controller. Thanks to this, the feedforward controller can take priority during frequency excursions without being affected by the dynamics of the integral controller. After the GRF action is complete, the integral controller restores the nominal value of DC voltage to the HVDC link. Additionally this section of the controller contains a saturation element to limit the energy extraction from the DC capacitor.

The different stages of the feedforward controller are shown in **Figure 15**.

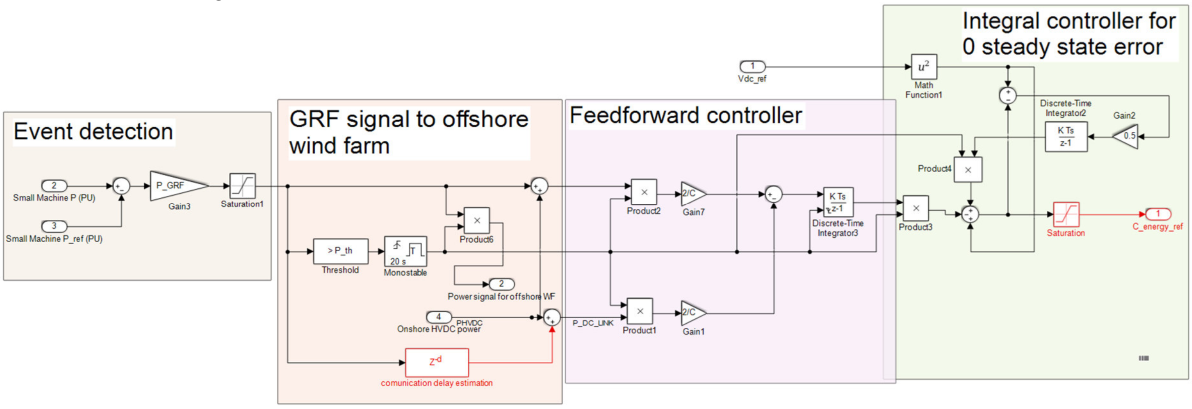

Figure 15 The GRF feedforward controller

3.4 Evaluation of the Generator Response Following Concept assuming constant wind speed and communication delay with feedforward controller.

Figure X show the behaviour of the multi-machine system during a frequency excursion with the GRF controller with feedforward for a case of communication delay of 150ms.

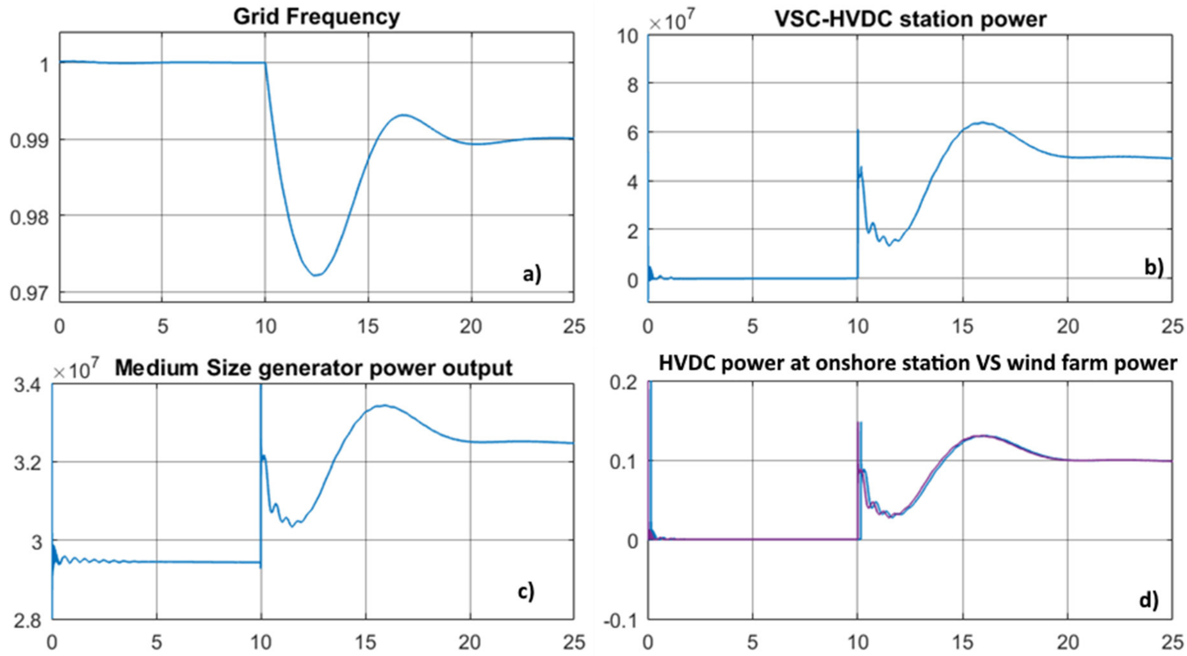

Figure 16 Behavior of the Multi-machine model for Generator-Response Following concept control with communication delay of 150ms and feedforward controller

As seen in Figure 16 b) the power output of the HVDC station follows the behavior of the medium size generator in a stable manner. The communication delay makes the power from the offshore wind farm to lag with respect to the GRF command. However, the power output of the HVDC station is immediate as seen in the graph HVDC power at onshore station vs wind farm power in Figure 16 d).
To enable immediate action of the onshore HVDC station during a frequency event, the feedforward controller extracts energy from the DC capacitors and injects it to the AC grid. **Figure 17** shows a comparison between a GRF controller action for the system with no communication delay and for the system with communication delay of 150ms. As seen in **Figure 17** a) the frequency response in both cases is very similar thanks to the action of the feedforward controller in the case of delay of communications. The action of the feedforward controller affects the magnitude of the DC voltage as seen in **Figure 17** b) however the DC voltage reduction does no compromise the proper functioning of the HVDC converter.

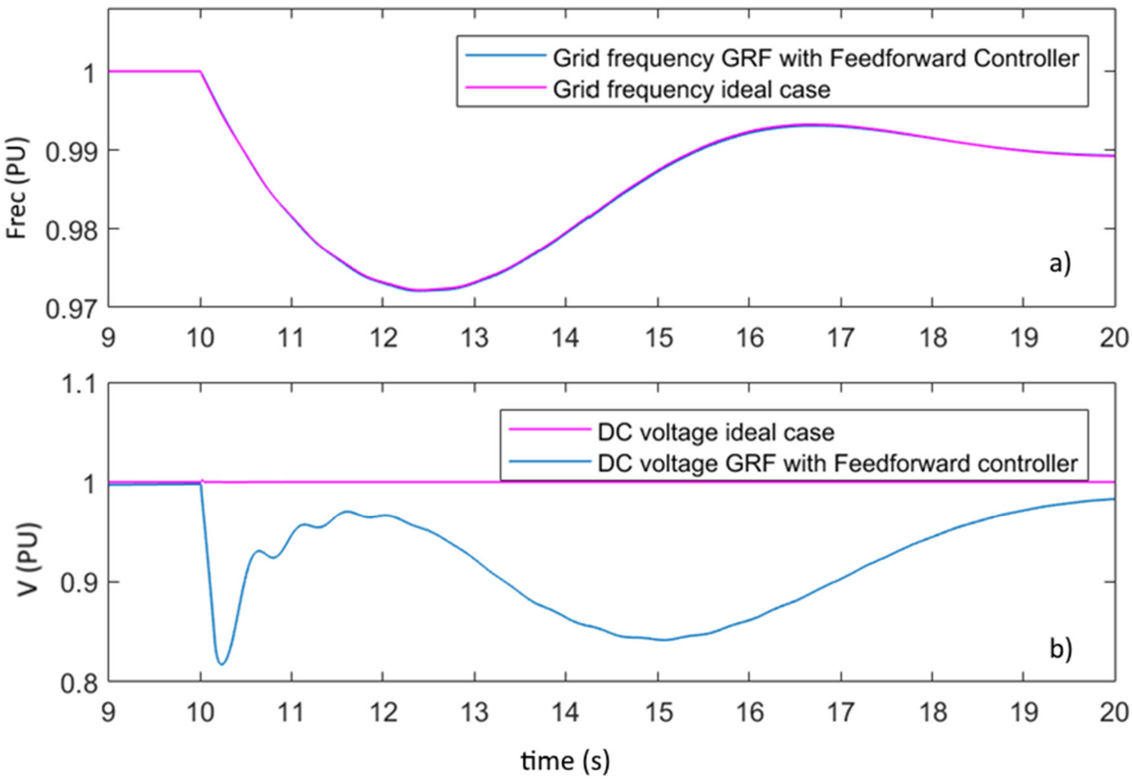

Figure 17 Comparison of HVDC DC voltage for a GRF action with no delay and with communication delay. a) Grid frequency b) HVDC voltage

3.5 Evaluation of the Generator Response Following Concept assuming variable wind speed and communication delay with feedforward controller.

Having a variable wind power generation implies having a continuous power adjustments from all the generators to keep the grid frequency constant. Each generator supplies power to the grid based in their droop controller and governor constants. The small-medium generator of the GRF concept will also change its power output based in the change of wind power provision. Since the GRF concept is designed to function only during mayor frequency perturbations, the GRF controller implements an actuation threshold value and the controller constant of the small-medium machine governor (specially the droop constant) were selected to reduce the sensitivity of the governor for small frequency excursions.

To demonstrate the action of the controller under a variable wind speed conditions Figure 18 shows the behavior of the GRF model multi-machine test model when a sudden loss of a generator at t=10s produces a sudden frequency drop. As seen in Figure 18 a) the frequency of the grid is affected by the variability of the wind power provision. At t=10s the frequency drops triggering an inertial and governor response from the small machine of the system as seen in Figure 18 b). Figure 18 b) shows that the small machine was working close to its set point prior the frequency excursion. The small difference between the small machine power output with its reference point is because of the droop control in the machine governor. When a frequency excursion happens, the DC capacitor of the onshore VSC-HVDC substation injects some active power to the grid by command of the feedforward controller. This causes the DC voltage to oscillate following the feedforward power provision command, as seen in figure Figure 18 c). Figure 18 d) shows the power output command from the GRF controller in blue. The PAC controller, as seen in the red plot in Figure 18 d), applies this power output command (after a short delay because of the communication channel). The GRF power command lasts for 20 seconds. After this, the power signal command resets and the PAC controller gradually decreases its power output following its internal dynamics. Finally, Figure 18 f) shows the power output of the VSC-HVDC system. This power output includes the energy provided by the GRF (i.e the feedforward controller and the PAC) and the wind power.

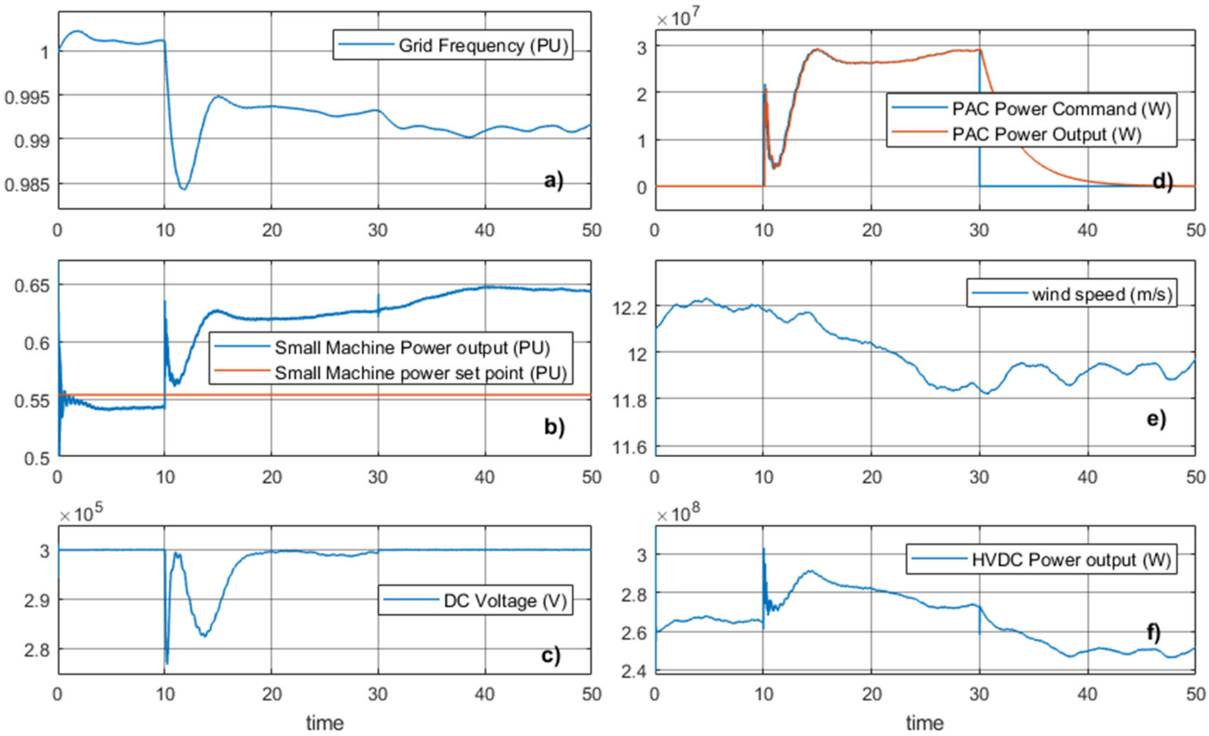

Figure 18 Behavior of the multi-machine system with a variable wind power input and the GRF controller

Figure 19 shows a comparison of the behavior of multi machine system when the GRF controller is enable vs when the GRF controller is disabled. The simulation with the GRF controller active are shown in blue and the simulations with the inactive GRF are shown in red. As seen in Figure 19 a), when the GRF controller is active, the frequency profile of the grid has a positive impact thanks to the extra power provided by the PAC-controlled offshore wind farm. Figure 19 b) shows the power output of the small machine. Here when the GRF is active, the extra power provided to the grid by the offshore windfarm reduces governor response of the small machine. When the GRF is inactive, the small machine is forced to provide more power output to try to compensate the frequency drop. Figure 19 c) Show the voltage profile of the HVDC link. When the GRF controller is active (blue plot), the feedforward action of the controller extracts energy from the DC capacitor to compensate the delay in power provision from the

PAC controlled offshore wind farm. This action makes the DC voltage to fluctuate, however this fluctuation is within the safe margin of operation of the HVDC system. The feedforward controller enforces this margin. Figure 19 d) shows the extra power output of the wind farm driven by the PAC controller. When the GRF is active, the PAC provides a power output following the power profile of the small machine as seen in the blue plot. When the GRF is inactive, the PAC commands no extra power provision from the wind farm as show in the red plot. Finally, Figure 19 f) shows the power output of the HVDC system. This power output follows the profile of the wind model. When the GRF is active, the HVDC power includes the energy provided by the GRF during frequency excursions (i.e the feedforward controller and the PAC) and the wind power. When the GRF is inactive, the HVDC power output is just the wind power minus the transmission and conversion losses.

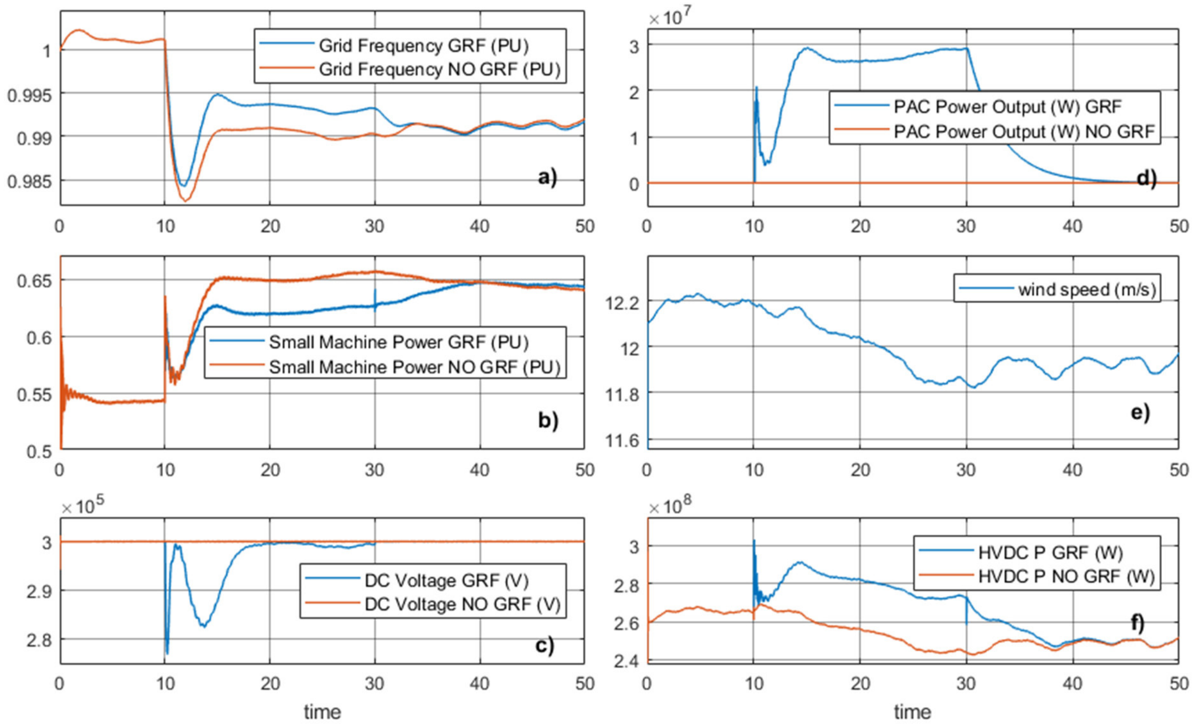

Figure 19 Comparison of the multi-machine system dynamics when the GRF controller is enabled/disabled.

To demonstrate the accuracy of the GRF controller in following the power output of the small-medium machine and the effects of modifying the governor constants of the small machine are shown in Figure 20. In this series of experiments the governor droop constant (D) is selected to be 0.06 (most sensitive to frequency variation), 0.09,0.2 and 0.6 (least sensitive to frequency variations). Figure 20 shows the effects of changing D in the grid frequency (Figure 20 a) the power output of the small machine (Figure 20 b) the HVDC dc voltage (Figure 20 c) The power provided by the PAC controller (Figure 20 d) and the HVDC power output (Figure 20 f). A seen in the plot in Figure 20 the GRF controller is able to follow the small generator in a wide range of governor settings. Another conclusion obtained from Figure 20 a) and b) is that the immediate power output response of the small generator during a frequency excursion is mostly based in its internal dynamics and not in the governor constants. As such, if the GRF is used to reduce the initial frequency drop of the grid, then the gain of the GRF controller should be increased. The effects of doing this are shown in Figure 21.

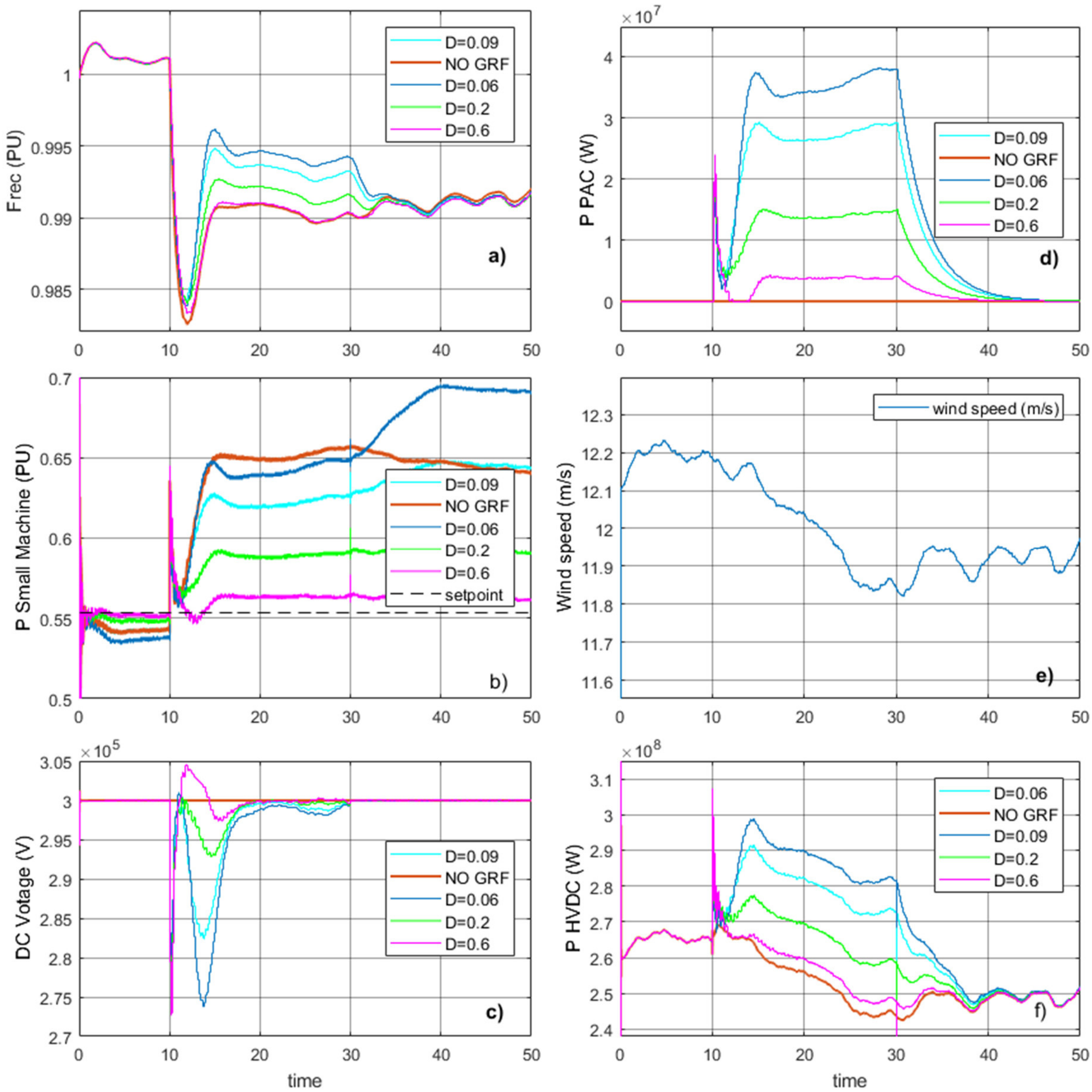

Figure 20 Effects of different droop control constants in the small generator when using the GRF controller

Figure 21 Shows the effects of changing the GRF controller gain for a small generator with 0.1 droop constant. The gain of the GRF defines the magnitude of the extra energy provision from the PAC-controlled wind farm and is obtained by multiplying the small generator power output in PU by a MW-defined gain G. The values of G defined for the simulation are 100MW, 300MW and 400MW. Figure 21 shows the effects of changing G in the grid frequency (Figure 21 a) the power output of the small machine (Figure 21 b) the HVDC dc voltage (Figure 21 c) The power provided by the PAC controller (Figure 21 d) and the HVDC power output (Figure 21 f). Ae seen in Figure 21 a) the impact of the loss of generation in the grid frequency decreases for higher values of G. Although the frequency response is similar to the cases presented in Figure 20, changing the value of G instead of D has other effects in the rest of the variables of the system (such as the dc voltage). The tuning of the G and D variables must be carried out based in the power handling capacities of the PAC-controlled wind farm and the desired dynamic response of the HVDC system. A proper tuning of the G and D variables can potentiate the advantages of the GRF controller and further improve the frequency performance of the grid.

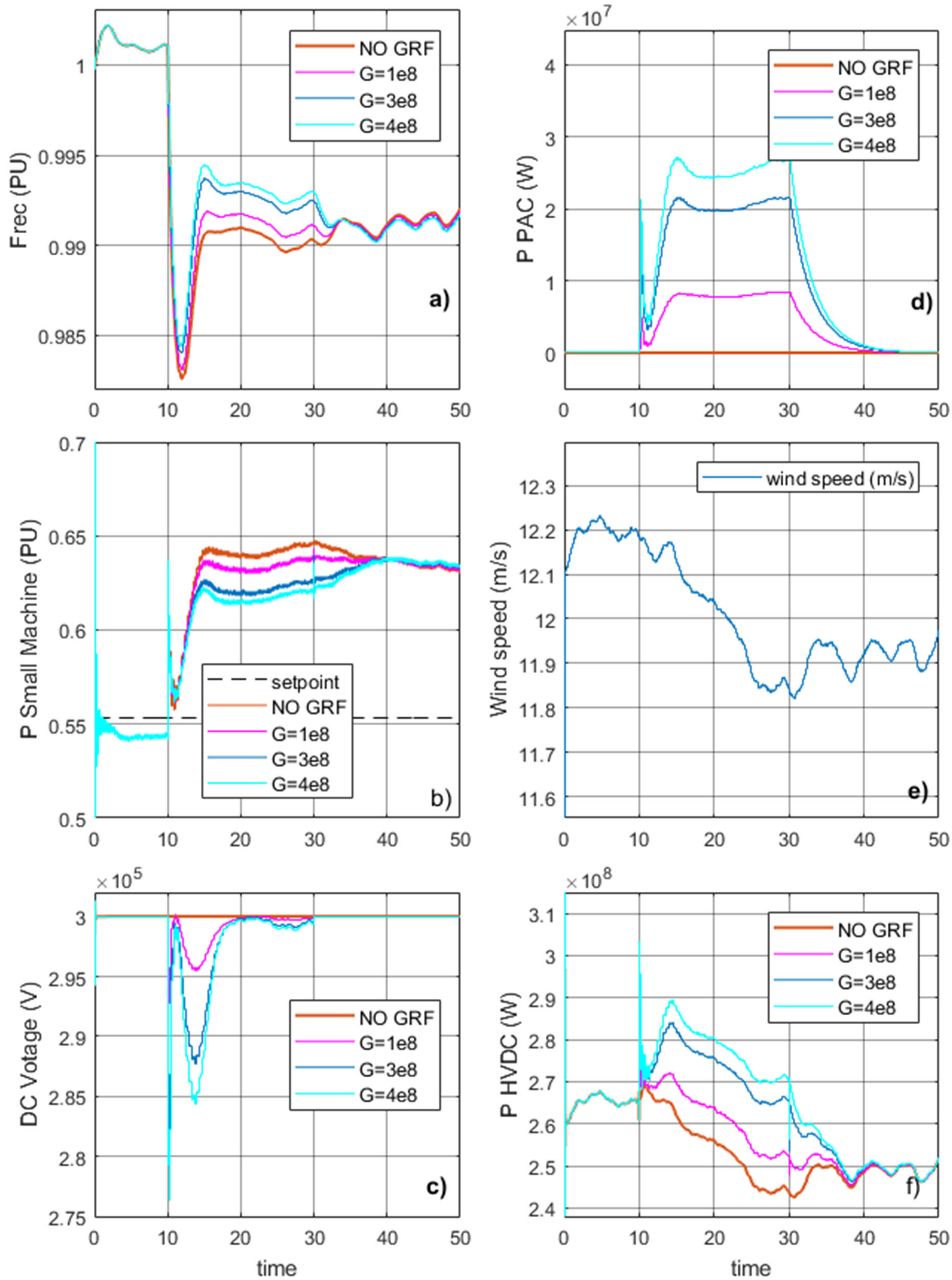

Figure 21 Effect of different gain values when using the GRF controller

4. Conclusions and Future work

The GRF concept presented offers a novel and timely solution to the ever-increasing need of developing systems that allow meeting renewable energy targets with improved flexibility. The innovation potential is significant when considering that industry and academia have repeatedly expressed the need for tools and strategies, such as the GRF concept, to enable the large-scale integration of wind power to the electric system.

Although the research efforts of this project focused in the development of a feedforward controller to handle communication delays. There is still a lot of room to improve the response the offshore wind farm to account to reduce HVDC voltage transients and minimize the disturbances to the feedforward controller. Additionally, the developed controllers require further validation in low-power experimental setups. These tasks can be covered in future iterations of the project.

Appendix

Experimental Prototype development at University of British Columbia.

Purpose of the visit.

This visiting stay at the Alpha Laboratory of Power Electronics of University of British Columbia, Canada had the purpose to develop a prototype and a real-time control system for testing a novel idea for improving power quality of DFIG wind turbine by controlling the amount of harmonic currents in the stator/rotor of the DFIG using the rotor side converter. In addition, this visit was used to create research and collaboration links with the host research group in order to maximize the impact of the Wind Energy and Control Centre research group at Strathclyde University in the areas of prototype developing and real-time control testing.

Brief Theoretical Background.

Wind generation systems are being increasingly installed in remote and/or offshore locations. The electric connections of these wind systems might be electrically "weak" and prone to voltage harmonic distortion. Nevertheless, the grid codes of several countries state that wind turbines must maintain an output current quality under certain range of grid voltage distortion. Advanced controllers for DFIG that eliminate the effect of harmonics in the stator currents have been proposed in recent literature. Among the universe of proposed solutions, the author of this report proposed a novel control solution based in Two degrees of Freedom Internal Model Controllers (2DF-IMC) and Synchronous reference frames. This novel controller fully eliminates harmonic currents in the DFIGs even under severely distorted AC voltages. Furthermore, the controller is very fast to detect and compensate harmonics without compromising the stability of the system. These features are unique and desirable among the universe of solutions available, especially if they can be corroborated experimentally.

Summary of activities carried out during the 1-month visiting scholar stay at the Alpha Lab of Power Electronics of University of British Columbia.

The initial stage of the scholar stay started by selecting the appropriate hardware devices for the prototype construction. Among the available equipment and instruments of the Alpha Lab, a 500W wound rotor induction machine was selected for the experiment. This machine provided access to the stator and rotor windings, making it suitable for the construction of a DFIG system. A 1kW DC prime mover/dymomenter was selected as the mechanical input of the generator and as a sensor for speed and position of the rotor shaft. A custom-made 2kW 3-phase VSC was selected as rotor side converter and two sets of instrumentation boards where assembled to measure the stator and currents, as well as the stator voltages. A control board system based on a 32-bit floating-point 150 MHz digital signal processor (the Texas Instruments F28335) was selected to implement the digital controller algorithm of the 2DF-IMC. Figure 23 shows the electrical diagram of the assembled prototype, naming its principal parts.
After the selection of the experiment components, the next stage consisted in measuring the induction machine parameters at different harmonic frequencies. Additionally, no-load and blocked rotor test where used to estimate machine parameters that could not be measured directly. To illustrate Figure 23 a) shows the measured variation of the rotor winding resistance at different harmonic frequencies.
After obtaining the relevant parameters from the machine, the next stage consisted in designing the digital controller to be executed by the DSP control board of the prototype. In order to do this, advanced coding tools for automatic code generation from Matlab where used. These tools enabled creating automatic C code from Simulink models that was compatible with the DSP compiler. Additionally, the generated code was based in timer interruptions for real-time

execution. As such, a highly complex program that reads 10 analog inputs using analog-to-digital converters, reads 2 digital inputs of a rotor position enconder, executes 6 closed-loop D2F-IMC controllers, executes a PLL, executes 3 abc-to-dq0 transformations and generates switching pulses for the 6 IGBTs of the VSC was designed in floating point architecture with a sampling frequency of 12kHz (i.e 83.3 microsecond step program execution). Figure 23 b) shows a capture of the Simulink model and Figure 23 c) shows a snapshot of the automatic generated C code of the digital controller.

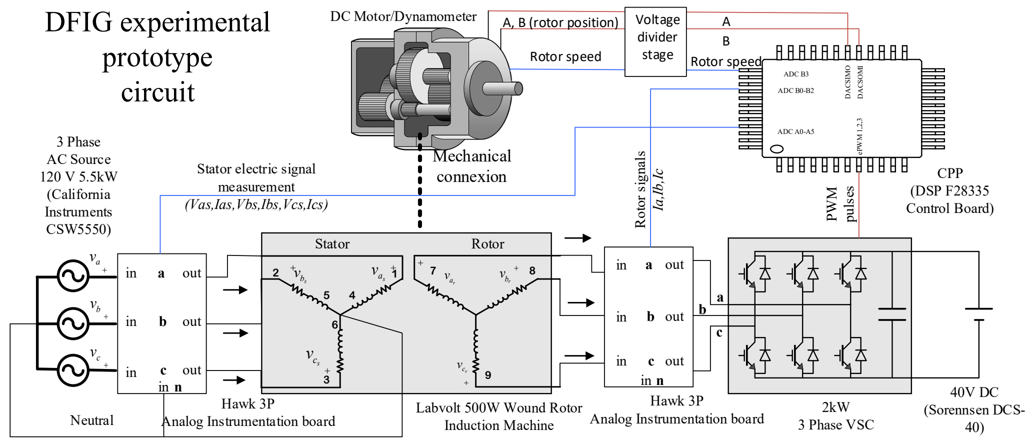

Figure 22 Electrical diagram of the DFIG prototype

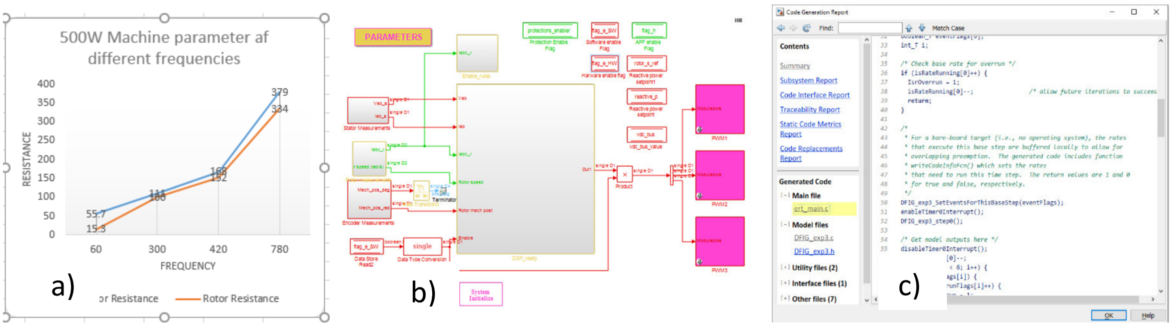

Figure 23 a) variation of rotor and stator parameters b) Simulink Code generation Model c) Generated C-code of the Simulink model.

The next stage of the work consisted in constructing the experimental platform and connecting it to a controlled 3-phase voltage source able to produce harmonic distortion. Figure 24 shows a picture of the built experimental platform naming its principal parts.

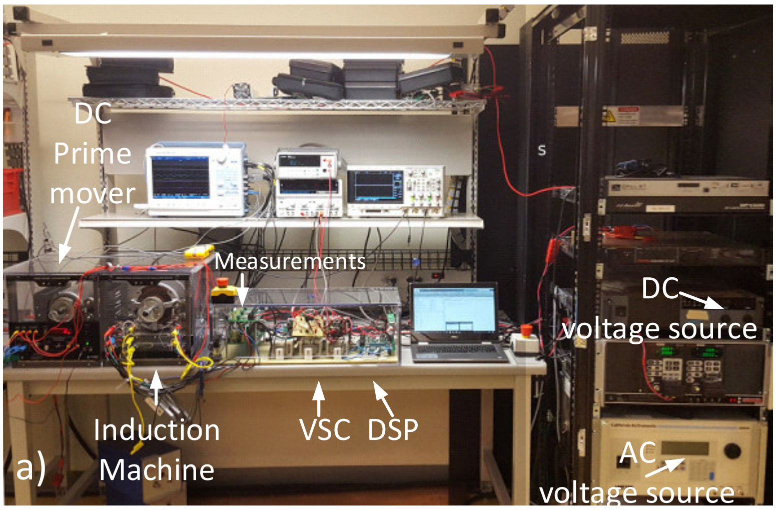

Figure 24 a) Full experimental prototype b) Electronic components of the experimental prototype c) Prime mover and induction machine of the experimental prototype.

The results of this investigation show an excellent performance of the DFIG controller in simulation and experiemental tests. To illustrate, Figure 25 shows the Behaviour of the DFIG rotor and stator currents as well as the stator active and reactive power for a speed change. As seen in the oscilloscope capture, the command of speed change triggers a current increase in both stator and rotor circuits that increase the active power consumption of the machine. However the reactive power is kept controlled at 0 VAR during this operation. This evidences the robustness of the speed and reactive power controller of the experimental DFIG setup.

Figure 25 Experimental results of the DFIG prototype for speed and reactive power control

To test the novel controller for active power filtering capabilites implemented in the DFIG a second experiment was carried out with AC voltage provision polluted with harmonic content. Here the pollution of the AC voltage will induce harmonic in the rotor and stator currents. However the controllers of the rotor side converter will remove the harmonic pollution in the currents using control over the rotor voltages.Figure 26 shows the simulated behaviour of a DFIG wind turbine when the active power filter feature is disabled/enable (red/green). At t=3s the grid voltage (va_s, vb_s, vc_s) is polluted with severe harmonic content which, in turn, produces harmonic distortion in the stator (ia_s, ib_s, ic_s) and rotor (ia_r, ib_r, ic_r) currents, and ripple in the power (P_s, Q_s) and torque (T_e) of the machine. At t=3.1s the active power filter of the DFIG controller is enabled and the harmonic distotion of the stator currents are eliminated to the full. This substantially reduces the ripple in the active power and the electrical torque.

Figure 27 shows the experimental results of the proposed technique where, just as in the case in the simulation case, the harmonics in the stator currents are eliminated and the ripple in the power is reduced after the enhaced controller is enbled.

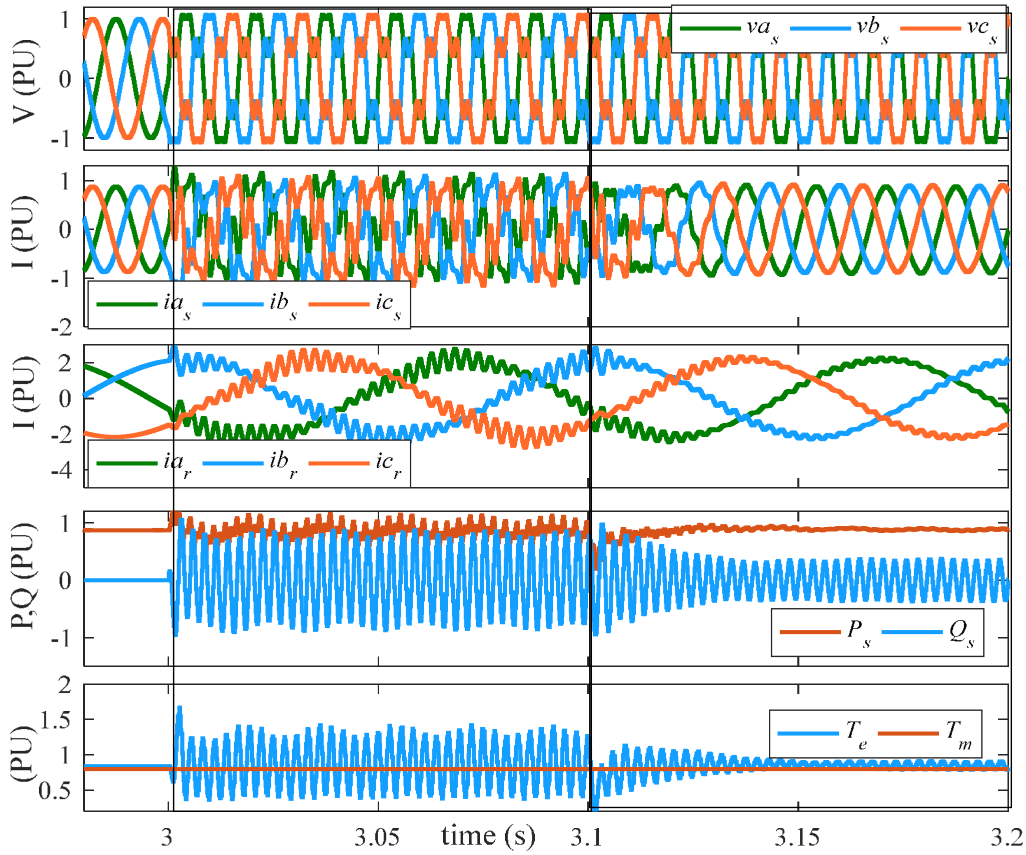

Figure 26 Simulation results of a DFIG wind turbine control with active power filter capabilities

Figure 27 Experimental results of a DFIG wind turbine control with active power filter capabilities

Figure 28 shows a detailed view of the stator and rotor currents when the harmonic filtering takes place. As seen in the figure, the stator and rotor are harmonic free even though the AC voltage is heavily polluted with harmonic content.

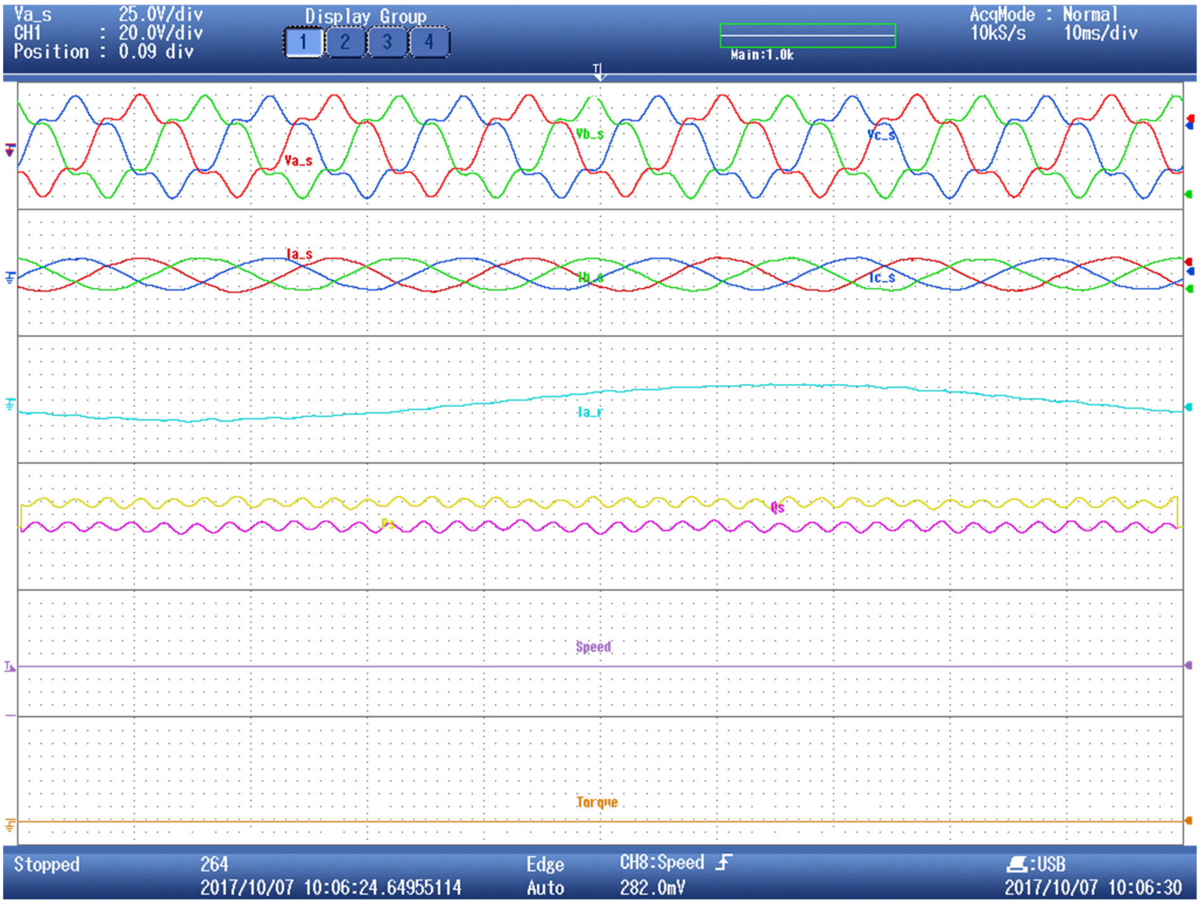

Figure 28 Experimental results of the DFIG prototype under AC voltage polluted with AC harmonics.

Poster presentation at Global offshore wind conference 2018.

Dynamic Wind Power Plant Control for System Integration

David Campos-Gaona, Olimpo Anaya-Lara, William Leithead

d.campos-gaona@strath.ac.uk, o.anaya-lara@strath.ac.uk w.leithead@strath.ac.uk

University of Strathclyde

Abstract

This project presents a holistic wind farm control approach that enables wind power plant to provide the full range of ancillary services including synthetic inertia at the wind farm level rather than single turbine level. In order to detect a power system event and select the magnitude of the service provision from the wind farm, a fully instrumented small/medium generator is used. By slaving the wind farm output to the generator natural response during power system events, the wind farm is able to provide a stable scaled-up range of ancillary services without relying in delayed or noisy grid frequency measurements.

Objectives

- Use the Power Adjusting Controller (PAC) hierarchical control approach to enable the provision of ancillary services at wind farm level rather than single turbine.
- Provide ancillary services from the offshore wind farm by slaving the PAC-enhaced wind farm controller output of a fully instrumented small generator during frequency event. This is called the Generator-Response Following (GRF) concept.
- Applying the Generator-Response Following (GRF) as a power system event-detection mechanism. This avoid the use of conventional frequency measurement devices prone to high noise, lack of accuracy and delay.
- Provide immediate response from the HVDC onshore wind power substation during a frequency event by applying a feed forward controller to deal with the delay in transmission of the GRF signal to the offshore wind farm.

Methods

The PAC controller:

- **Allows the wind turbine power output to be adjusted via an input AP**
- **Is a generic controller that can be applied to any asynchronous variable speed horizontal axis wind turbine without alteration to nor knowledge of the turbine MPPT controller.**
- **does not affect the normal operation of the turbine.**

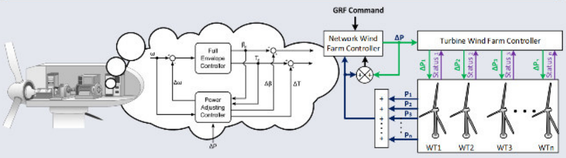

The GRF concept:

- **A small fully-instrumented (PSS, AVR) generation unit at the wind plant point of connection**
- **A Master-slave controller for provision of ancillary services from the wind turbine that mimics the natural response, droop control and inertia of the small generator at a much greater scale level.**
- **A feedforward controller for immediate response of the wind farm based in the control of the energy of the HVDC capacitors at the onshore substation.**

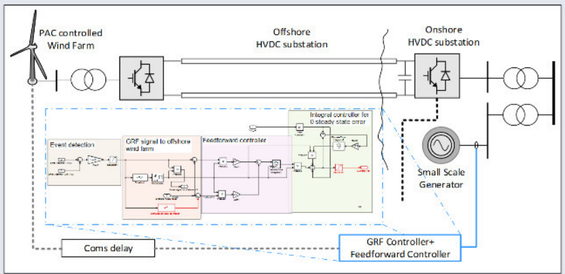

Results

The result is a stable scaled-up synthetic inertia provision from the wind farm during system events that mimics the response of the synchronous generator. This has a noticeable positive impact in the transient dynamics of the grid frequency.

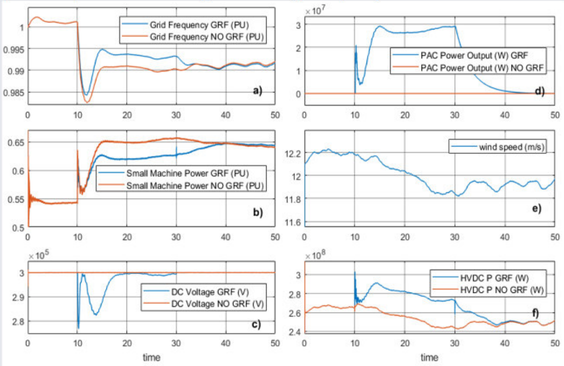

To demonstrate the accuracy of the GRF controller in following the power output of the small-medium machine and the effects of modifying the governor constants of the small machine are shown in figure 2. In this series of experiments the governor droop constant (D) is selected to be 0.06 (most sensitive to frequency variation), 0.09,0.2 and 0.6 (least sensitive to frequency variations). Figure 2 shows the effects of changing D in the grid frequency (Figure 2 a) the power output of the small machine (Figure 2 b) the HVDC dc voltage (Figure 2 c) The power provided by the PAC controller (Figure 2 d) and the HVDC power output (Figure 2 f). A seen in the plot in figure 2. The GRF controller is able to follow the small generator in a wide range of governor settings.

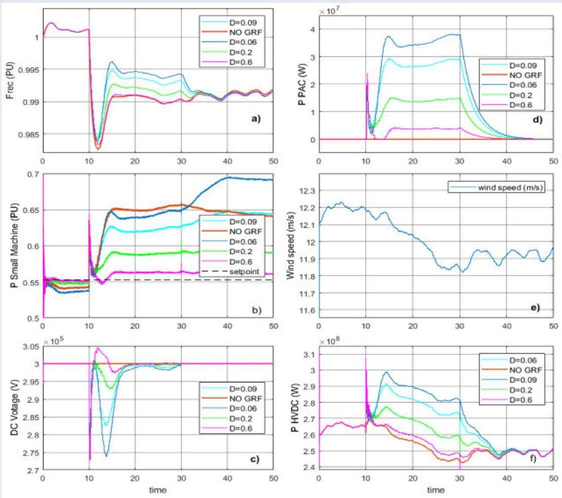

Conclusions

The GRF concept presented offers a novel and timely solution to the ever-increasing need of developing systems that allow meeting renewable energy targets with improved flexibility. The innovation potential is significant when considering that industry and academia have repeatedly expressed the need for tools and strategies, such as the GRF concept, to enable the large-scale integration of wind power to the electric system

References

1. H. Holttinen, J. Kiviluoma, N.A. Cutululis, A. Gubina, A. Keane, F. Van Hulle, 2012. Ancillary services: technical specifications, system needs and costs, Deliverable 2.2, REserviceS.
2. C. Bjerge, JR. Kristoffersen, How to run an offshore wind farm like a conventional power plant. Modern Power Systems 2007; 27: 31–33. ISSN 02607840.
3. Hur, S.-H., Leithead, W. E., *Curtailment of wind farm power output through flexible turbine operation using wind farm control*, EWEA2014, Barcelona, Spain, 2014.
4. Stock, A., *Augmented Control for Flexible Operation of Wind Turbines*, PhD Thesis, University of Strathclyde, 2015.
5. Stock, A., Leithead, W.E., *Providing frequency droop control using variable speed wind turbines with augmented control*, EWEA2014, Barcelona, Spain, 2014.

2018 GLOBAL OFFSHORE WIND 19–20 June Manchester, UK

Global Offshore Wind 2018 – Manchester - 19-20 June 2018